63-3-4

ASTIA Document No. 05000 4

THE UNIVERSITY OF MICHIGA

APPLIED RESEARCH IN MICROWAVE AND QUANTUM ELECTRONICS

INTERIM SCIENTIFIC REPORT NO. 2

Period Covering August 5, 1962 to February 5, 1963

ELECTRON PHYSICS LABORATORY
Department of Electrical Engineering

By: J. E. Boers
H. K. Detweiler
G. I. Haddad
G. Hok
G. T. Konrad
Y. C. Lim
R. J. Lomax
N. A. Masnari
J. E. Rowe
A. Singh
C. P. Wen
C. Yeh

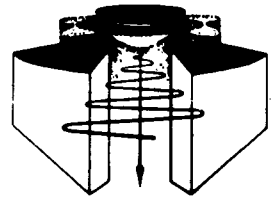

Approved by: J. E. Ro

February, 1963

CONTRACT WITH:
ELECTRONIC TECHNOLOGY LABORATORY, AERONAUTICAL SYSTEMS DIVISION, WRIGHT-PATTERSON AIR FORCE BASE, OHIO. DEPARTMENT OF THE AIR FORCE,
PROJECT NO. 4156, TASK NO. 415603, CONTRACT NO. AF-33(657)-8050

OFFICE OF RESEARCH ADMINISTRATION • ANN ARBO

Qualified requesters may obtain copies of this report from ASTIA.

THE UNIVERSITY OF MICHIGAN
ANN ARBOR, MICHIGAN

INTERIM SCIENTIFIC REPORT NO. 2

FOR

APPLIED RESEARCH IN MICROWAVE AND QUANTUM ELECTRONICS

This report covers the period August 5, 1962 to February 5, 1963

Electron Physics Laboratory
Department of Electrical Engineering

By: J. E. Boers
H. K. Detweiler
G. I. Haddad
G. Hok
G. T. Konrad
Y. C. Lim
R. J. Lomax
N. A. Masnari
J. E. Rowe
A. Singh
C. P. Wen
C. Yeh

Approved by: J. E. Rowe
J. E. Rowe, Director
Electron Physics Laboratory

Project 05000

CONTRACT NO. AF-33(657)-8050
DEPARTMENT OF THE AIR FORCE
PROJECT NO. 4856, TASK NO. 415603
PLACED BY: ELECTRONIC TECHNOLOGY LABORATORY
AERONAUTICAL SYSTEMS DIVISION
WRIGHT-PATTERSON AIR FORCE BASE, OHIO

February, 1963

ABSTRACT

High-Conductivity Materials for Microwave Tubes

Several techniques for brazing a wire helix in a beryllium oxide envelope are presented. One scheme proved to be quite satisfactory. Heat tests on the helix structure are described showing that good thermal contact between the helix and the envelope has been obtained. The power dissipating capability of the structure has been increased substantially over what has been possible previously.

Cold tests on an X-band helix mounted in a beryllium oxide envelope indicate that dielectric losses are slightly higher than in conventional schemes but not detrimental to good tube operation.

Low-Noise Investigations

In an electron gas in equilibrium no appreciable organized motion or medium-like wave propagation is shown to be possible unless one of its boundaries is an emitter operating strongly temperature limited. The initial work on an analysis for accelerated electron flow is described, whereby it will be possible to ultimately reach conclusions of a corresponding nature.

A space-harmonic analysis useful in traveling-wave maser design is described. The design of such devices is thereby greatly facilitated.

Plasmas and Quantum Electronics

Some preliminary computer results presented in this report indicate the validity of the theoretical formulation for both double-beam and beam-plasma systems.

The experimental work on the microwave plasma amplifier is described. The work to date concerned itself mainly with the production of a suitable cesium plasma. Densities in the order of 10^{11} and 10^{12} electrons per cc have been obtained by contact ionization.

A number of interesting aspects eventually to be used in an experimental millimeter-wave plasma oscillator are described. Among these are field emission into a cesium vapor and schemes for increasing the plasma density by magnetic as well as geometrical means of confinement.

The design of the major components to be used in a high-power millimeter-wave generator is described. Cold tests on the extended interaction buncher are presented.

Crossed-Field Electron Gun Studies

It is shown that crossed-field guns in general can generate a laminar beam of limited convergence if the cathode width does not exceed some maximum value. The Poisson cell in conjunction with an analog computer was used to obtain these results.

Experimental results found in the electron beam analyzer for a simple crossed-field gun as well as a multi-electrode gun are presented. Comparison is made with theory.

Data obtained from a hybrid gun is described. The results are shown to be not conclusive for the evaluation of the gun performance.

Improvements in the digital computer program for solution of crossed-field gun problems are presented. Automatic calculation of nonuniform emission from the cathode and other features to add flexibility to the program have been incorporated.

TABLE OF CONTENTS

LIST OF ILLUSTRATIONS

LIST OF TABLES

PERSONNEL

Scientific and Engineering Personnel		Time Worked in Man Months*
G. Hok	Professors of Electrical Engineering	1.54
J. Rowe		.04
C. Dolph	Professor of Mathematics	.16
C. Yeh	Associate Professor of Electrical Engineering	.62
R. Lomax	Visiting Assistant Professor of Electrical Engineering	2.41
G. Haddad	Instructor of Electrical Engineering	1.01
A. Singh	Research Engineer	1.81
J. Boers	Associate Research Engineers	1.48
G. Konrad		1.48
J. Kurtz		1.06
H. Detweiler	Assistant Research Engineers	5.55
N. Masnari		2.53
W. Rensel		.23
C. Wen		.09
A. Collins	Research Assistants	1.00
T. DeMassa		1.84
S. Salinger		.65
D. Terry		.29
Service Personnel		18.70

* Time Worked is based on 172 hours per month.

REPORTS ISSUED DURING THE LAST PERIOD

R. J. Lomax, "An Analog Method of Determining Electrode Shapes of Electron Guns Having Curved Trajectories", Tech. Report No. 54; November, 1962.

G. Hok, "Noise Propagation in a Nonuniform Electron Gas", Tech. Report No. 58; March, 1963.

INTERIM SCIENTIFIC REPORT NO. 2

FOR

APPLIED RESEARCH IN MICROWAVE AND QUANTUM ELECTRONICS

I. GENERAL INTRODUCTION (G. T. Konrad)

The purpose of this study is to conduct applied research in microwave and quantum electronics. The program is meant to be quite general and flexible in nature so that novel ideas for the generation of electromagnetic radiation in the microwave through optical range may be investigated promptly.

Work areas for this program embody investigations of techniques in the realm of plasma, low noise, and quantum electronics to include the related areas and associated devices. In detail, these areas of investigation are as follows for the present.

A. High-thermal-conductivity materials for high-power microwave devices.

B. Various low-noise studies including multi-dimensional analyses and various maser schemes for millimeter-wave operation.

C. The interaction of electromagnetic waves with dense plasmas in both relativistic and nonrelativistic domains.

D. Generation of high-frequency, high-power electromagnetic radiation.

E. Research on the improvement of crossed-field convergent flow electron guns.

These are the same general areas that have been described in Interim Scientific Report No. 1 and were continued during the past period.

New results and the status of the various investigations are presented in detail in their respective sections in this report.

II. HIGH-THERMAL-CONDUCTIVITY MATERIALS FOR MICROWAVE TUBES (H. K. Detweiler)

A. Introduction

The investigation of high-thermal-conductivity materials for use in microwave tubes has for the present been reduced to the investigation of a single material, beryllium oxide. This ceramic material has electrical and physical properties adequate for most applications, and in addition has thermal characteristics far superior to other insulators.

Current study has been centered on overcoming a difficulty in obtaining good thermal contact between a helix and the BeO tube in which it is supported. This problem came to light during tests wherein the helix was heated by d-c current and helix temperature monitored as a function of power dissipated on the helix. Poor contact was evidenced by the development of hot spots at locations of very poor contact and in a lower than expected power handling capability. Progress made in this area of endeavor is described below.

Since at frequencies near X-band and above the small size required makes the use of fluted tubing impractical, the properties of a helix mounted in a smooth BeO tube are being investigated. Cold test data for an X-band geometry are reported.

The current status of the work on waveguide windows and on the solution of the radial heat flow problem are also presented.

B. Experimental Work

B.1 Beryllium Oxide Brazing Techniques. The thermal contact problem has been seen to be a serious obstacle to the realization of the predicted power handling capability of the helix mounted in beryllium oxide. Consequently, considerable effort has been concentrated on finding a solution to this problem.

One method of improving contact being investigated is to embed the helix in the BeO tubing. It is proposed to accomplish this by plasma-spray deposition of the BeO tube around the helix. This technique has met with some success. A short section has been supplied by an outside vendor for evaluation. This piece, while being a good job of plasma spraying, was found to be somewhat marginal for our application in that it was not mechanically strong enough and was quite porous. Both of these difficulties can be at least partly eliminated by high temperature firing and post-sintering, i.e., sintering after the plasma-spray deposition of the BeO. The vendor is proposing to modify his plasma-spray technique so as to improve the quality of the BeO body. Definite indications as to the practicality of this method of overcoming the contact problem should be forthcoming shortly.

A second method of improving contact is to braze the helix into the ceramic tubing, thereby creating a metallic bond between them. At the beginning of this period a technique had been developed whereby a copper- or nickel-plated tungsten helix was placed in contact with the titanium-coated beryllium oxide and vacuum fired at an appropriate temperature. This technique was partly successful in that it was possible to obtain a braze in this manner. The process was, however, unsuccessful in that the brazing was generally not uniform, reproducible,

or predictable. It is possible that these difficulties could have been resolved had not another problem led the way to the eventual solution.

A problem attendant to the above brazing technique from its inception was the evaporation of the helix plating material onto the titanium coated BeO during the vacuum firing. The resulting coating on the BeO was found to be impervious to attack from the hydrofluoric acid mixture which was intended to remove the titanium. Initially it was felt that this coating was merely copper over titanium and work proceeded on developing means of removing it. It was found to be possible to remove the copper coating by reverse electroplating, but a more effective means was to use a mixture of 5 percent hydrofluoric acid and 10 percent nitric acid thus removing both copper and titanium.

Having determined how to remove copper and titanium coatings from BeO, further braze tests were made. A tungsten helix with a 0.1 mil copper plating was loaded into a BeO fluted tube which was coated with 0.050 mil of titanium and vacuum fired at 1050-1100°C for 5 minutes. It appeared that a braze had been made and it was attempted to chemically remove the copper and titanium from the walls of the tubing using the acid mixture. It was found that most, but not all, of the coating was removed quite quickly, the remainder giving no evidence of being affected. At this stage the bond appeared to be intact. Further chemical etching had no apparent effect on the remaining coating but did eventually deteriorate the bond. It was then concluded that the copper and titanium on the walls had alloyed and this alloy was quite resistant to chemical attack. Subsequent removal of the helix showed brazing had taken place but that it was not uniform nor was there much evidence of the formation of fillets. At points along the helix where brazing had occurred,

microscopic examination revealed BeO particles attached to the helix, indicating that the bond was strong and resistant to chemical attack, but that the BeO itself had been weakened in the area of the braze and had broken loose when the helix was removed. These results indicated that a change was necessary in the brazing technique.

A close examination of the braze test pieces after firing revealed a very interesting phenomenon. The copper which evaporated from the helix during brazing had adhered to the titanium coated BeO but not to the bare portion. Because of this discovery and in hope of minimizing evaporation from the helix, it was decided to leave the ceramic bare and to vacuum deposit the titanium on the copper plated helix. This coating was accomplished by placing the helix on the axis of a helical filament which consisted of 2-3 strands of 0.015 inch tantalum wire covered by 0.010 inch titanium wire wound at approximately 18 TPI. The filament temperature was slowly raised to above the melting point of titanium and the evaporating titanium was deposited on the helix. By varying the amount of titanium on the filament, evaporating time, and spacing between the helix and filament it was possible to control the thickness of the titanium coating.

The first braze test using this technique was performed on a one-inch length of helix having a copper plating 0.86 mil thick on a 0.1 mil thickness of titanium, placed between two uncoated pieces of BeO. This test piece was vacuum fired by r-f induction heating for a period of 2-1/2 minutes at 1100°C. Because of outgassing of the parts it was necessary to slowly raise the temperature to this level over a time interval of about 15 minutes. The pressure in the bell jar was 3×10^{-6} mm Hg during brazing.

Inspection of this test piece showed that bonding had taken place between the helix and the ceramic. Study of the region of the braze under a microscope revealed the formation of fillets at the contact points. However, there seemed to be insufficient wetting of the BeO by the copper-titanium alloy. Since the titanium promotes wetting[1], it was decided to increase the percentage of titanium available for the braze. This change is also desirable from the standpoint that an increased percentage of titanium will result in a lower brazing temperature. From an inspection of the copper-titanium phase diagram[2] it is seen that the lowest melting point alloy between these constituents occurs at about 75 percent copper, 25 percent titanium by weight. For the above test the composition of the brazing alloy was approximately 94 percent copper and 6 percent titanium.

It should be noted that this particular brazing process has solved the two major problems previously encountered. Since the coatings of titanium and copper on the helix are quite uniform, the brazing and fillet size are quite uniform as long as contact is made between the helix and BeO. Also the evaporating copper does not adhere to the BeO which is found to be very clean at the completion of brazing.

It appears that this brazing process is a satisfactory solution to the thermal contact problem. There is, however, a drawback in that the copper-titanium alloy remains on the helix surface and is not removable by acid etching. Because of the high resistivity of titanium it is suspected that this surface coating may have a high resistivity

---

1. Kohl, W. H., Materials and Techniques for Electron Tubes, Reinhold Publishing Corp., New York, p. 505; 1960.

2. Hansen, M., Constitution of Binary Alloys, McGraw-Hill Book Co., Inc., New York, New York, pp. 643-645; 1958.

also. If such is the case, a plating of a lower resistivity metal, such as copper, can be applied to the helix surface. The thickness of this plating should be approximately equal to the skin depth so as to minimize r-f losses. It is also necessary that the helix be in contact with the BeO before brazing in order that brazing take place. Thus great care must be exercised in loading the helix into the envelope.

Further brazing tests were performed in order to work out the details of the process. The various parameters of the process such as plating thicknesses, relative amounts of copper and titanium, firing times and temperatures were varied in order to determine their effect on the braze obtained. Satisfactory brazes were obtained with a thickness of 0.1 to 0.8 mil of copper, 0.03 to 0.07 mil of titanium, and firing temperatures of from 1000 to 1100°C for 2-7 minutes. It was found that exceptionally good and consistent results were obtained by using a 0.1 mil thickness of copper, 0.05 mil thickness of titanium, and firing at 1034°C for 2-1/2 minutes. In order to minimize stresses due to the different coefficients of expansion of tungsten and BeO, after firing the temperature was reduced to 900°C and held there for 2 minutes before allowing the helix to cool to room temperature. The process as described above was used to braze helices into BeO tubes for the heat tests described later.

As mentioned above, the copper-titanium plating remaining on the helix after brazing has been cause for some concern. An alternative brazing technique was attempted as a means of circumventing this problem. Instead of evaporating titanium onto the copper plated helix a piece of titanium foil 0.25 mil thick was placed between the helix and BeO. Vacuum firing was done at 1034°C for 5 minutes. Brazing took place with

uniform fillets forming. However, the copper-titanium alloy flowed out of the braze area up the helix and onto the BeO. The electrical properties of this configuration would most likely be unsatisfactory due to nonuniformities. Although this problem could very likely be overcome with further work, development of this technique has been delayed pending electrical testing of the helix brazed by the previous technique.

The promise shown by the copper-titanium brazing technique warranted the preparation of a sample for heat testing. The beryllium oxide tube used in this test had been used previously for testing molybdenum and chromel helices which had been loaded into the tube under pressure. The data obtained from these tests have been reported previously[3] and will be compared to the present results. The dimensions of the tube are

I.D. = 0.205 inch on the flutes

O.D. = 0.315 inch

t_w = 0.040 inch

w_f = 0.020 inch

h_f = 0.015 inch.

The helix dimensions are

2a' = 0.187 inch

TPI = 18

d_w = 0.020 inch

length = 5-3/4 inch

flat width = 0.011 inch.

The outside diameter of the helix was 0.206 inch before loading into the tube and hence it had to be compressed. The plating thickness of copper

3. Detweiler, H. K., Dolph, C. L., Rowe, J. E., "Applied Research on High-Thermal-Conductivity Materials for Use in Microwave Tubes", Final Report, Electron Physics Laboratory, The University of Michigan; December, 1961.

and titanium on the helix was 0.11 mil and 0.055 mil, respectively. Firing took place at 1030°C for a period of 2-1/2 minutes. Inspection of the helix turns visible at each end revealed the formation of fillets at the points of contact. It was found after completion of the braze that the turns could not be moved, indicating that brazing had taken place. Aside from having the helix brazed into the tube, the test piece is the same as discussed previously[4].

B.2 Tests on Power Handling Capabilities. To determine the power handling capability of a helix supported in this fashion, d-c power was applied to the helix and measurements taken of voltage, current and the thermocouple potentials. Two methods were used for finding the helix temperature. The first was a direct method using the temperature as read by the thermocouple attached to the helix at its center. The validity of the assumption that the helix temperature is given accurately by this reading is somewhat doubtful due to the frequent development of hot spots at or near the thermocouple location. Rather than this being a coincidence, it is felt that connection of the thermocouple may actually be the cause of a hot spot because of distortion of the helix during the spot-welding process. For this reason, later test models have omitted this thermocouple. When a hot spot does occur near the thermocouple, the temperature as determined from the thermocouple potential is appreciably higher than the mean helix temperature.

The second method was to calculate the mean helix temperature from its change in electrical resistance. Strictly speaking, the calculation should take into account the different temperature behavior of the tungsten wire and the copper-titanium alloy on its surface. However, due

4. ibid.

to the thinness of this plating, and therefore its high resistance in comparison to that of the wire, the temperature behavior of the combination is nearly identical to that of the tungsten alone. A few sample calculations made to test this assumption proved its validity for the helices to which it was applied. Although this method does not take into account that the hot turns are dissipating appreciably more power by radiation than the rest, it is felt that the temperature calculated in this way is more representative of the helix temperature than that obtained from the thermocouple reading. Consequently, this method was employed for calculating the temperature used in presenting the test data.

Several test runs were made on this model with the results being quite consistent. The first test showed a higher temperature rise than did the second and third tests, indicating that the helix very likely expanded and shifted sufficiently at some of the hot spots to come into contact with the tubing and braze to it. Data from the second and third tests were located on the same curve, showing that any shifting that was going to take place did so during the first test. The results are shown in Fig. II.B.1, curve E, where the mean helix temperature rise is plotted as a function of power input to the helix. Also shown are the results previously reported for various test models. The dimensions of these models are given in Table II.B.1. It should be noted that a helix of different dimensions was used for the present tests than had been used previously. However, since the TPI of the present helix is approximately 1.5 times as large and the wire diameter 2/3 as large, the helix surface area and contact area with the BeO is very nearly the same. Therefore, the test results can be directly compared.

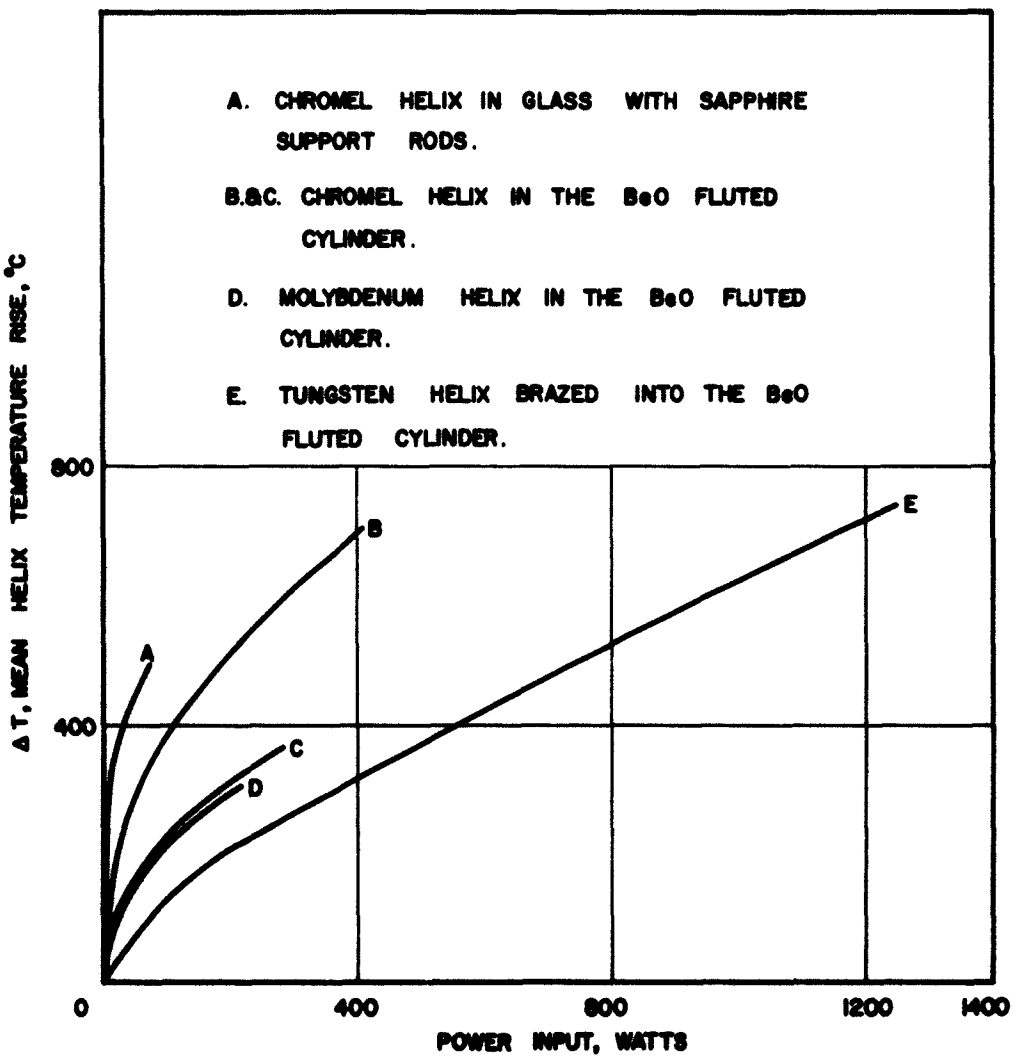

FIG.II.B.1 HELIX TEMPERATURE VS. POWER INPUT FOR HELICES MOUNTED IN GLASS WITH SAPPHIRE SUPPORT RODS AND IN A BeO FLUTED CYLINDER.

Table II.B.1

Dimensions of Test Pieces

	A	B and C	D
Envelope:	Type 7052 glass	BeO	BeO
	I.D. = 0.245 inch	I.D. = 0.205 inch on flutes	I.D. = 0.205 inch on flutes
	O.D. = 0.304 inch	O.D. = 0.315 inch	O.D. = 0.315 inch
		t_w = 0.040 inch	t_w = 0.040 inch
		w_f = 0.020 inch	w_f = 0.020 inch
		h_f = 0.015 inch	h_f = 0.015 inch
Helix:	Chromel A	Chromel A	Molybdenum
	d_w = 0.0285 inch	d_w = 0.0285 inch	d_w = 0.030 inch
	I.D. = 0.156 inch	I.D. = 0.156 inch	I.D. = 0.152 inch
	O.D. = 0.2055 inch	O.D. = 0.2075 inch	O.D. = 0.2078 inch
	Flat width = 0.018 inch	Flat width = 0.016 inch	Flat width = 0.017 inch
	T.P.I. = 11.32	T.P.I. = 11	T.P.I. = 12
	Length = 5-3/4 inches	Length = 5-3/4 inches	Length = 5-3/4 inches
	Sapphire rod diameter = 0.020 inch		

It is seen from the curves of Fig. II.B.1 that the results for the test model with the brazed helix are considerably better than obtained for previous models. At a power input of 200 watts, for instance, the brazed helix is nearly 100°C cooler than the best previous model. At comparable temperatures this brazed helix dissipated 2-4 times as much power. Compared to the helix mounted in glass, this helix dissipated from 11 to 25 times as much power. For a temperature of 600°C the brazed helix was found to have a power dissipation capability 47 percent of that predicted by theoretical calculations. An interesting aspect of curve E is that the variation of ΔT with input power is nearly linear, indicating that almost all of the power is being dissipated by conduction.

The success of the above test justified further experimental testing of brazed helix models. Since there were no more vacuum tight BeO fluted tubes available, it was necessary to use porous tubes and perform the tests in a vacuum bell jar. Initial tests pointed up difficulties with the thermocouple and the thermon used to insure good contact between the BeO and the cooling coils. The thermocouple seemed to promote hot spots and the thermon lost its heat transfer properties when heated in the vacuum. To overcome these difficulties, the thermocouple was omitted and the thermon was replaced by pure tin. A low melting temperature bismuth-lead alloy was also used but it began to melt at relatively low power levels. Curves of the mean helix temperature rise as a function of power input for the three heat transfer agents are shown in Fig. II.B.2. It is seen that tin is the best of the three for this application and the results obtained in this test are the best to date.

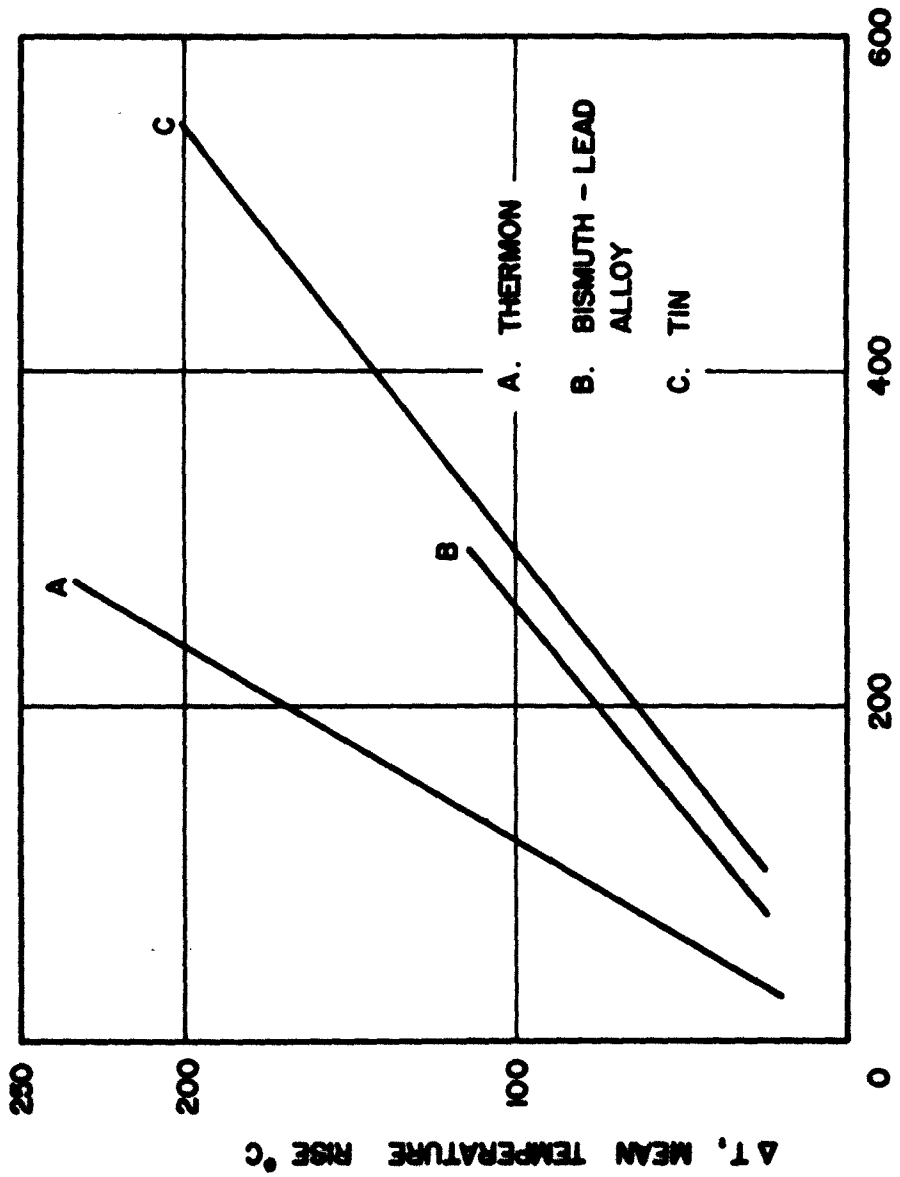

FIG. II.B.2 HELIX TEMPERATURE VS. POWER INPUT FOR A HELIX BRAZED IN A BeO FLUTED CYLINDER USING VARIOUS HEAT TRANSFER AGENTS.

The dimensions of the BeO tube for these tests are

I.D. = 0.201 inch

O.D. = 0.320 inch

t_w = 0.035 inch

w_f = 0.025 inch

h_f = 0.025 inch

$\tan \alpha$ = 0.357.

The helix dimensions are

2a' = 0.186 inch

TPI = 18

d_w = 0.020 inch

length = 5-3/4 inch

flat width = 0.011 inch.

The plating thickness of copper was 0.16 mil and of titanium 0.07 mil. Brazing was done at 1034°C for a period of 2-1/2 minutes.

A calculation of the theoretical power handling capability for this helix showed that at a temperature of 200°C the actual power dissipation obtained experimentally was 53 percent of that predicted. While the agreement between predicted and experimentally obtained dissipation is quite good, the problem of hot spots has not been entirely overcome. It is felt that this is primarily due to nonuniformities in the tubing. Further testing for brazed helices is planned upon receipt of additional fluted tubing.

Since the electrical properties of the brazed helix are very important, it will be necessary to cold test this structure to ascertain whether the brazing has adversely affected its electrical characteristics. The tests are planned for the next period pending shipment of additional tubing.

B.3 Metallizing of BeO Tubes. The possibility of surface metallizing BeO tubes for vacuum tightness is still being investigated. Although no further work has been done on the plasma-spray metallizing, the process developed for helix brazing was adopted for surface metallizing. Initial tests employed thin vacuum-deposited layers of copper and titanium in proportions of approximately 10 to 1, respectively. Firing was done in a vacuum at 1030°C for 2 minutes. The resulting metallized coating appeared to be quite adherent and nonporous although in some locations the coating bubbled up and then peeled. It is felt that this condition was caused by dirt or grease on the tube surface. Further work on this technique is planned. Also scheduled for the next period are tests of the moly-manganese process, which can now be attempted due to the recent acquisition of a high-temperature furnace.

B.4 R-f Cold Tests of an X-Band Helix. Extensive r-f cold tests have been carried out on an X-band helix mounted in a smooth-bore BeO tube. In these tests, coupled-helix couplers were used to couple r-f energy onto and off of the helical structure. The dimensions of the various components are listed below:

BeO tube: I.D. = 0.098 inch
O.D. = 0.158 inch

Helix: Mean helix diameter = 0.085 inch
Wire diameter = 0.014 inch
TPI = 24
Flat width = 0.007 inch

Coupler: Mean helix diameter = 0.173 inch
Wire diameter = 0.015 inch
TPI = 9.5

Coupling length = 4-1/2 turns

Dielectric thickness = 0.037 inch

Shield I.D. = 0.262 inch.

Measurements were taken of the VSWR of each coupler with the helix terminated and also of the VSWR of both couplers with the output coupler terminated in a matched load. Curves of VSWR vs. frequency for these combinations are shown in Fig. II.B.3. Except for the high frequency end, above about 11.4 kmc, the couplers are satisfactory.

These couplers were used to determine the guide wavelength, λ_g, for the helix mounted in the BeO tube. From this parameter the phase velocity, v_p, and $\gamma a'$ can be calculated. These results are plotted in Figs. II.B.4, II.B.5 and II.B.6. The dielectric loading factor, DLF, and the synchronous voltage were also determined and are shown in Figs. II.B.7 and II.B.8. The DLF is seen to be rather low, about 63 percent, which is slightly lower than the predicted 70 percent. This increased dielectric loading resulted in the synchronous voltage being lower than expected.

Measurements were also made of the helix insertion loss as a function of frequency for different lengths of helix. From these data, the helix and coupler loss were calculated and are presented in Figs. II.B.9 and II.B.10.

In general, these cold tests showed that the helix in a smooth-bore BeO tube performed about as had been anticipated with the exception that a slightly lower DLF was obtained. In spite of this, it is felt that this helix supporting method is practical from the standpoint of its electrical characteristics. Since cold testing of the X-band structure has been completed, attempts will now be made to satisfactorily braze a

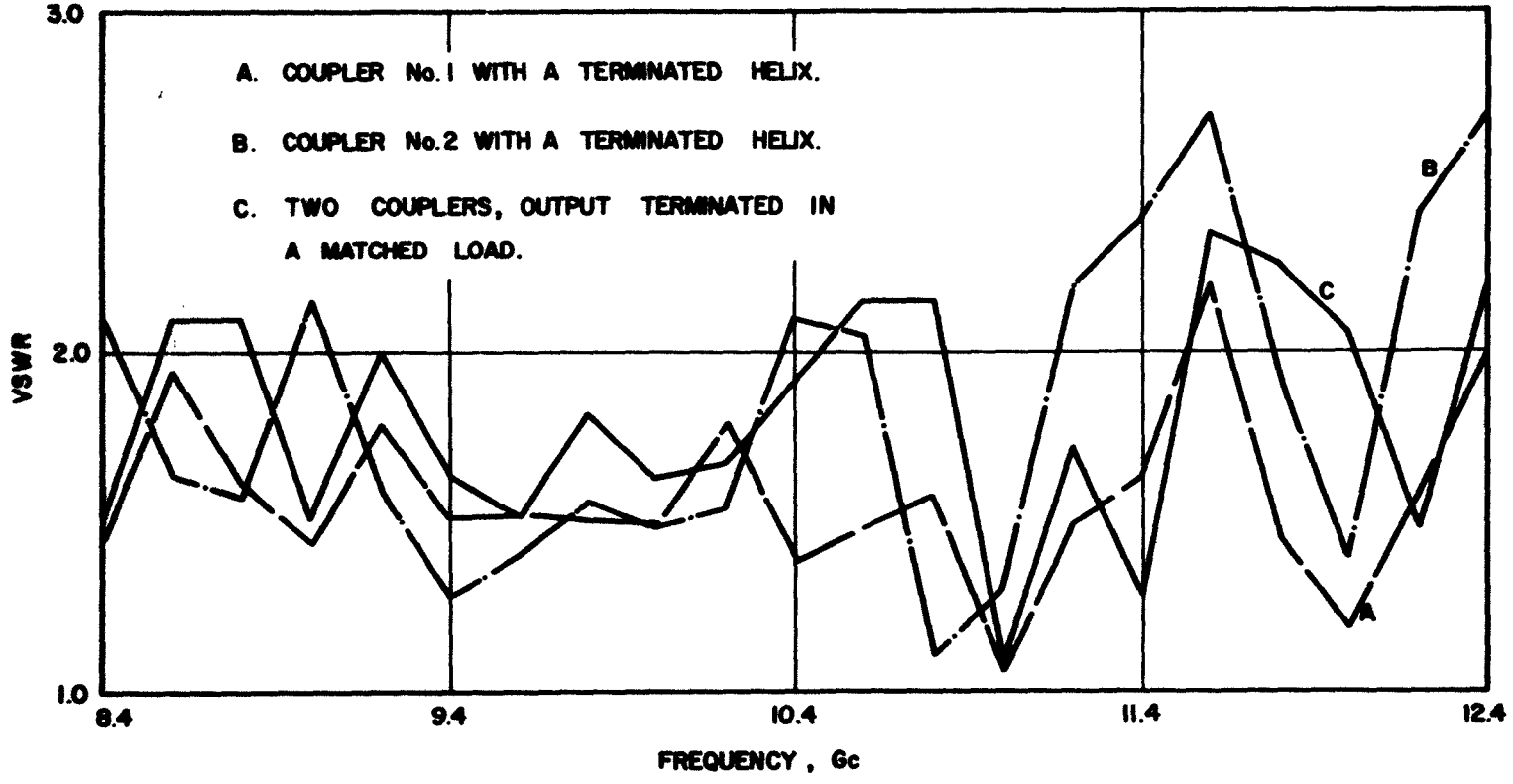

FIG. II.B.3 INPUT VSWR VS. FREQUENCY OF COUPLED-HELIX COUPLERS.

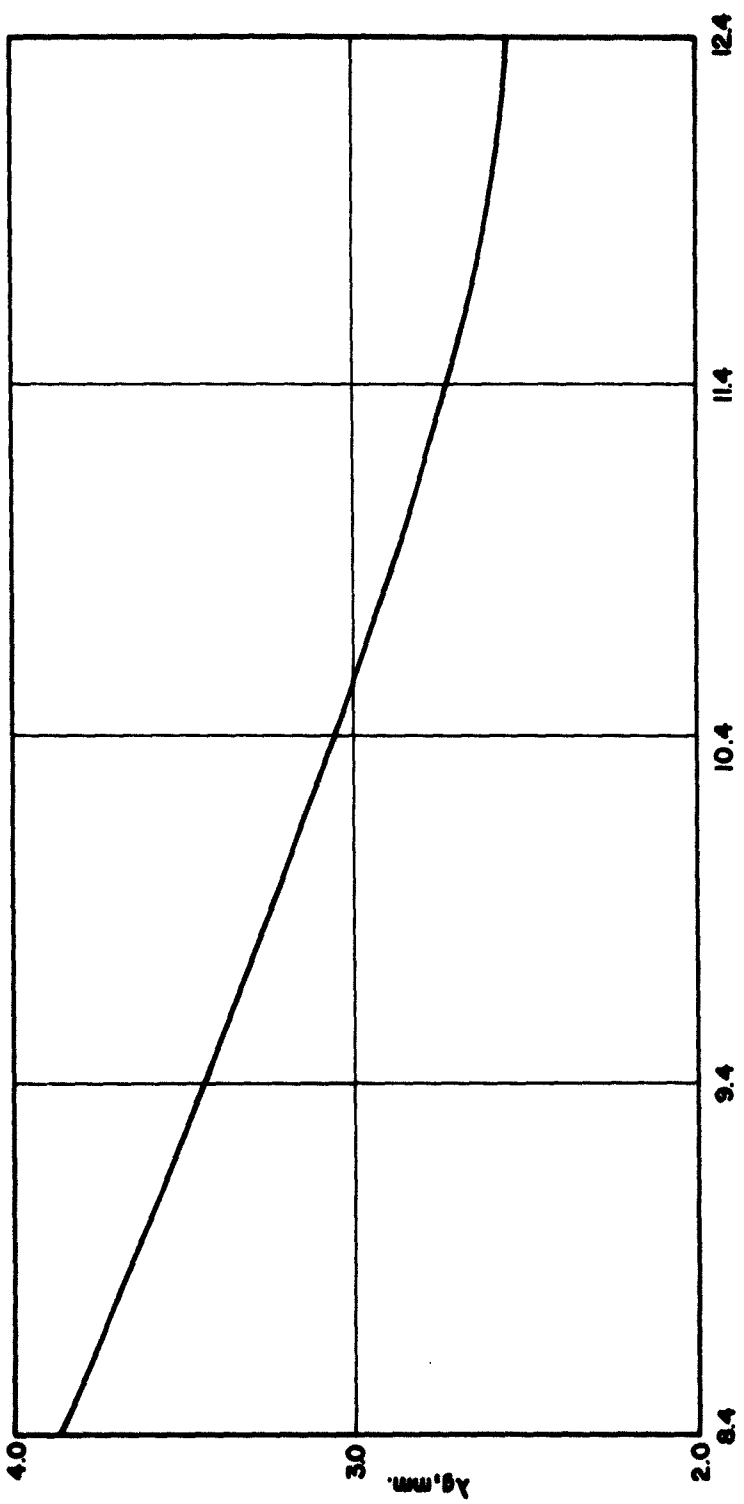

FIG. II.B.4 GUIDE WAVELENGTH, λ_g VS. FREQUENCY.

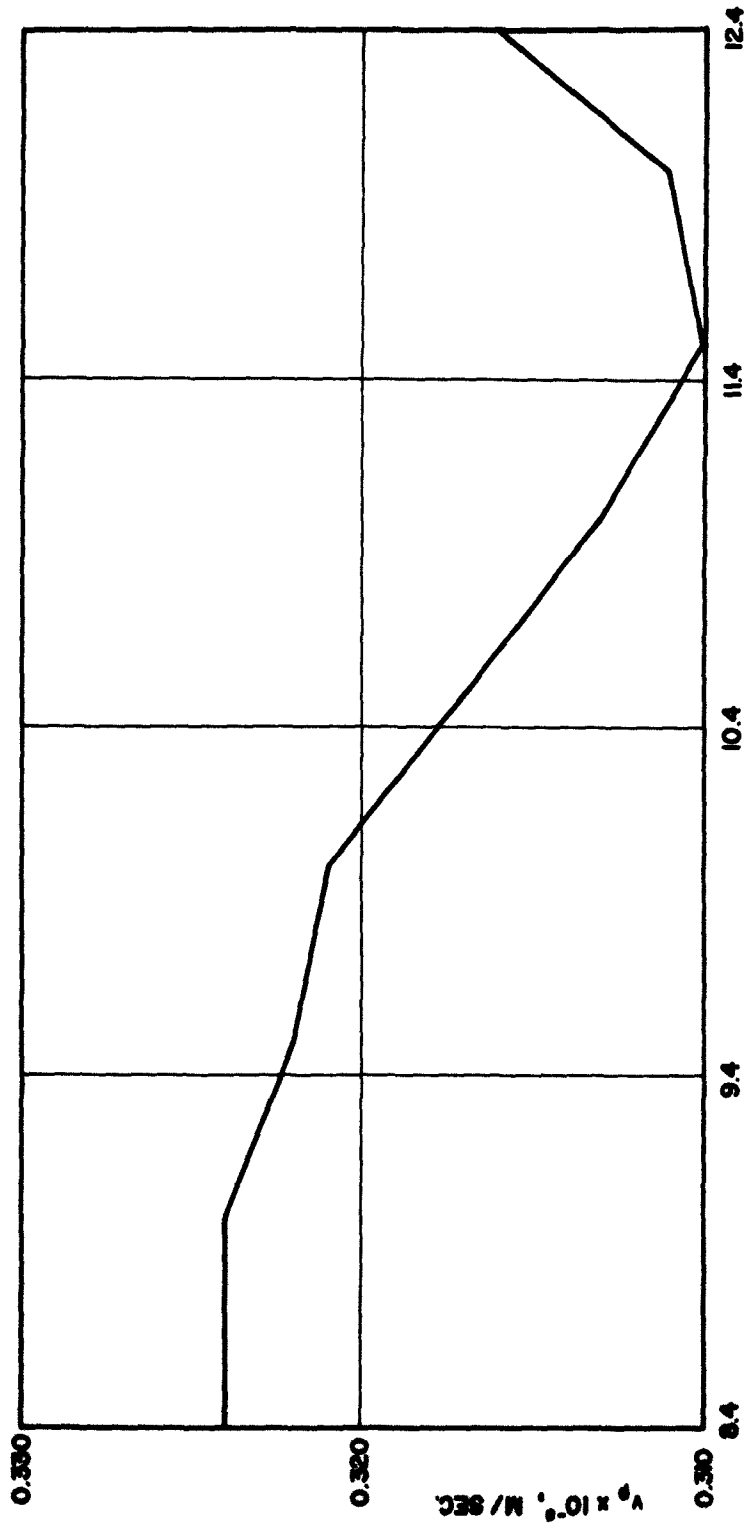

FIG. II.B.5 PHASE VELOCITY, v_p, VS. FREQUENCY.

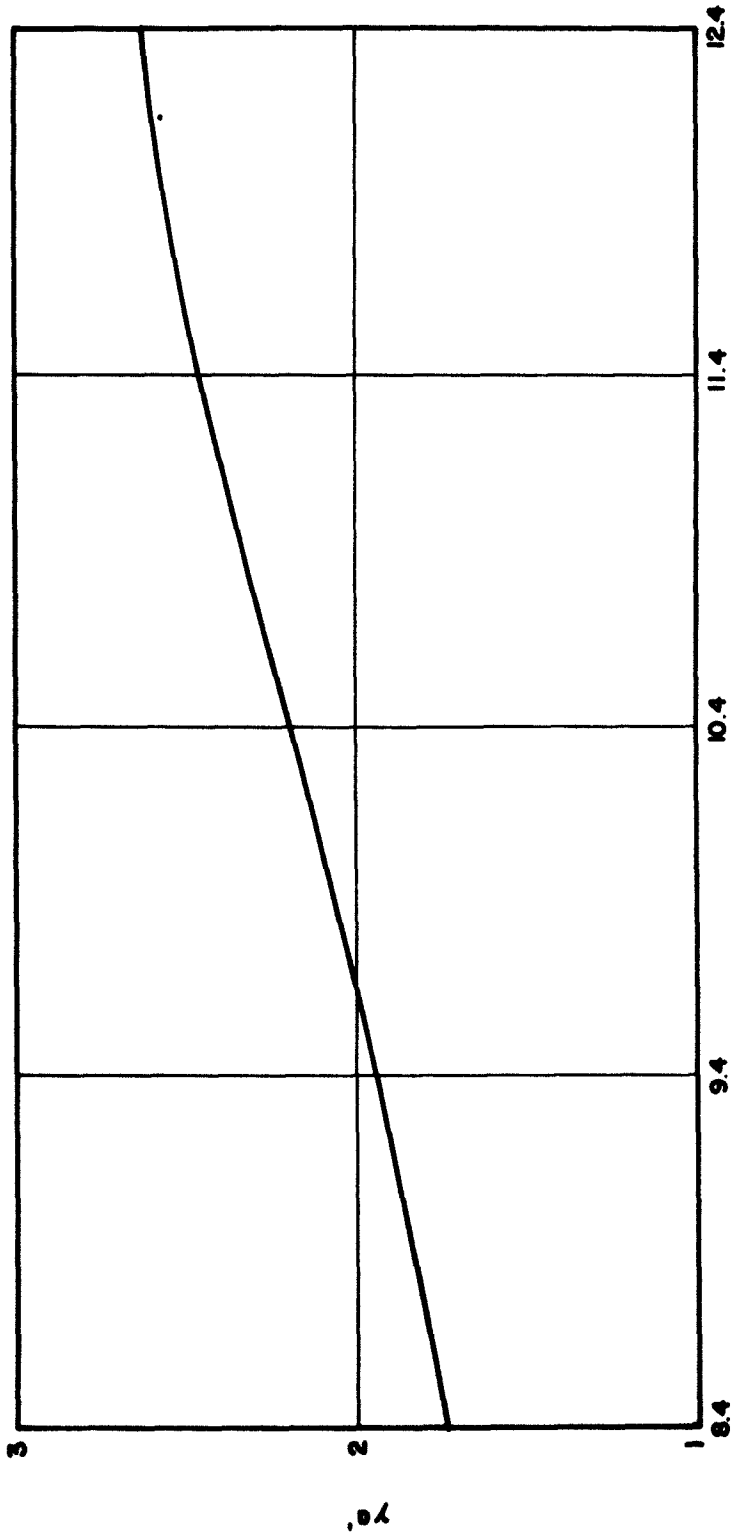

FIG. II.B.6 γ_a' VS. FREQUENCY.

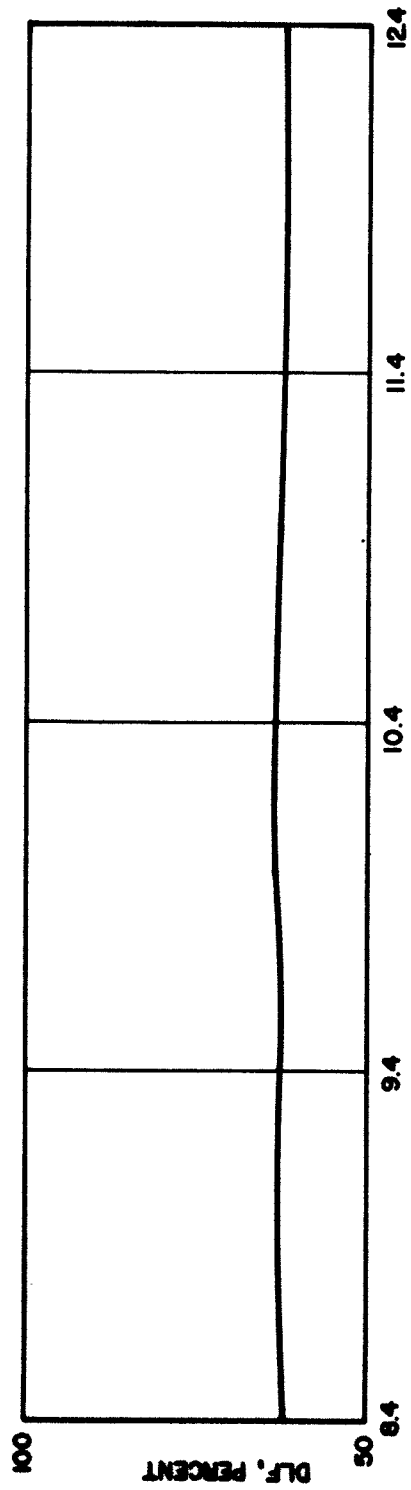

FIG. II.B.7 DIELECTRIC LOADING FACTOR, DLF, VS. FREQUENCY.

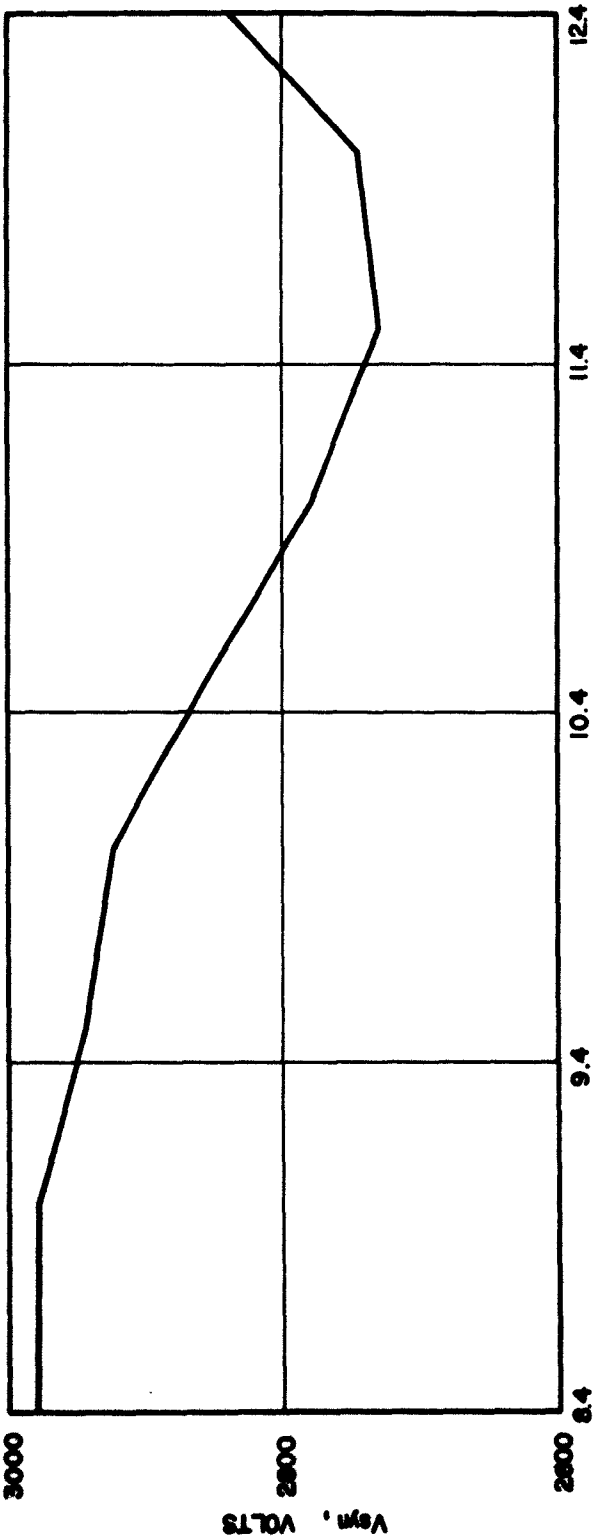

FIG. II.B.8 SYNCHRONOUS VOLTAGE VS. FREQUENCY.

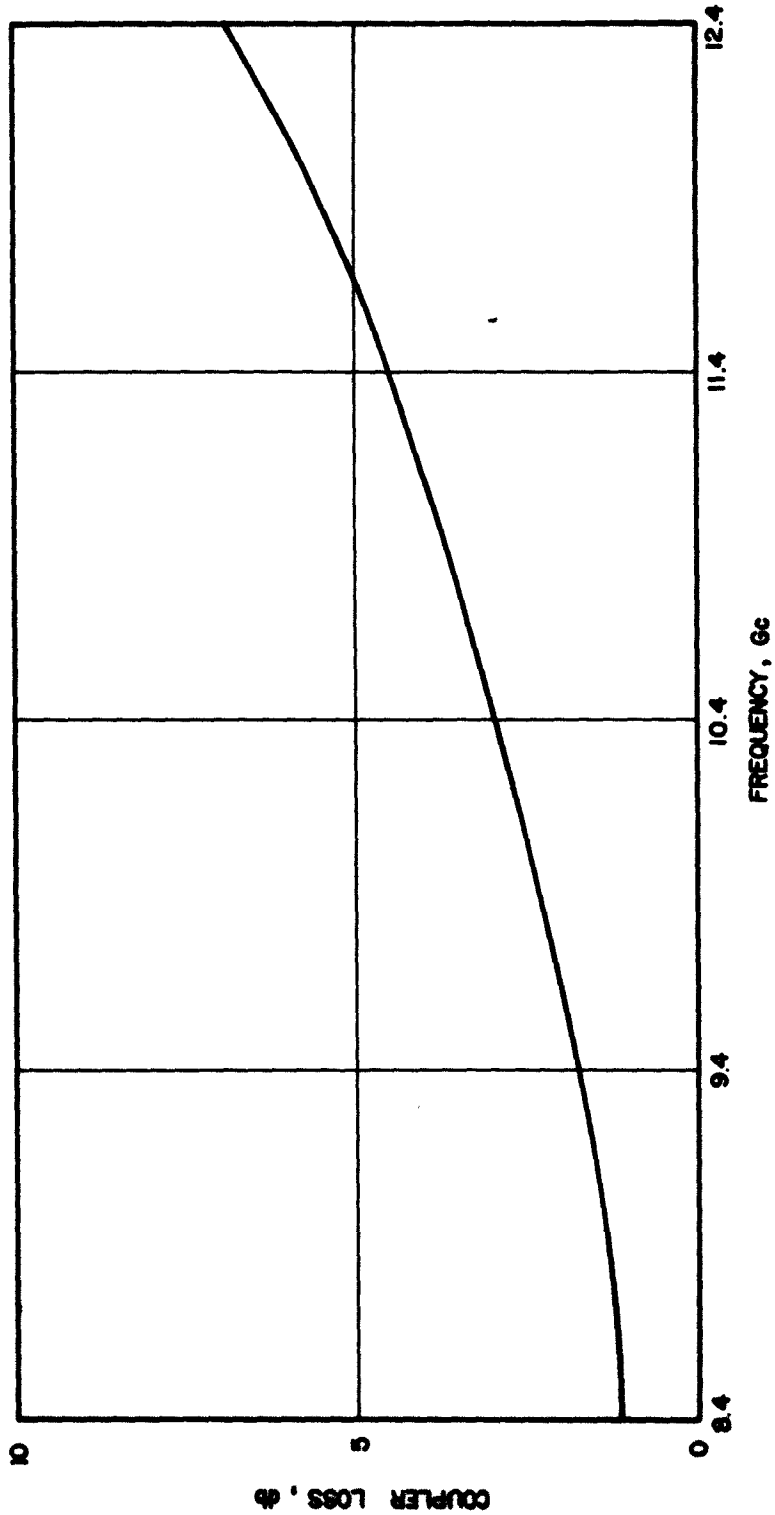

FIG. II.B.9 COUPLER LOSS VS. FREQUENCY.

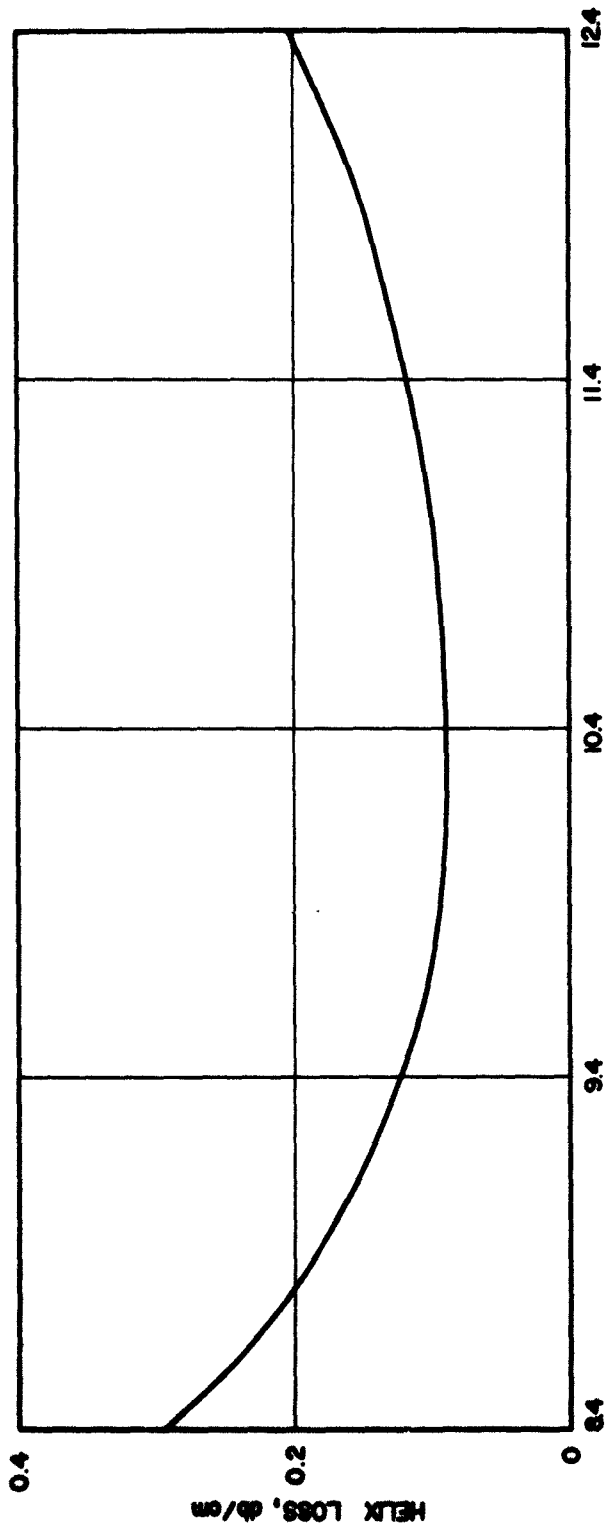

FIG. II.B.10 HELIX LOSS VS. FREQUENCY.

helix into the tube. Heat tests will be performed when samples are ready.

Recently, several BeO waveguide windows were received. They are, for the most part, free of flaws and have been successfully metallized on the edges for brazing into a holder. Testing is to take place during the next period.

C. Mathematical Investigation

The radial heat flow problem presented previously[1] has been programmed for numerical solution on a digital computer. The particular case analyzed is that of no inward heat loss from the helix, i.e.,

$$\frac{\partial T_1(r_1,t)}{\partial r} = 0 \quad . \qquad \text{(II.C.1)}$$

Numerical solution of this problem will be carried out shortly.

D. Conclusions

A technique has been developed for brazing a tungsten helix into beryllium oxide tubing. D-c heat tests of the brazed helix have shown it to have appreciably higher power handling capability than a pressure loaded helix and about 50 percent of that predicted by theoretical calculations. When more dimensionally-uniform fluted tubing is available, the problem of poor thermal contact should be overcome. Cold tests of the X-band helix mounted in BeO and the coupled-helix couplers revealed a satisfactory performance over most of the band. Recent shipments of smooth-bore beryllium oxide tubing and waveguide windows have shown a considerable improvement in quality. The evident advances in manufacturing

1. Boers, J. E., et al, "Applied Research in Microwave and Quantum Electronics", Interim Scientific Report No. 1, Electron Physics Laboratory, The University of Michigan, p. 12; August, 1962.

techniques are very encouraging and it is hoped that the desired BeO fluted tubing may be available soon.

E. Program for the Next Period

During the next period work will continue along the following lines:

1. Cold tests of the electrical properties of the brazed-helix structure will be carried out for the S-band fluted tubes and the X-band smooth-bore tubes. Additional work on the brazing technique will be done upon receipt of additional fluted tubes. Evaluation will be made of the properties of the helix embedded in plasma-sprayed BeO pending successful fabrication of this item.

2. Additional attempts will be made to surface metallize BeO tubes for vacuum tightness.

3. Tests will be performed on the BeO waveguide windows.

4. Numerical computation of the solution to the radial heat flow problem will take place.

III. LOW-NOISE INVESTIGATIONS

A. Analysis of Multivelocity Low-Noise Streams (G. Hok)

A.1 Introduction. Since the writing of the first interim report six months ago a technical report on "Noise Propagation in a Nonuniform Electron Gas" has been completed, which presents in more detail the work summarized in Section III.C of the first interim report as well as results of subsequent work in this area.

The study concerns the propagation of noise as compressional waves in an electron gas in various states of equilibrium or flow. The approach

employed here is to derive partial differential equations involving the first three moments of the velocity distribution from Boltzmann's transport equation, Poisson's equation and a postulate that the vibrations of the gas be adiabatic. Those solutions which satisfy the well known conditions for negligible Landau damping are accepted as physically significant; all other solutions are rejected, since Landau damping is dissipative and increases the entropy of the gas, contrary to the assumption of adiabatic variations.

A.2 Equilibrium Electron Gas. In the technical report closed-form solutions are obtained for plane compressional waves in a highly nonuniform electron gas in equilibrium between two infinite plane emitters. As a first step the set of differential equations for the perturbations of the stationary state are transformed to a pair of first-order linear differential equations analogous to those for a tapered transmission line or waveguide

$$\frac{\partial}{\partial z}\left(\frac{a_{11}}{a_{00}}\right) = \frac{\partial i_1}{\partial z} = -\frac{j\omega}{\sigma}\frac{1}{a_{00}}a_{12} \quad , \qquad \text{(III.A.1)}$$

$$\frac{\partial a_{12}}{\partial z} = -\frac{j\omega}{3\sigma}a_{00}\left(\frac{a_{11}}{a_{00}}\right) = -\frac{j\omega a_{00}}{3\sigma}i_1 \quad , \qquad \text{(III.A.2)}$$

where σ is the steady-state one-dimensional root-mean-square electron velocity and a_{00} is the steady-state number density (electrons per unit volume). The perturbations a_{11} and a_{12} represent the above mentioned velocity moments and are defined by

$$a_{1n} = \frac{1}{n!}\int_{-\infty}^{+\infty} H_n\left(\frac{u}{\sigma}\right)\rho_1(u)\,du \quad , \qquad \text{(III.A.3)}$$

where $H_n(x)$ is the nth Hermite polynomial and $\rho_1(u)$ is the perturbation of the distribution density function in velocity space.

By alternative elimination of one of the perturbation variables the following two second-order differential equations are obtained:

$$\frac{\partial^2 i_1}{\partial z^2} + \frac{\partial}{\partial z} \log a_{00} \frac{\partial i_1}{\partial z} + \frac{\omega^2}{3\sigma^2} i_1 = 0 \ , \qquad \text{(III.A.4)}$$

$$\frac{\partial^2 a_{12}}{\partial z^2} - \frac{\partial}{\partial z} \log a_{00} \frac{\partial a_{12}}{\partial z} + \frac{\omega^2}{3\sigma^2} a_{12} = 0 \ . \qquad \text{(III.A.5)}$$

The electron density a_{00} varies widely with z; the solutions of these equations will be different for different functions $a_{00} = a_{00}(z)$. The expression

$$a_{12} = A\sqrt{a_{00}} \exp (\pm j\gamma z) \qquad \text{(III.A.6)}$$

is easily shown to be the solution, if $b = (a_{00})^{-1/2}$ satisfies the equation

$$\frac{\partial^2 b}{\partial z^2} = -\left(\gamma^2 - \frac{\omega^2}{3\sigma^2}\right) b = -g^2 b \ , \qquad \text{(III.A.7)}$$

where g is a parameter independent of position, time and frequency.

The differential equations of the unperturbed state of the electron gas have the solution

$$a_{00} = Ag^2 [\sinh (gz + C)]^{-2} \ , \qquad \text{(III.A.8)}$$

where g and C are constants of integration determined by the boundary conditions at the emitting surfaces and A involves the emitter temperature and universal constants only.

From the last two members of Eq. III.A.7 the following relations may be derived by definition of a new parameter ω_c

$$\gamma^2 = \frac{\omega^2}{3\sigma^2} - g^2 = \frac{\omega^2}{3\sigma^2}\left(1 - \frac{\omega_c^2}{\omega^2}\right) , \qquad \text{(III.A.9)}$$

$$\omega_c^2 = 3\sigma^2 g^2 . \qquad \text{(III.A.10)}$$

Thus ω_c is a cutoff frequency quite analogous to the plasma resonance frequency in an electron plasma of uniform density. But its value depends not only on the electron density but also on the space derivatives of the density

$$g^2 = -\frac{1}{b}\frac{\partial^2 b}{\partial z^2} = \frac{1}{2}\frac{1}{a_{oo}}\frac{\partial^2 a_{oo}}{\partial z^2} - \frac{3}{4}\left(\frac{1}{a_{oo}}\frac{\partial a_{oo}}{\partial z}\right)^2 . \qquad \text{(III.A.11)}$$

Depending on the boundary conditions at the emitting surfaces three different alternatives are possible.

1. The density or its mathematical extrapolation beyond the emitting surfaces has a minimum at a finite distance from the emitters. Then

$$\omega_c^2 < 0 .$$

2. The extrapolation of the density has an asymptotic minimum at infinite distance. Then

$$\omega_c^2 = 0 .$$

No real cutoff frequency exists in these two alternatives. The phase velocity of the adiabatic wave solutions is ($\sqrt{3}\,\sigma$) or smaller. Consequently the Landau damping would be excessive and these solutions are not physically significant. The electron gas does not show any appreciable medium-like wave-propagating behavior under these conditions.

3. In the third alternative one of the emitters is so poor that it operates temperature limited at the equilibrium temperature. Then

$$\omega_c^2 > 0 \quad .$$

A plasma cutoff frequency exists and for a certain range of frequencies immediately above this frequency the phase velocity of the adiabatic solutions is large compared to the thermal electron velocities. The Landau damping is consequently small and these solutions describe adequately a medium-like wave propagation in the electron gas.

The conclusions are then that under the conditions described as alternative 1 and 2 above, the electric interaction between the electrons is incapable of producing any appreciable "organized motion" or "medium-like behavior"; in alternative 3, on the other hand, such behavior occurs, and despite the nonuniform density a uniform plasma resonance frequency and a uniform phase velocity exist throughout the gas.

A.3 Accelerated Electron Flow. A considerable amount of work has been devoted to the extension of the same analysis as applied in the preceding case to the electron flow in a space-charge-limited diode or electron gun. The electron velocity distribution is here no more Maxwellian; since it is reasonably stable, however, this circumstance may not be a serious roadblock. The expansion of the electron gas flowing through the gun is not everywhere reversible, i.e., not adiabatic, because of the irreversible sorting of the electrons at the potential minimum. The idea of postulating, as previously, an adiabatic perturbation on a steady state which is no longer of constant entropy does not seem reasonable. However, the fact that an equilibrium gas with a potential minimum has no medium-like behavior provides some intuitive basis for the assumption that the gas is in a completely random and incoherent

state at least up to the minimum. Beyond the minimum the steady expansion becomes at least to a limited extent reversible, so that an adiabatic perturbation may be used as a working hypothesis in the same way as previously, subject to the final test for small or large Landau damping.

Instead of the relation in Eq. III.A.3 for the velocity-moment variables the present case requires the form

$$a_{1n} = \frac{1}{n!} \int_{-\infty}^{+\infty} H_n\left(\frac{u-u_o}{\sigma}\right) \rho_1(u)\, du \quad , \tag{III.A.12}$$

where u_o and σ^2 are the mean and variance, respectively, of the unperturbed z-directed velocity distribution; they are both functions of z.

A number of transformations of the convection-current variable are required in order to obtain from the basic differential equations relationships closely analogous to Eqs. III.A.1-2 and III.A.4-5. Note in the latter pair that all coefficients are real, and that only the last coefficient in each depends on the frequency and this in a very simple manner.

The following transformations accomplish this purpose

$$i_1 = u_o a_{1o} + \sigma\, a_{11} \quad , \tag{III.A.13}$$

$$i_2 = \exp\left\{-\int \frac{j\omega u_o}{\Gamma}\, dz\right\} i_1 \quad , \tag{III.A.14}$$

$$i_2 = \frac{C_1}{u_o} \int \frac{u_o}{\Gamma}\, dz\, i_3 = Q i_3 \quad , \tag{III.A.15}$$

where

$$\Gamma = 3\sigma^2 - u_o^2 \tag{III.A.16}$$

and C_1 is a constant that may be chosen arbitrarily.

The differential equation for i_3 then is

$$\frac{\partial^2 i_3}{\partial z^2} + \frac{\partial}{\partial z} \log (Q^2 u_o \Gamma) \frac{\partial i_3}{\partial z} + \omega^2 \frac{3\sigma^2}{\Gamma^2} i_3 = 0 \quad . \qquad \text{(III.A.17)}$$

A change of the independent variable makes the last coefficient a constant; let

$$d\theta = \frac{\sqrt{3}\,\omega\sigma}{\Gamma} \, dz \qquad \text{(III.A.18)}$$

giving

$$\frac{\partial^2 i_3}{\partial \theta^2} + \frac{\partial}{\partial \theta} \log (Q^2 u_o \Gamma) \frac{\partial i_3}{\partial \theta} + i_3 = 0 \quad . \qquad \text{(III.A.19)}$$

Clearly the product $Q^2 u_o \Gamma$ corresponds to a_{oo} in the equilibrium case. We can consequently formulate a condition corresponding to Eq. III.A.11. If g^2 is independent of θ and z, closed form solutions analogous to Eq. III.A.6 exist; if g^2 in addition is positive, the electron stream has a plasma cutoff frequency and medium-like wave propagation with small Landau damping.

The properties of this parameter g^2 have not yet been investigated for nonequilibrium conditions. The highly transcendental unperturbed relationships suggest, however, that g^2 is not a constant. Most likely it is a slowly varying function, so that the true solution may piecewise be represented by solutions for constant g^2. Better approximations to continuous solutions may possibly be obtainable along similar lines to the well known WKB-method in quantum mechanics.

A.4 Conclusions. The conclusions given above at the end of Sections A.2 and A.3 may be summarized as follows:

In an electron gas in equilibrium no appreciable "organized motion" or "medium-like wave propagation" is possible, unless one of its boundaries

is an emitter operating strongly temperature limited. In the latter case, a constant "plasma resonance frequency" exists despite the widely varying electron density. In a frequency band immediately above this cutoff frequency propagation of compressional waves takes place with negligible attenuation.

The corresponding analysis of accelerated electron flow is in progress but has not yet yielded equally specific results.

A.5 Program for the Next Period. Equation III.A.19 will be studied further. Evaluation of a parameter g^2 analogous to the one given by Eq. III.A.11 will be attempted. Investigation will be carried out concerning approximate solutions in various regions and under various operating conditions of an electron gun in order to gain some insight into the propagation, transformation, growth or decay of noise waves originating in the hot region close to the cathode.

B. Low-Noise Microwave Tube Theory (C. P. Wen)

B.1 Density Function Analysis. During this period the density function noise analysis program was written and checked out on the IBM-7090 digital computer. The stepwise solution of the problem proceeds as follows:

a. Integration of a finite number of velocity classes from the potential minimum to the cathode for unit current input to each velocity class,

b. Application of the cathode boundary conditions to the density function to find the actual current associated with each velocity class,

c. Integration from the potential minimum to the anode,

d. Calculation of the noise quantities S, Λ, Π and Φ,

e. Calculation of noise figure from

$$F_{min.} = 1 + \frac{T_c}{T}\left[S(a,\zeta_j,\xi) - \Pi(a,\zeta_j,\xi)\right] .$$

The numerical work was completed assuming 15 velocity classes and no reduction of noise figure was observed. Examination of the equations revealed that this was due to a forced correlation among velocity classes leaving the potential minimum. Parts of the program are now being rewritten to eliminate this difficulty. Numerical results should be available in approximately one month.

B.2 Program for the Next Period. The density function calculations will be completed and the results compared with those of the Monte Carlo study. The design of an experimental vehicle to check the theoretical results is presently nearing completion and its construction will commence in the near future.

C. Traveling-Wave Maser Studies (G. I. Haddad)

C.1 Introduction. It is very desirable in the design of traveling-wave masers that one be able to predict closely the slowing factor of the slow-wave structure and the field configurations in it without having to resort to detailed measurements which can be very time consuming, especially at millimeter wavelengths. In order to achieve this a space-harmonic analysis which is applicable to several forms of dielectrically-loaded ladder lines, which are useful in traveling-wave maser applications, has been developed. Since this theoretical work and the extensive results that have been obtained from it will be included in detail in a technical report to be issued in the near future, a very brief summary is included here.

C.2 Space Harmonic Analysis of Dielectrically-Loaded Ladder Lines. The method of analysis employed here was originated by Fletcher[1] in connection with his work on the interdigital circuit. This method is employed here to study the effect of a dielectric, placed along the array of conductors forming the slow-wave circuit, on the dispersion characteristics and the field configuration. The results of such a study should prove very useful in the design of traveling-wave masers utilizing such structures as the Karp, Meander-line, Comb, and other structures containing arrays of conductors.

The detailed analysis and the approximations assumed will be discussed in detail in the technical report.

The effects of several dielectrics on the characteristics of the Karp-type slow-wave structure have been investigated in great detail and the results are now being tabulated. Materials with relative dielectric constants of 9 (ruby), 100 and 256 (rutile) have been considered since they have proven to be good maser materials.

Information on the following subjects can be learned from this analysis:

a. The slowing factor of the slow-wave structure can be obtained as a function of frequency over the entire passband. This is very important in designing a traveling-wave maser since the gain of such a device is directly proportional to the slowing factor. From this analysis one would be able to wisely use the active maser material to shape the ω-β diagram to his choice.

---

1. Fletcher, R. C., "A Broad-Band Interdigital Circuit for Use in Traveling-Wave Type Amplifiers", Proc. IRE, vol. 40, No. 8, pp. 951-958; August, 1952.

b. The input impedance to the structure can be calculated, which would give some guidance for developing better matches over a wide frequency range.

c. From a knowledge of the r-f field configuration in the structure, the filling factor and the polarization of the r-f fields can be determined. This would then give a guide as to the location of the isolating material and the orientation of the maser material in the Karp-type slow-wave structure in order to maximize the gain.

d. The characteristics of higher order passbands can be obtained from such an analysis. Operation in higher order passbands was suggested in Interim Scientific Report No. 1 for traveling-wave masers with signal frequencies higher than pump frequencies. This will also result in physically larger structures.

e. The characteristics of multiple ladder structures can be determined from such an analysis. Such multiple ladder structures, as suggested in Interim Scientific Report No. 1, should lead to larger structures and thus to a wider dynamic range in traveling-wave maser amplifiers.

C.3 Experimental Work. The effort that was directed toward the experimental work has mainly consisted of measuring the effect of different dielectric materials on the dispersion characteristics of the Karp-type slow-wave structures. These measurements were made at X-band for different configurations of ruby material placed at various positions in the structure. Measurements are now being performed on rutile and should be completed soon. These measurements are intended to check the validity of the above theory and thus are very essential.

The twelve-inch magnet has been set up and aligned and is ready for use. A platform around the magnet has been completed. It is hoped that more effort will be spent in the next period on the experimental program outlined in Interim Scientific Report No. 1.

C.4 Conclusions. The space-harmonic analysis of dielectrically-loaded Karp-type slow-wave structures should lead to improved design criteria of traveling-wave masers in any frequency range. The information that can be obtained from such an analysis has already been cited. Such information is highly useful in traveling-wave maser design.

C.5 Program for the Next Period. The program for the next period will consist of:

a. The completion of the theoretical and experimental investigations of dielectrically-loaded ladder lines and the writing of a technical report on this subject.

b. Proceeding with the experimental work as outlined in the previous interim scientific report.

IV. PLASMAS AND QUANTUM ELECTRONICS

A. Cerenkov Radiation Device (G. T. Konrad)

A.1 Introduction. The object of the work conducted under this phase of the program is to obtain coherent power in the millimeter- and submillimeter-wave regions. Initially it is planned to pass a bunched electron stream in the vicinity of a dielectric material such that $u_o > v_p$, where u_o is the electron velocity and v_p is the velocity of light in the dielectric medium. In order to obtain a substantial amount of coherent power in the millimeter-wave region the electron beam is bunched at X-band while the Cerenkov radiator to be employed is designed

to operate at a higher harmonic. The initial work is planned at a wavelength of 2 mm Hg.

A.2 Electron Gun. The gun to be used in this experiment is a conventional, convergent, solid beam gun operating at 100 kv. A final beam diameter of 0.6 mm Hg is desired in the interaction space. This will be achieved with a cathode current density of 0.5 amp/cm^2 and an area convergence ratio of 70:1. The design of the gun is quite straightforward except for the necessary electrode spacings capable of standing off 100 kv under cw conditions. It is expected that some field emission problems may exist in the gun causing localized heating on electrode surfaces and ultimate voltage breakdown. Provided the spacings are large enough it should be possible to overcome these difficulties by careful fabrication of parts and by observing good vacuum techniques. One other area where some problems are expected should be mentioned. Space-charge effects in this gun are quite small, whereas thermal velocities have a pronounced effect on broadening the electron beam. These problems will be worked out experimentally in the beam analyzer once the gun is constructed. At the present time a digital computer program similar to the one for crossed-field guns described in Section V.E of this report is used to finalize the design of the 100 kv gun.

A.3 Extended Interaction Buncher. In order to obtain a considerable amount of coherent millimeter-wave power by Cerenkov radiation it is necessary to bunch the electron beam. The bunching will be carried out at a substantially lower frequency than the millimeter-wave output in order to make use of high-power cw sources presently available. It is planned to do the first experiments at X-band. At the near-relativistic electron speeds (600 kv for the present) to be encountered here the

harmonic content of the bunched beam may be expected to be quite substantial.

It is desirable to have some flexibility in this experiment in choosing the optimum operating frequency, hence a broadband circuit for bunching the beam is necessary. At the same time, however, an efficient interaction is desirable. For these reasons an extended interaction buncher was chosen for this experiment. The circuit consists of a number of cavities coupled to each other inductively by holes in their common walls and is terminated by reflecting planes at each end. A photograph of a typical circuit section is shown in the lower part of Fig. IV.A.1. An end-section and a waveguide transition to the slow-wave circuit are also shown in this figure.

The ω-β diagram for this circuit was determined by means of the set-up shown in Fig. IV.A.2. Here coaxial input lines are used to loosely couple into the resonant section of the circuit. Figure IV.A.3 shows the ω-β diagram obtained experimentally. It may be seen that this circuit will operate in the first space-harmonic for this application. At a frequency of 10 Gc a synchronous voltage of 68.2 kv may be computed by use of the ω-β diagram if relativistic effects are taken into account.

The interaction impedance was measured by perturbation of the phase velocity on the structure by means of a sapphire rod. The result is shown in Fig. IV.A.4.

In order to couple r-f energy onto the structure a step-transition will be used. This transition affords an impedance match from RG-52/U waveguide to the coupled cavity circuit. To date a VSWR of less than 2:1 has been achieved over a bandwidth of 20 percent for a single transition. Further work is necessary to improve this match.

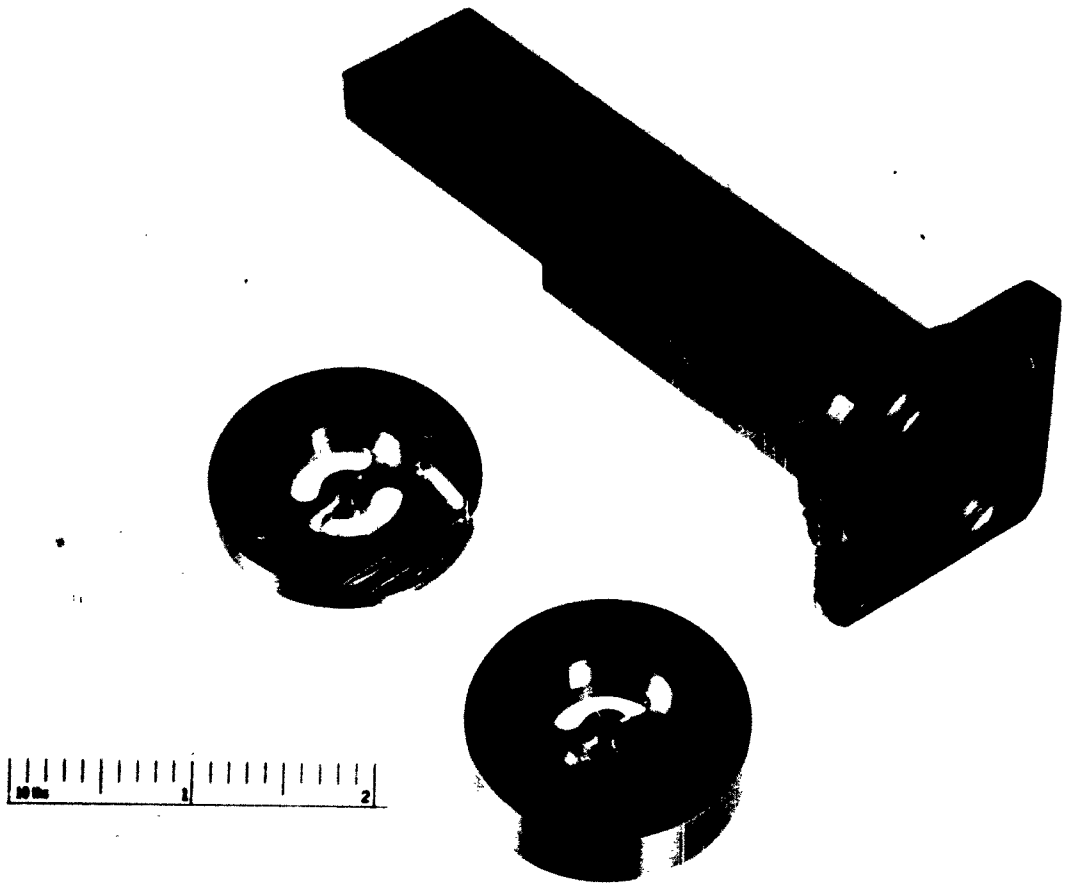

FIG. IV.A.1 BUNCHING CIRCUIT COMPONENTS.

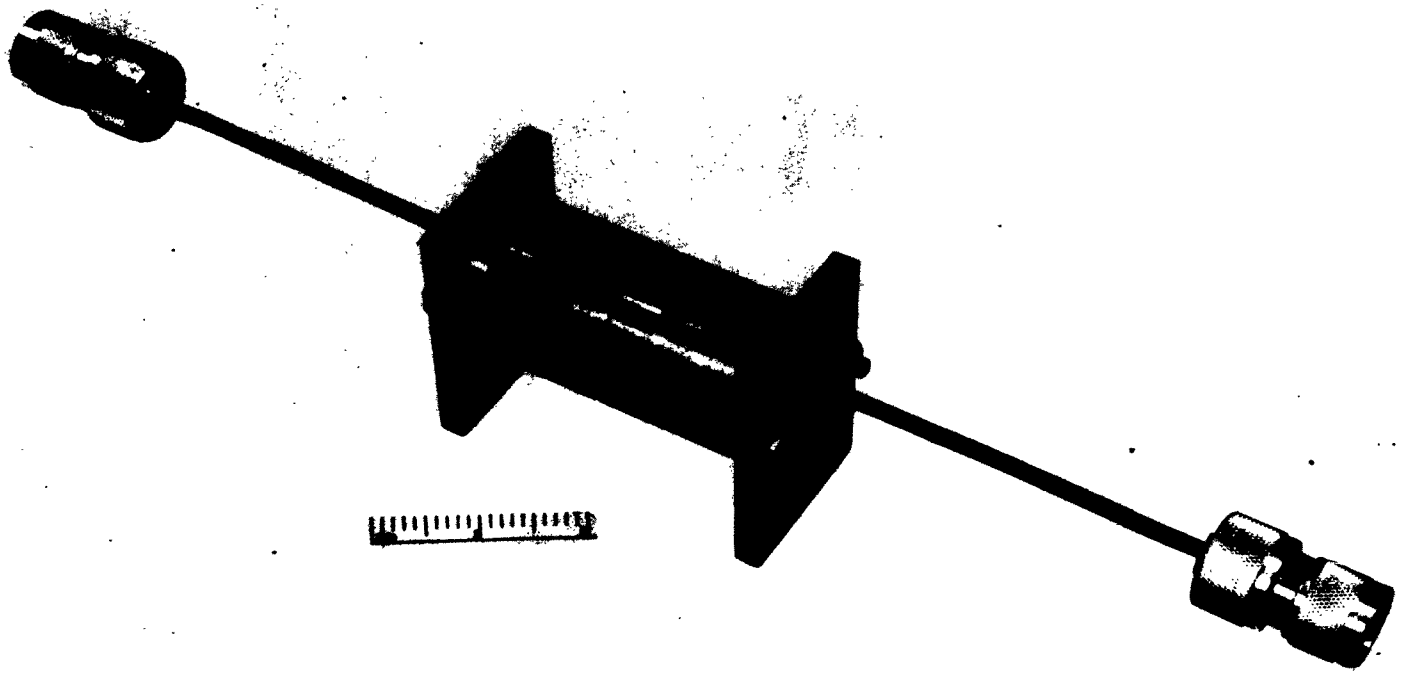

FIG. IV.A.2 RESONATING STRUCTURE FOR BUNCHER COLD TESTS.

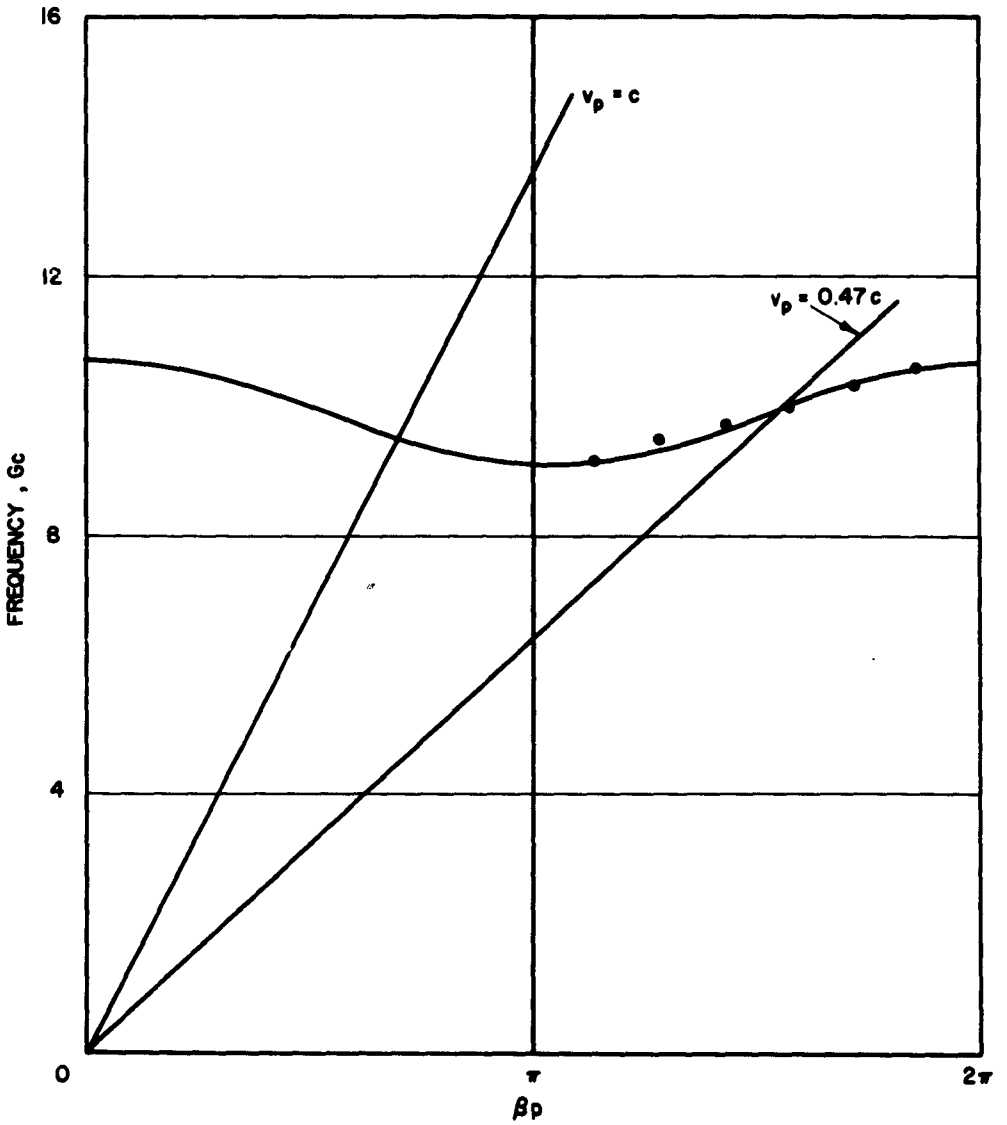

FIG. IV.A.3 ω-β DIAGRAM FOR THE X-BAND BUNCHING CIRCUIT. (p = 1.098 cm)

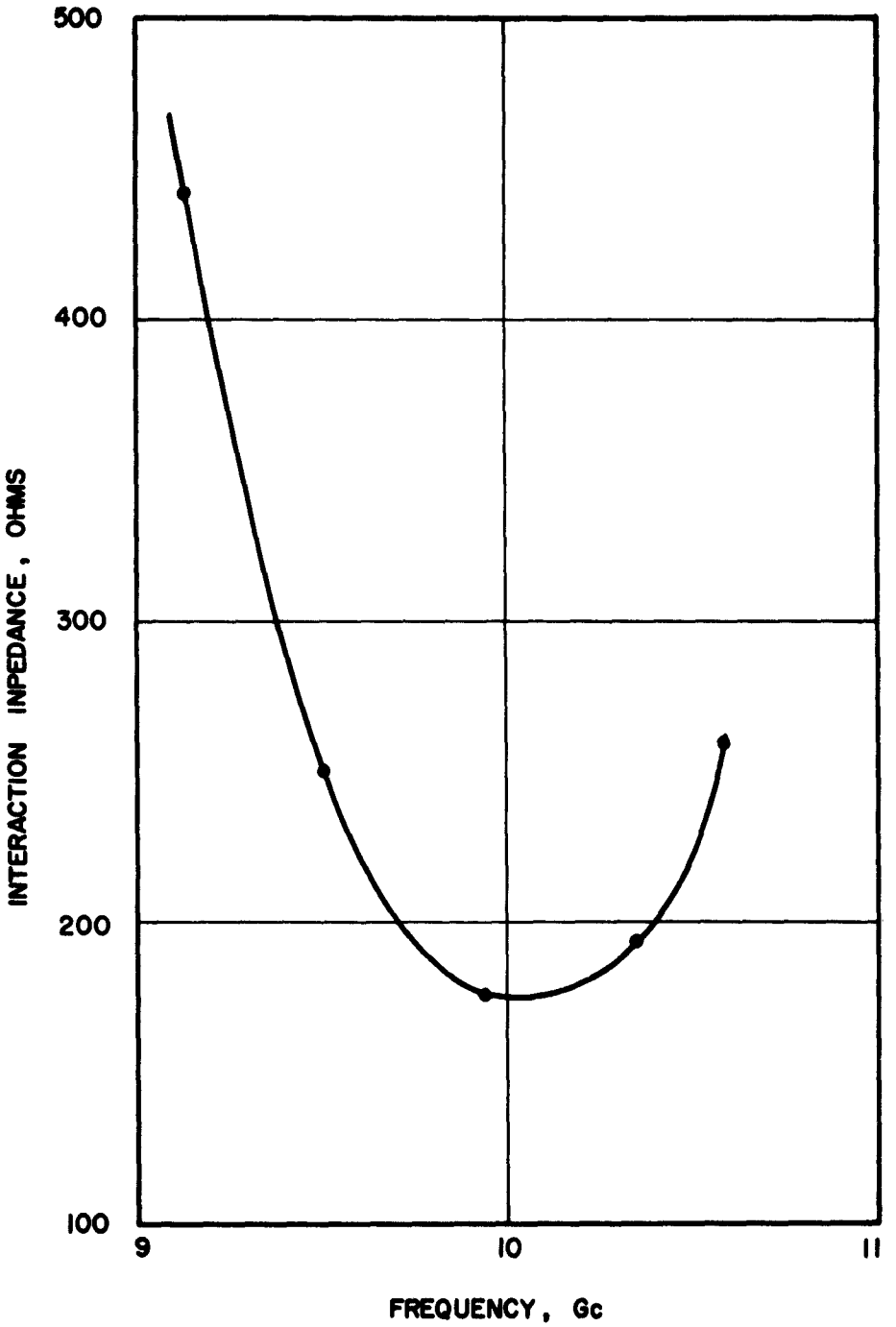

FIG. IV.A.4 INTERACTION IMPEDANCE OF THE X-BAND BUNCHING CIRCUIT.

A.4 Depressed Potential Operation. It will be advantageous to operate the device with a depressed potential collector in order to improve the overall efficiency. The spent electron beam will be collected at the gun anode potential, while in the Cerenkov coupler the beam potential will be raised to 600 kv. This technique affords of course another advantage. The high-voltage supply will have to be capable of yielding only a small fraction of the total beam current. This is a very important consideration from a cost standpoint.

A.5 Conclusions. The electrical design of the major components has been completed while the mechanical design is well under way. Cold tests on the extended interaction circuit indicate that X-band bunching will be possible over a frequency band of at least 20 percent.

A.6 Program for the Next Period. Further work will be done on the r-f transition to the buncher. The values of Q and insertion loss for the resonant circuit will be determined. The digital computer checkout of the electron gun will be completed and the gun will be constructed. Some tests will be made in the beam analyzer. The high-voltage bushing and the vacuum chamber will be constructed and tested. Since the high-voltage supply is available it will be possible to make high-voltage checks.

B. Millimeter Wave Plasma Oscillator (A. Singh)

B.1 Introduction. The objectives during this period have been as outlined at the end of the last period. Additional data was obtained on field emission into cesium vapor. Experimental studies were conducted on the effect of a conical intermediate electrode and a converging magnetic field, on the electron temperature and the plasma density in a gas discharge. Various features of the proposed experimental tube were examined

and a detailed design was prepared. The tube parts have been built and are now being assembled.

B.2 Stability of Field Emission into Cesium Vapor.

a. Effect of Vapor Pressure. Data on extremes of fluctuations of the type shown for a cesium vapor pressure of 2×10^{-6} mm Hg in Fig. IV.E.8 of Interim Scientific Report No. 1 were also taken at other values of vapor pressure. Interesting features were observed at 10^{-5} mm Hg, 10^{-3} mm Hg and 3×10^{-3} mm Hg, the curves for which are shown in Figs. IV.B.1 through 3.

The phenomenon is complex. Thus at 10^{-5} mm Hg, as the average emission current is raised, the oscillations gradually die out. They are not observed between 35 μa and 45 μa, but start again as the current is raised further. At 10^{-3} mm Hg, no oscillations are observed until the current rises to 45 μa, after which they gradually start. At 3×10^{-3} mm Hg, no oscillations were observed as such, except that the emission current was suddenly observed at a lower value of applied voltage, as the emission current rose above 25 μa.

It is presumed that ionization of Cs atoms plays an increasing role as the vapor pressure rises. The state of the emitting surface will be altered not only by the heating effect of high-density emission current, but also by the ionic bombardment of the surface.

At the higher vapor pressure, the negative corona discharge is an appropriate model to describe the phenomenon due to ions. Similar instabilities have been observed for the negative corona[1]. The main emphasis in the usual negative corona studies has however been on

1. Brown, S. C., Basic Data of Plasma Physics, The Technology Press, New York, pp. 271-272; 1959.

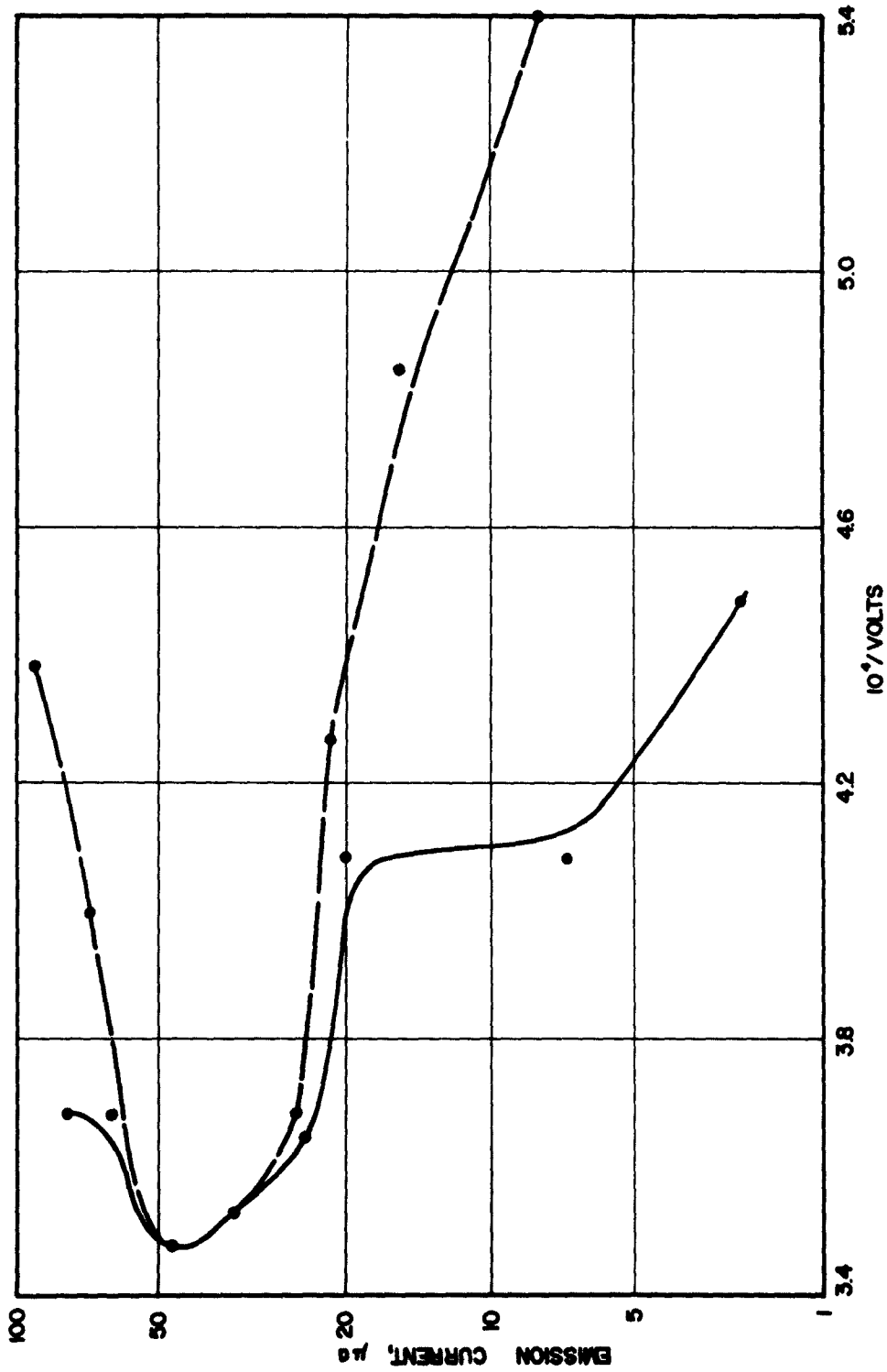

FIG. IV.B.1 EXTREMES OF INSTABILITY FOR FIELD EMISSION INTO Cs VAPOR AT 10^{-5} mm Hg.

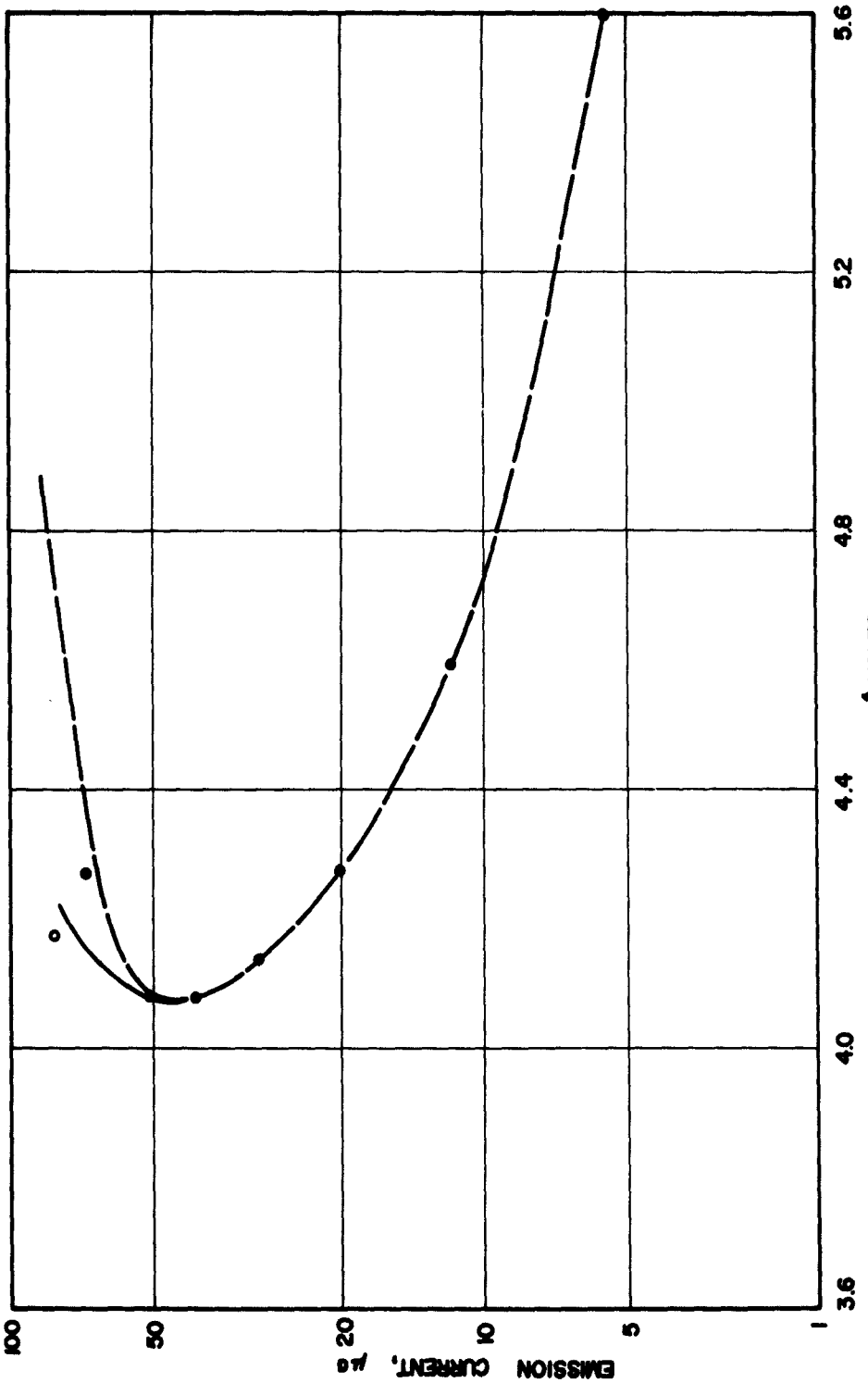

FIG. IV.B.2 EXTREMES OF INSTABILITY FOR FIELD EMISSION INTO Cs VAPOR AT 10^{-3} mm Hg.

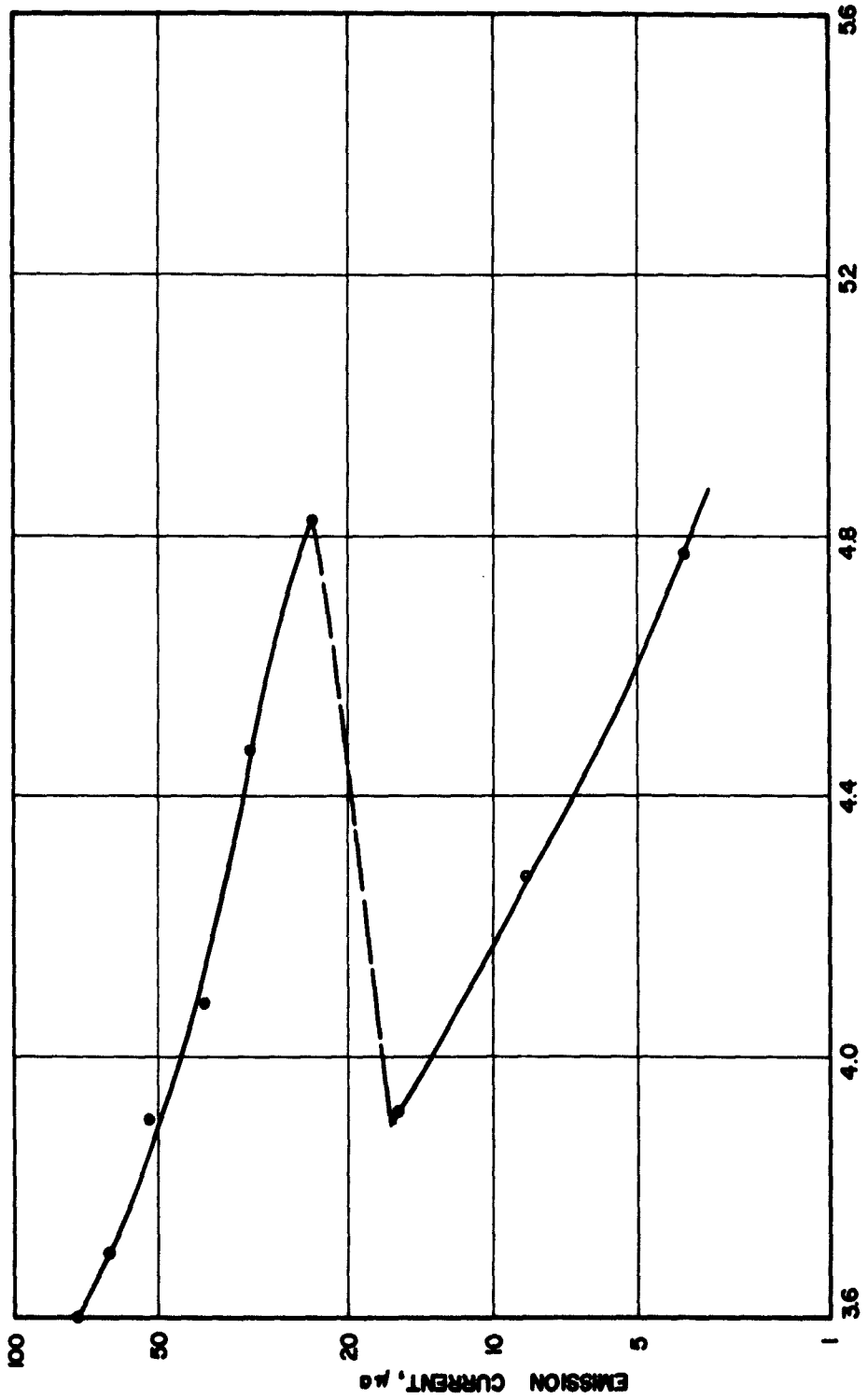

FIG. IV.B.3 EXTREMES OF INSTABILITY FOR FIELD EMISSION INTO Cs VAPOR AT 3×10^{-3} mm Hg.

photo-emission and secondary emission from the cathode, whereas here field-emission also plays a major role.

b. Effect of Heating the Field Emitter. It was also observed that the history of previous heating of the field emitter by means of the supporting loop affected the stability. Such a clean-up tended to reduce the emission and increase the stability. Data was also taken, keeping the loop hot, by passing various amounts of heater current while emission current was being drawn. This also tended to reduce the limits of fluctuation.

It was noticed that after the tube had been idle for a few weeks the leakage resistance became low, owing to the presence of a layer of cesium on the glass walls. It rose to the range of 500 megohms again, when the tube was heated up by heater tape.

Although the tube had not been originally designed for a study of possible r-f oscillations in the emission stream, an attempt was made to detect these with suitable modifications and appendages. The tube was covered with silver paint, except at leads for the emitter and the collector. A resistance of 680 kilo-ohms was introduced in series with the emitter, the former being shielded in a coaxial line. The fluctuations across the resistance were examined on an oscilloscope and a spectrum analyzer. The results of this preliminary experiment were negative.

B.3 Effect of Electrode Geometry and Magnetic Field on Plasma Density in a Gas Discharge. An important feature of the experimental tube proposed during the last period was an anticipated increase in plasma density by using a conical intermediate electrode between the anode and the hot cathode and a converging magnetic field. Two tubes to study these features were designed, built and tested. A schematic diagram of the second tube is shown in Fig. IV.B.4.

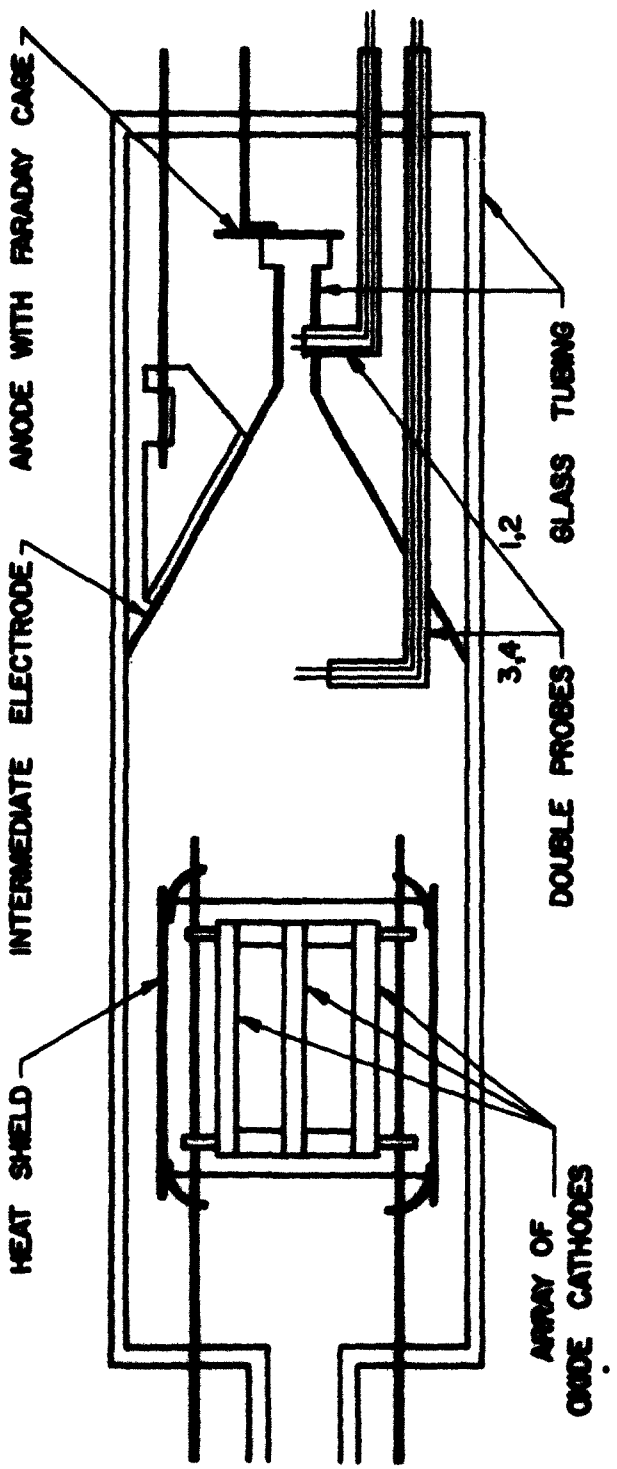

FIG. IV.B.4 SCHEMATIC DIAGRAM OF EXPERIMENTAL TUBE FOR STUDY OF PLASMA PARAMETERS.

Six oxide coated cathodes were arranged in a cylindrical array and were capable of yielding 120 ma in a vacuum environment. The array and heat shield are appropriate for a gas discharge tube, since the hidden faces of the cathode can also inject electrons into the plasma.

Langmuir probes were used for determination of plasma temperature and density. They consisted of tungsten wire of 0.0105 inch diameter, the length of the two pairs being 0.079 inch and 0.118 inch respectively.

The anode was provided with a Faraday cage to reduce the effects of secondary emission of electrons. The larger diameter of the cone was 1.97 inch and the smaller diameter was 0.150 inch.

After the tube was evacuated and baked, the cathodes were broken down and activated. Argon could be introduced up to a controllable pressure by leading off small quantities of the gas from a flask to the region between two stop-cocks, to be finally led into the manifold. Experiments were conducted in the range of pressure from 10 microns to 300 microns of mercury.

The intermediate electrode behaved like the grid in a thyratron. In order to start the discharge, it was momentarily touched to the anode. Afterwards it was left at floating potential for most measurements. If the potential was made more positive than the floating potential, the current drawn by the intermediate electrode rose rapidly. If it was made more negative, the current in the reverse direction rose to a saturation value. The discharge current to the anode was largely unaffected in this process.

When the discharge current flowing to the anode was varied by varying the series resistance connected externally, the anode potential

and floating potential of the intermediate electrode remained almost unchanged.

Double probe measurements were taken by plotting individual points as well as by photographing a trace on an oscilloscope. The former method gave accurate results. The latter, though less accurate, made it possible to survey the effect of a wide range of parameters. In particular, since the probe characteristic could be obtained very quickly, the discharge current could be raised to relatively high values for a few seconds at a time.

Figure IV.B.5 shows the variation of plasma density at the wide and narrow end of the cone as a function of discharge current for Argon at a pressure of 70 microns, with no applied magnetic field. The increase of density between the two locations by almost one order of magnitude is clearly seen. Also the density is seen to be nearly proportional to the discharge current. This curve is based on hand-plotted data.

Figure IV.B.6 shows the effect of variation of pressure and magnetic field on the plasma density at the throat of the cone. This is based on photographic traces. The accuracy, though not as good as in the previous case, was sufficient to indicate the following general trends:

1. The plasma density is further increased by about an order of magnitude by the application of the converging magnetic field.

2. As magnetic field is increased, the plasma density tends to saturate. This happens at lower values of magnetic field for lower pressures.

3. At a magnetic field strength above 500 gauss, the density in general decreases with increase of pressure. At zero magnetic field the

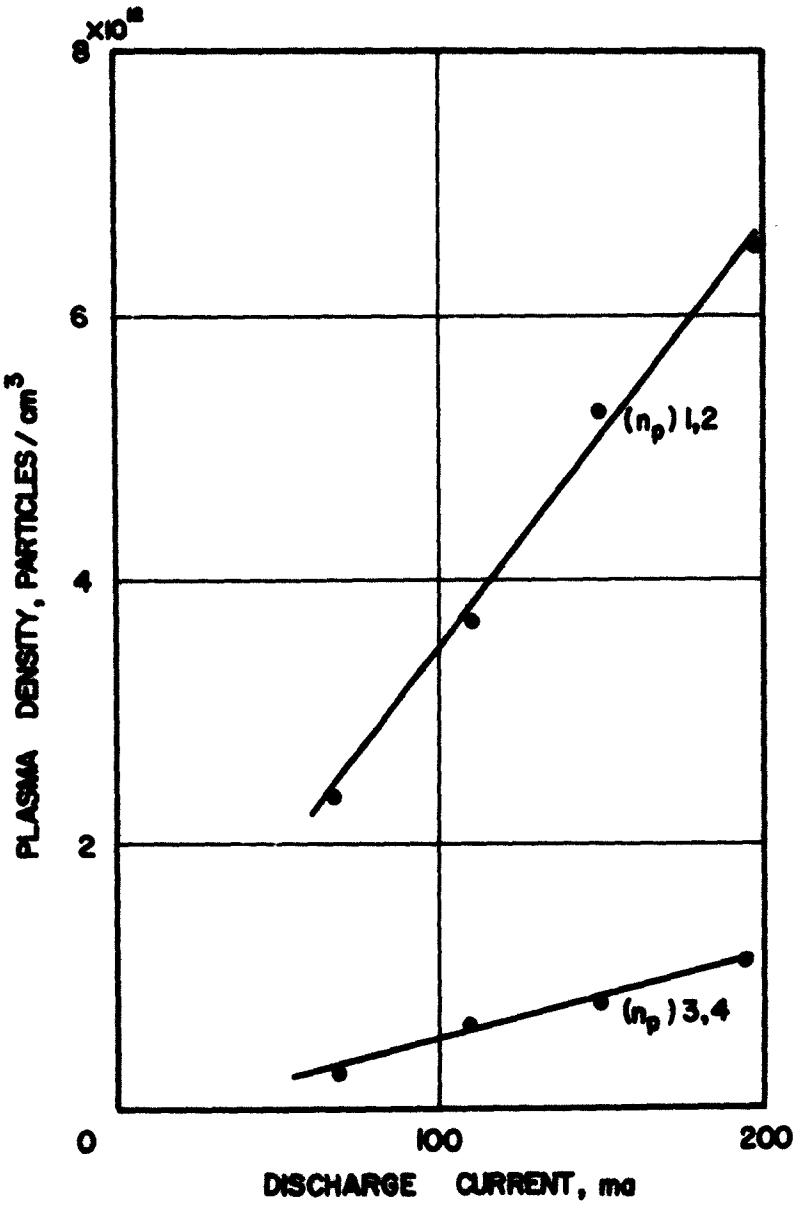

FIG. IV.B.5 VARIATION OF ION DENSITY WITH DISCHARGE CURRENT.

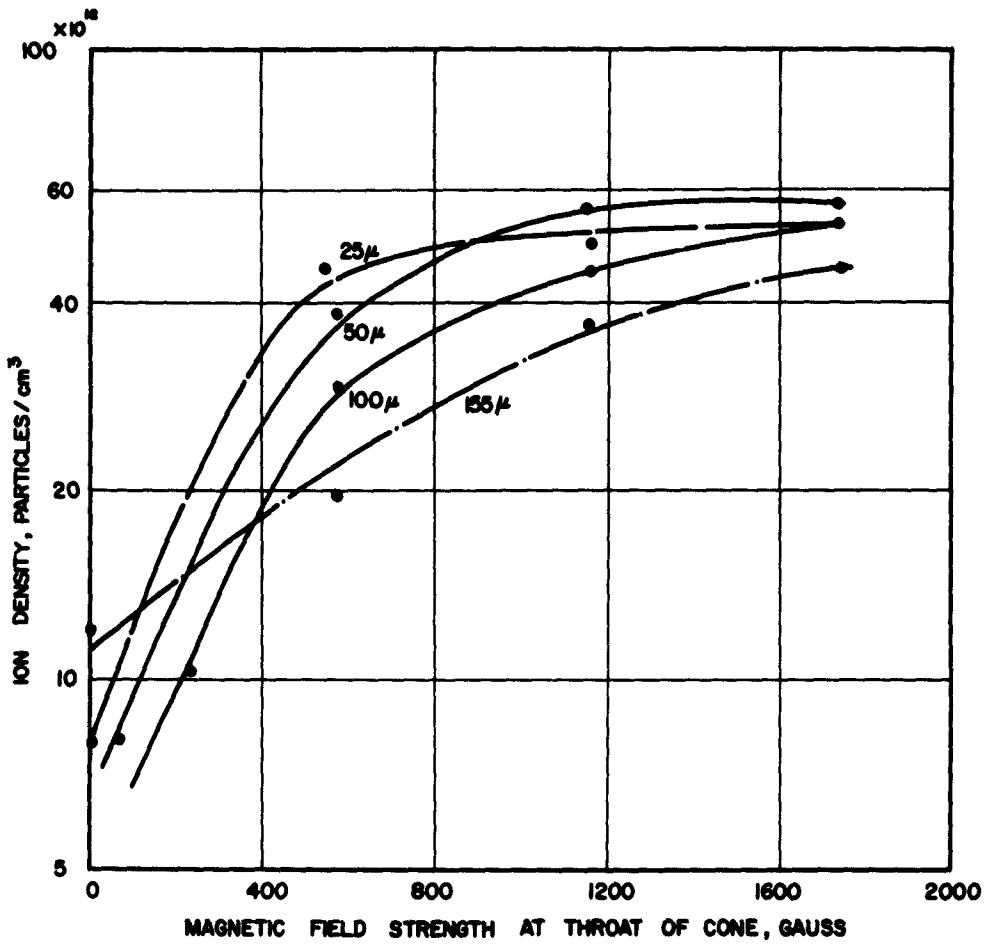

FIG. IV.B.6 VARIATION OF ION DENSITY WITH MAGNETIC FIELD.

trend appears to be reversed, although the data is insufficient at present to confirm this. Further data is being taken.

The data on electron temperature exhibits the trend that this parameter increases with decreasing pressure and is comparatively insensitive to current and magnetic field variations.

B.4 Design Considerations for the Experimental Millimeter-Wave Device. Detailed consideration was given to the various aspects of the device whose basic features were discussed in Interim Scientific Report No. 1. The salient points are given below.

a. Coupling Methods. Along with the basic features of the experimental tube, reported in Interim Scientific Report No. 1, a direct coupling to a cavity resonator was contemplated.

It was considered worthwhile to explore the possibility of using a dielectric-tube resonator for coupling power out of the beam-plasma system. In this case, depending upon the choice of dielectric constant and dimensions of the tube, the phase velocity of the electromagnetic wave can be made to synchronize with the electron beam velocity. This has been done for relativistic electron beams[2], using materials such as teflon, with a dielectric constant of 2.08. The minimum ratio of phase velocity achieved, to velocity of light in vacuum, is $1/\sqrt{\epsilon_2}$, where ϵ_2 is the dielectric constant. Obviously, if comparatively low accelerating voltage is desired, high values of ϵ_2 have to be explored. With this in view, sapphire (Al_2O_3) and titania (TiO_2) were considered. In both these materials, the dielectric constant depends upon the orientation

2. Becker, R. C., and Coleman, P. D., "The Dielectric Tube Resonator, a Device for the Generation and Measurement of Millimeter and Sub-Millimeter Waves", Proc. of Symp. on Millimeter Wave, Polytechnic Institute of Brooklyn, Polytechnic Press, pp. 191-222; 1960.

chosen, with respect to the optical axis. For the sake of symmetry it would be best to make the optical axis parallel to the axis of the tube. Since the electric field is primarily parallel to the axis inside the dielectric material, a simple approach to the initial design of the resonator would be to take a value of dielectric constant close to the one corresponding to the optical axis. Thus an effective dielectric constant of 8.5 was chosen for sapphire and 100 for titania.

Design of a dielectric tube resonator essentially involves numerical solution of a boundary value problem. Given the value of the dielectric constant ϵ_2 and the ratio v_p/c_o, of phase velocity to velocity of light in vacuum, design curves can be computed. These give the relationship between a/λ_o and b/λ_o for different possible modes, where a and b are the inner and outer radii of the tube, respectively, and λ_o is the wavelength in free space. Becker and Coleman's paper gives these curves for $\epsilon_2 = 2.08$ and $v_p/c_o = 0.80$.

A computer program was set up so that these design curves could be obtained for other values of ϵ_2 and v_p/c_o. These are shown for $\epsilon_2 = 8.50$, $v_p/c_o = 0.40$, and $\epsilon_2 = 100$, $v_p/c_o = 0.15$, in Figs. IV.B.7 and IV.B.8 respectively.

Assuming $\lambda_o = 8$ mm Hg, and choosing the mode group TM_{01n} where n represents the number of half wavelengths along the tube, the dimensions of the resonators for different cases are as shown in Table IV.B.1. Here L represents the length of the tube.

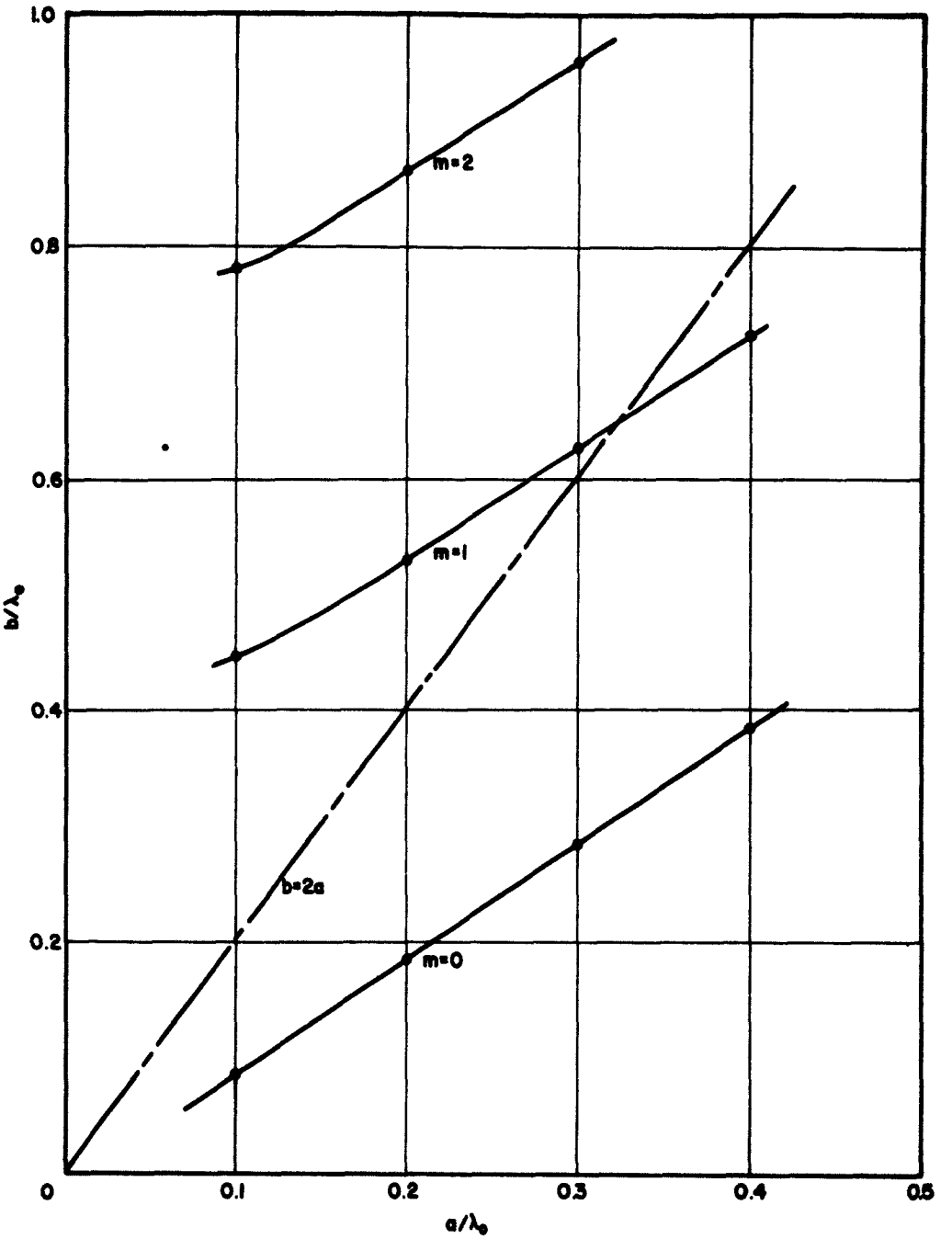

FIG. IV.B.7 DESIGN CURVES FOR DIELECTRIC TUBE RESONATOR, $\epsilon_2 = 8.50$, $v_p/c_o = 0.40$.

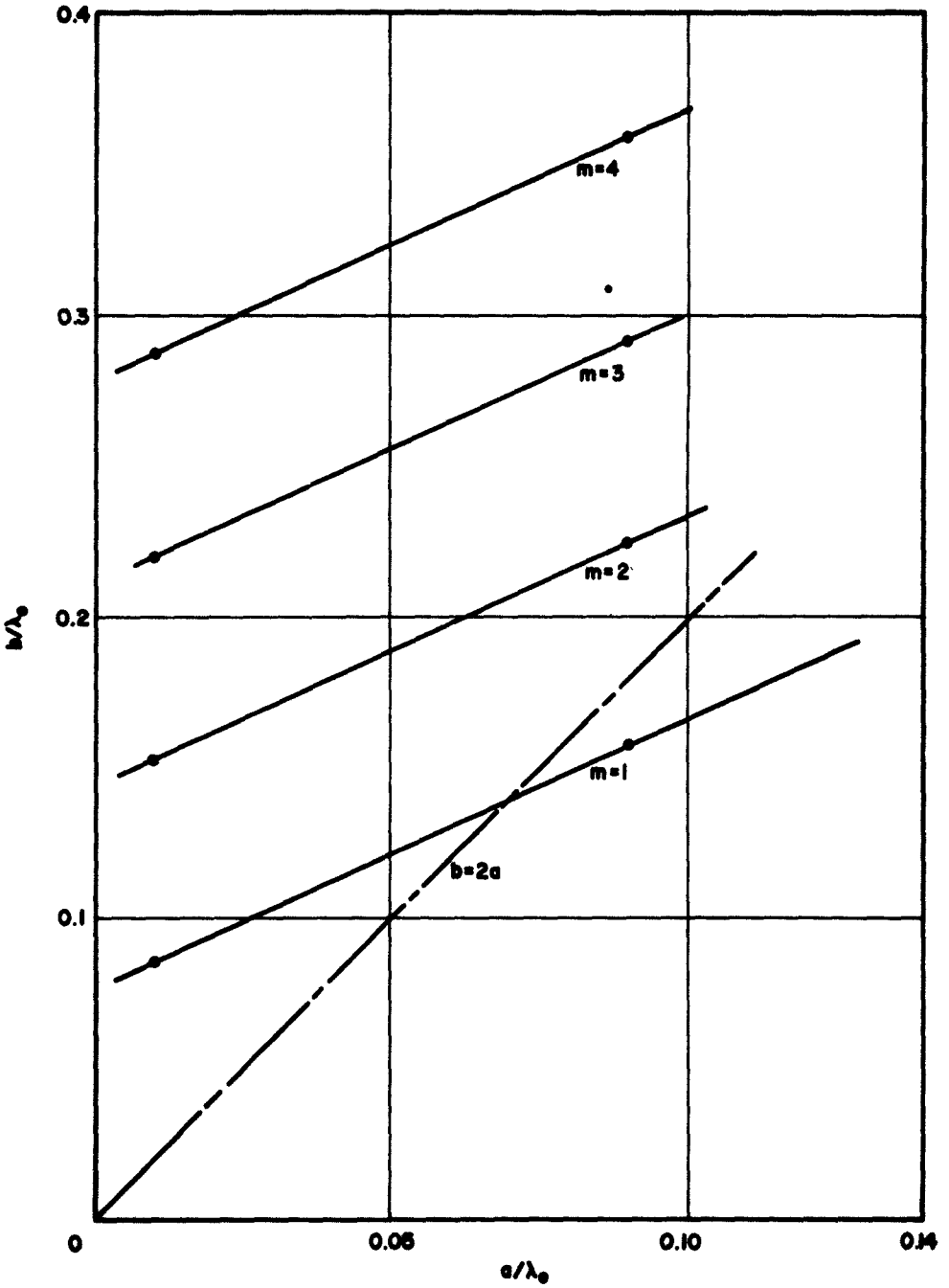

FIG. IV.B.8 DESIGN CURVES FOR DIELECTRIC TUBE RESONATOR, $\epsilon_2 = 100$, $v_p/c_0 = 0.15$.

Table IV.B.1

Dimensions of Dielectric Tube Resonator for TM_{01n} Mode

with λ_o = 8 mm Hg

Material	ϵ_2	v_p/c_o	Accelerating Potential in kv	a in cm	b in cm	n	L in cm
Sapphire	8.50	0.40	4.7	0.260	0.520	8	1.28
Rutile	100	0.15	5.8	0.056	0.112	8	0.480
Rutile	100	0.15	5.8	0.103	0.154	16	0.960

b. Amplification Per Unit Length. Before deciding on the final choice, it is advisable to consider the gain to be expected in a beam-plasma interaction for the various conditions. The estimation was based on the analysis given by Bogdanov[3] et al. The amplification per unit length is expressed as

$$\xi = 8.69\, \gamma_{pe}\, q \quad , \qquad \text{(IV.B.1)}$$

where $\gamma_{pe} = \omega_{pe}/v_e$ is the plasma wave number of the electron stream and q is a gain parameter. This parameter is a function of $(\omega_p^2/\omega^2 - 1)$ and $\gamma_e\, a_e$, where ω_p is the plasma radian frequency, γ_e is the electron wave number, and a_e is the radius of the electron beam. The analysis is strictly valid only for a beam in a plasma of infinite extent. In general the value of the gain parameter q is high for small values of $((\omega_p/\omega)^2 - 1)$ and large values of $\gamma_e\, a_e$. This means that the plasma frequency should be a little higher than the operating frequency and for a given beam diameter, a slower beam would give greater amplification per

3. Bogdanov, E. V., Kislov, V. J., Tchernov, F. S., "Interaction Between an Electron Stream and Plasma", Proc. of Symp. on Millimeter Waves, Polytechnic Press, pp. 57-71; 1960.

unit length. However, for larger values of $\gamma_e a_e$, the q vs. $[(\omega_p/\omega)^2 - 1]$ curve is more sharply peaked than for smaller values of $\gamma_e a_e$, so that the plasma density would need to be more closely controlled for a given operating frequency.

All in all, the desideratum of larger gain per unit length also leads to the desirability of smaller v_p/c_o, and thus of a larger ϵ_2 for the dielectric material.

A gain calculation for reasonable parameters associated with a titania resonator gives the following figures. Assume

$$\frac{v_p}{c_o} = 0.15 \quad , \quad a_e = 0.005 \text{ cm} \quad , \quad \lambda_o = 0.8 \text{ cm} \quad ,$$

$$\left[\left(\frac{\omega_p}{\omega} \right)^2 - 1 \right] = 0.1$$

and beam current = 20 ma. Then $\omega_p = 1.05\ \omega = 2\pi \times 39.5 \times 10^9$ rad/sec, the required plasma particle density = 1.93×10^{13}/cc, the plasma frequency for the beam electrons = 6.5×10^8/sec, q = 1.25, $\gamma_{pe} = 0.907$, and ξ = 10 db/cm. This is a reasonable figure to start with.

Taking reasonable parameters for sapphire, one changes v_p/c_o to 0.40 keeping all other parameters the same, the plasma frequency for the electron beam = 4.0×10^8/sec $\gamma_{pe} = 0.209$, and ξ = 0.64 db/cm. Thus for the range of parameters chosen, it is more attractive to try a titania tube resonator first.

c. Detailed Design. A detailed design was worked out with the following features as shown in Fig. IV.B.9.

1. The unit is demountable.

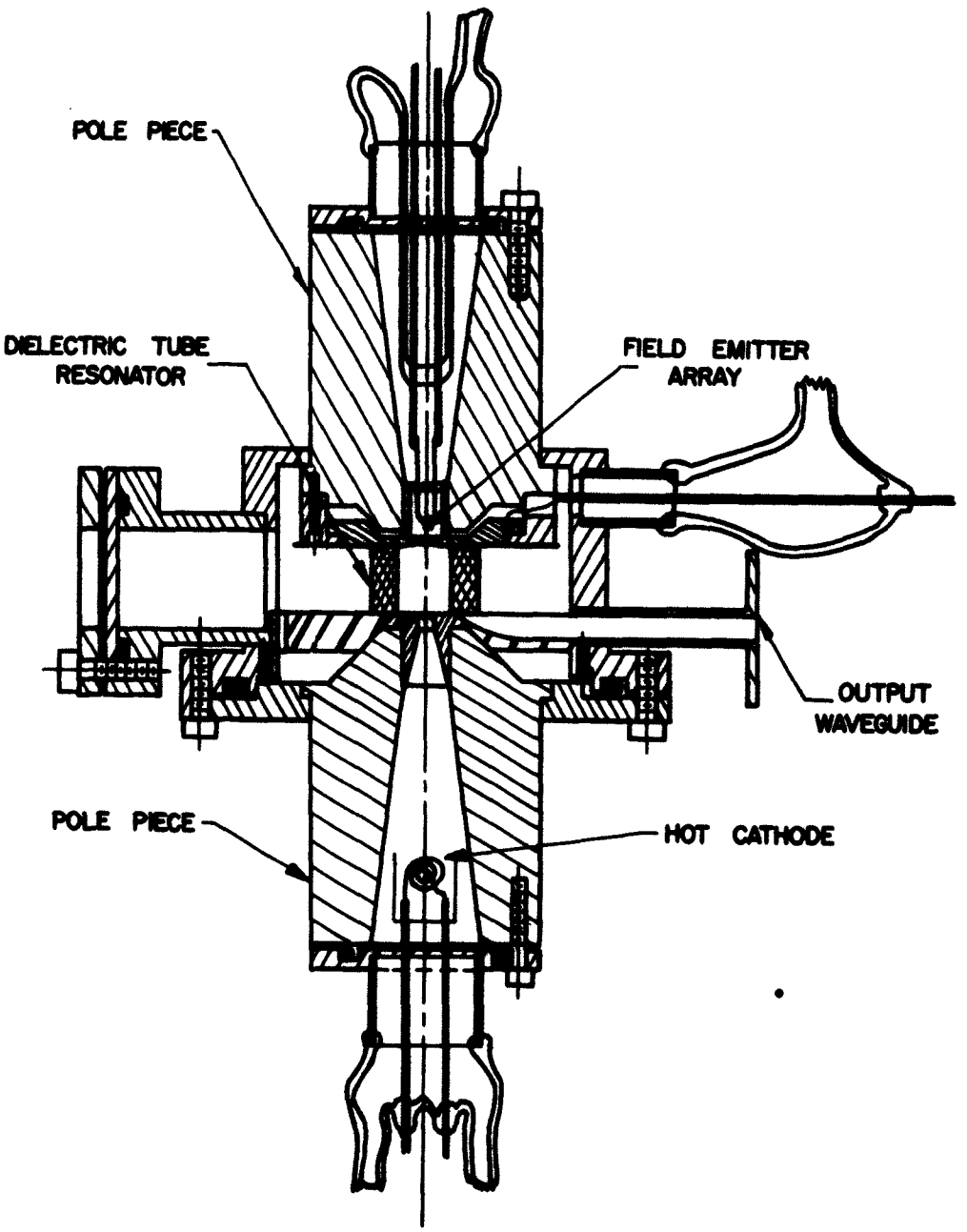

FIG. IV.B.9 ASSEMBLY DRAWING FOR EXPERIMENTAL MILLIMETER WAVE PLASMA OSCILLATOR.

2. An inner subassembly can be inserted which has either a dielectric-tube resonator or a cavity resonator coupled to the outside through a waveguide. Alternatively, in the same place, another assembly can be put for plasma diagnostic purposes.

3. A side window is provided for viewing or supporting the auxiliary structures needed for diagnostics.

4. The two cathodes on the opposite sides, one for generating the plasma and the other for the beam, can be removed and replaced.

5. The pole pieces are designed to fit into an existing electro-magnet and thus provide a field strength of up to 8,000 gauss in the interaction space. The pole tips were designed by using an electrolytic tank as analog. Variation of field in the longitudinal as well as transverse direction was studied in the analog as well as with finished pole pieces.

6. Suitable mechanical details were arranged for holding opposite sides of the dielectric tube resonator, and applying different potentials to them, while making it possible to couple to the resonator by means of a waveguide.

The detailed drawings of the parts were made, and almost all the parts have been fabricated already. The jigs and fixtures needed for assembly have been designed and made. The tube is now being assembled.

B.5 Conclusions. Different types of instability were observed in field emission into cesium vapor. It was in general reduced by keeping the field emitter hot.

The plasma density in a gas discharge was increased by nearly two orders of magnitude by introducing a conical intermediate electrode and a converging magnetic field. The effects of different parameters were studied.

The experimental millimeter-wave plasma oscillator was designed and partially assembled. Much of the information gained on the initial experiments will be useful in the successful operation of the device.

B.6 Program for the Next Period. Further data on the experimental tube will be taken. The assembly of the plasma oscillator is expected to be completed and tests on it will be undertaken.

C. Microwave Plasma Amplifier (R. J. Lomax and C. Yeh)

C.1 Experimental Plasma Tube. In order to gain some experience as a first step toward the design of an electron beam-plasma amplifier, the experimental tube described in the first interim report was constructed. This consisted of a glass tube 32 mm in diameter containing two flat spiral tungsten filaments. About half of the tube was enclosed by a brass water jacket fastened to the glass tube with Thermicon, a high thermal conductivity cement. After baking out the tube, cesium was introduced by internally breaking the tip of a small glass ampule previously sealed onto the tube. The cesium had to be kept outside the oven during baking by putting a long stem on the ampule to prevent chemical interaction with the glass at the baking temperature of 400°C.

Previous experience had shown that condensation of cesium on the electrode lead out wires could cause short circuits and consequently these leads were covered with glass all the way from the base to near the electrodes. In order to make electron temperature and density measurements, a probe was inserted halfway along the side of the tube.

The completed tube after admission of the cesium and removal from the vacuum pump was mounted coaxially in a cylindrical traveling-wave tube magnet which is capable of producing a field of up to 750 gauss. The glass envelope was cooled by blowing air between the tube and the magnet

wall. The water jacket cools only that part of the tube remote from the filaments, however, the temperature of this region is somewhat lower than the region cooled by air alone and therefore is dominant in controlling the vapor pressure. Since the cesium tends to condense in this coolest region, the tube was mounted vertically with the water jacket downwards. The relatively long glass-insulated leads passing through this region afford a long leakage path for any cesium which may condense.

C.2 Method of Measurement. The tungsten filaments were directly heated, consequently it was necessary to avoid spurious plasma currents which flow when a voltage is applied to heat the filaments. This was achieved by using unsmoothed half-wave rectified 60 cps alternating current and confining measurements to the half cycle in which no current flows. Separate isolated heater supplies were provided in case it was desired to apply a potential difference between the electrodes at the two ends of the tube.

As soon as the tube was baked out, but before the cesium was introduced, the temperature/current characteristic of each filament was measured with an optical pyrometer making due allowance for the change in emissivity of the tungsten with temperature. Using these results, the temperature of the filaments could be determined subsequently from the filament current. The temperature characteristic must be taken at an early stage because evaporation of tungsten and condensation of cesium considerably reduce the light transmission of the glass after a short period of operation, and in any case, once the tube was mounted in the magnet, it was not possible to see it easily.

The tube was set up in the magnet and a variable power supply connected to the probe, but while preliminary adjustments were being made and

before any quantitive information had been obtained the tube failed. This was due to a crack which appeared in the probe region and was thought possibly to be due to the probe having been heated excessively by electron bombardment when it was positive with respect to the plasma. As a result of this experience, it was decided to make changes in the design of the tube and in the method of measurement.

The new tube is shown in Fig. IV.C.1. The envelope is increased in diameter in the plasma region to increase the separation between the hot filaments and the glass and in addition the probes are made of a heavier material. An initial attempt to bring the probes out through the side of the tube was abandoned in favor of bringing glass insulated probes out through the tube base--a method which proved to be mechanically sounder.

In order to reduce the power dissipation at the probe, it was decided to use a pulsed power supply rather than a d-c supply. To achieve this, the pulse generator, the circuit of which is shown in Fig. IV.C.2a, was designed. This gives a pulse of variable amplitude up to 300 volts and of variable length centered in the period when no filament current flows. In order to ensure automatic synchronization of the pulse, it is generated by shaping and amplifying the 60 cps line supply used for the filaments.

The measurement of the pulse current/voltage characteristic is made using the circuit of Fig. IV.C.2b. Unfortunately, when the double probe was tested after completion of the tube, it was found that an internal short circuit had developed which necessitated the use of the probe as a single probe. The current is measured by passing it through a small resistor and measuring the voltage dropped across the resistor.

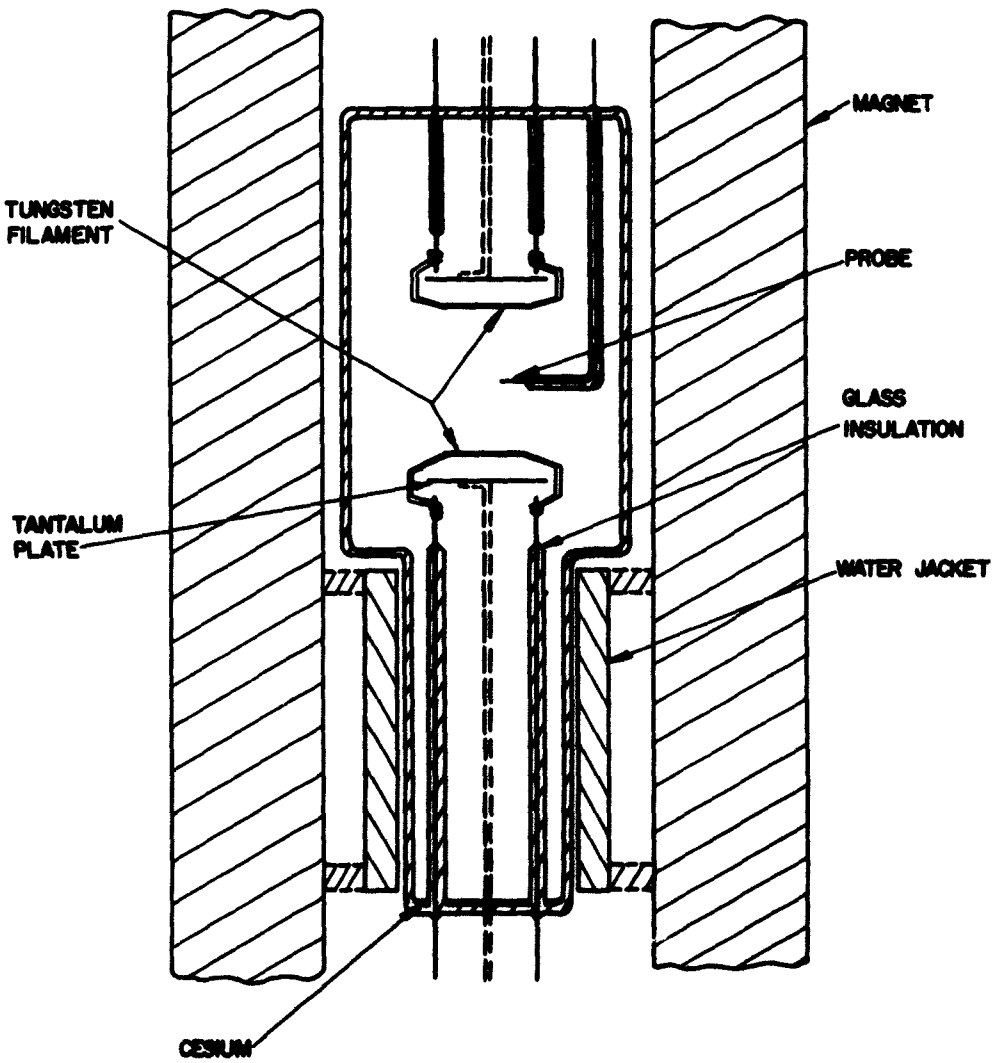

FIG. IV.C.1 SCHEMATIC DIAGRAM OF AN EXPERIMENTAL PLASMA TUBE.

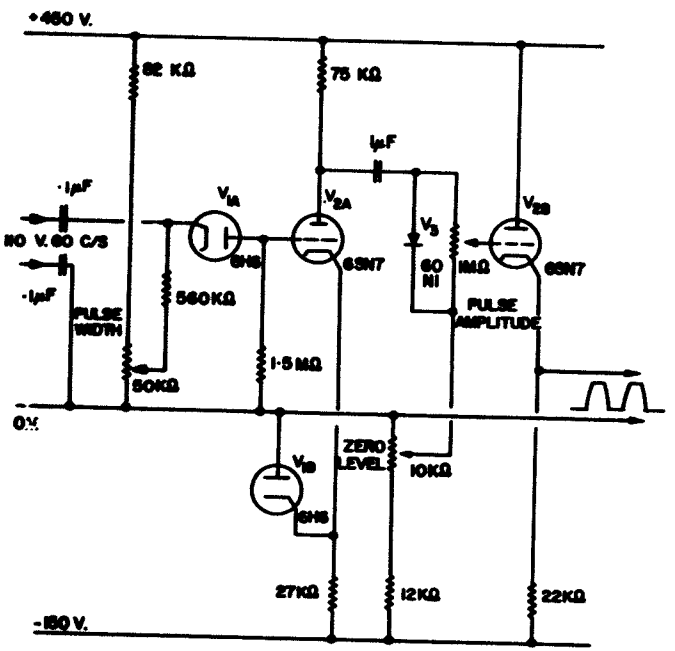

a. PULSE GENERATOR

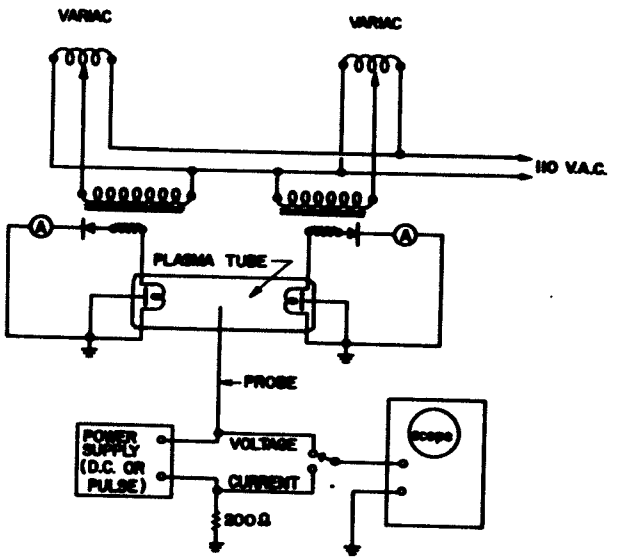

b. CURRENT—VOLTAGE MEASUREMENT CIRCUIT

FIG. IV.C.2 EXTERNAL ELECTRIC CIRCUITS.

Because of the pulse nature of the probe voltage, both the voltage and current must be measured with an oscilloscope. For rapid observation of the effect of certain changes, the probe voltage was used to produce the X-deflection of the oscilloscope while observing current in the Y-direction, thus current/voltage plots could be obtained directly. For high accuracy though, it was better to take quantitative readings using the conventional saw-tooth deflection and measuring both voltages and currents as a Y-deflection.

C.3 Interpretation of the Measurement. In Fig. IV.C.3, the natural logarithm of the electron current to the probe, i.e., probe current plus ion saturation current, is plotted against the probe voltage V_p. According to the theory for a planar probe[1], the plot of $\ell n\ i_e$ vs. V_p should be a straight line if the distribution of the electron velocities is Maxwellian. The electron temperature can then be determined by

$$T_e = \frac{e}{km_o} = \left(\frac{11{,}600}{m_o}\right)^\circ K \quad , \qquad \text{(IV.C.1)}$$

where the slope of the straight line is expressed as

$$m_o = \frac{d}{dV_p}(\ell n\ i_e) \quad . \qquad \text{(IV.C.2)}$$

Figure IV.C.3 shows a gradual bending of the curve. It should not necessarily be concluded that the velocity distribution of the electrons is not Maxwellian, but that probably these results are due to a gradual change of the effective probe area caused by an increase in the size of the sheath around the probe. Thus the slope of this line would be steeper

1. Dickson, L. D., "Survey of Diagnostic Techniques Used to Determine Temperature and Density in Plasmas", Technical Report No. AF-95, The Johns Hopkins University Radiation Laboratory, AD No. 275762, 82 pp.; May, 1962.

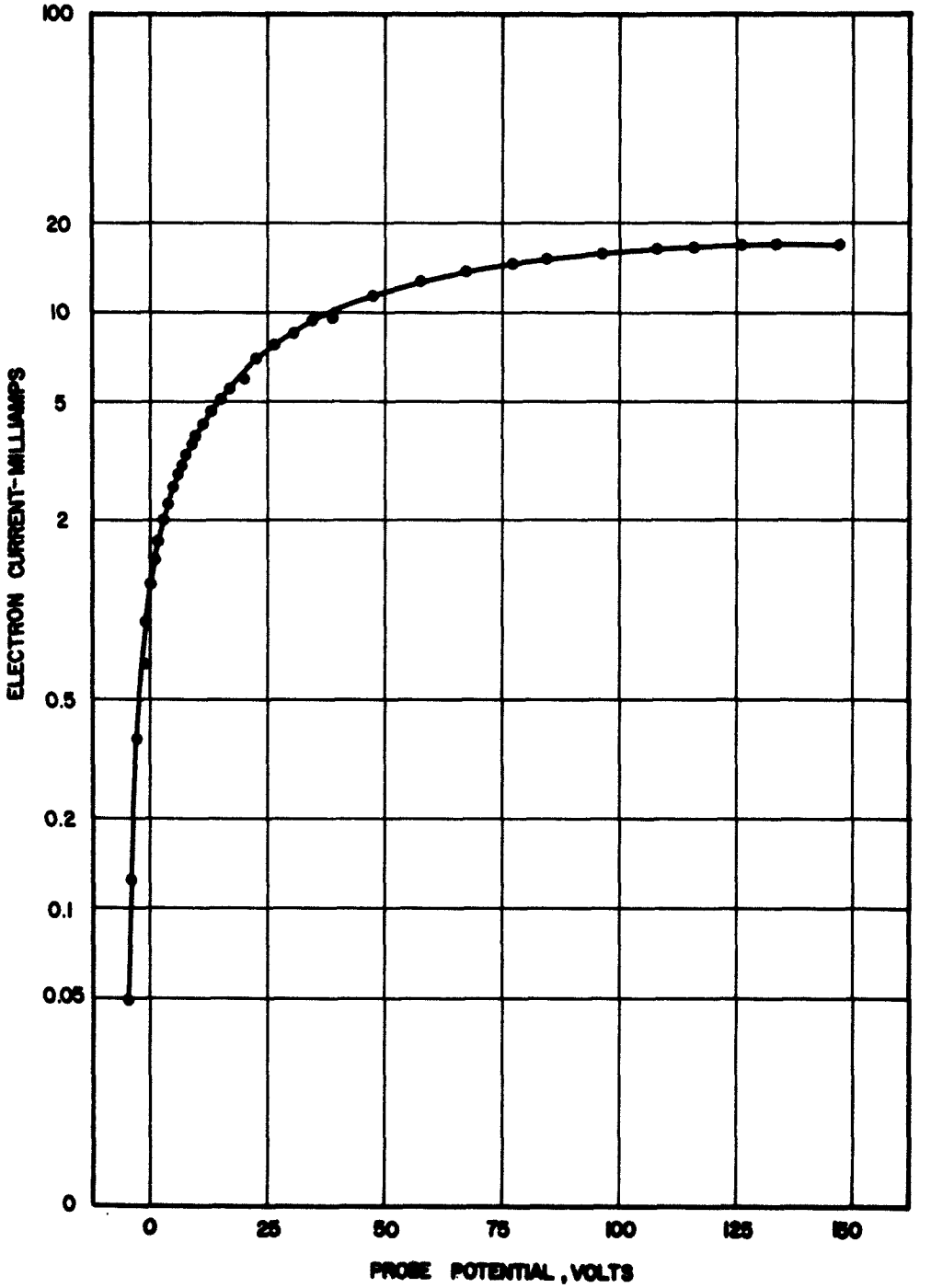

FIG. IV.C.3 PROBE CURRENT AND PROBE POTENTIAL CHARACTERISTICS AS MEASURED BY SINGLE PROBE METHOD.

if the probe area were constant and consequently the temperature determined by this method should be too high. This seems to be the case. The changing effective area of the probe also influences the saturation current. As a result, any conclusions drawn from these measurements must be regarded with suspicion.

A second measurement was made by using the plates behind each filament in the same way as a floating double probe. Although the dimensions of the plates and their separation do not really qualify them to be called a double probe, the results obtained from this measurement should yield the correct order of magnitude. A typical characteristic is shown in Fig. IV.C.4. It is estimated from this curve that the electron temperature is approximately 2600°K. Assuming an ion temperature close to the temperature of the envelope (320°K) and assuming that the positive ion and electron densities are the same, an electron density between 10^{11} and 10^{12} electrons per cc is obtained. Both results seem reasonable.

The asymmetry in the characteristic curve is not completely explained, but may be due to asymmetries in the tube, or more likely, to a difference of pressure between the two ends of the tube.

C.4 Conclusions. Although no firm quantitative results have been obtained so far, it is felt that much has been learned about the technology of the cesium plasma from the preliminary experiments. It is believed that the double probe method for measuring the electron density is more reliable and the result of 10^{11} to 10^{12} electrons per cc in this tube is reasonable.

C.5 Program for the Next Period. In the next period it is hoped to begin the building of a tube which will include an electron beam as

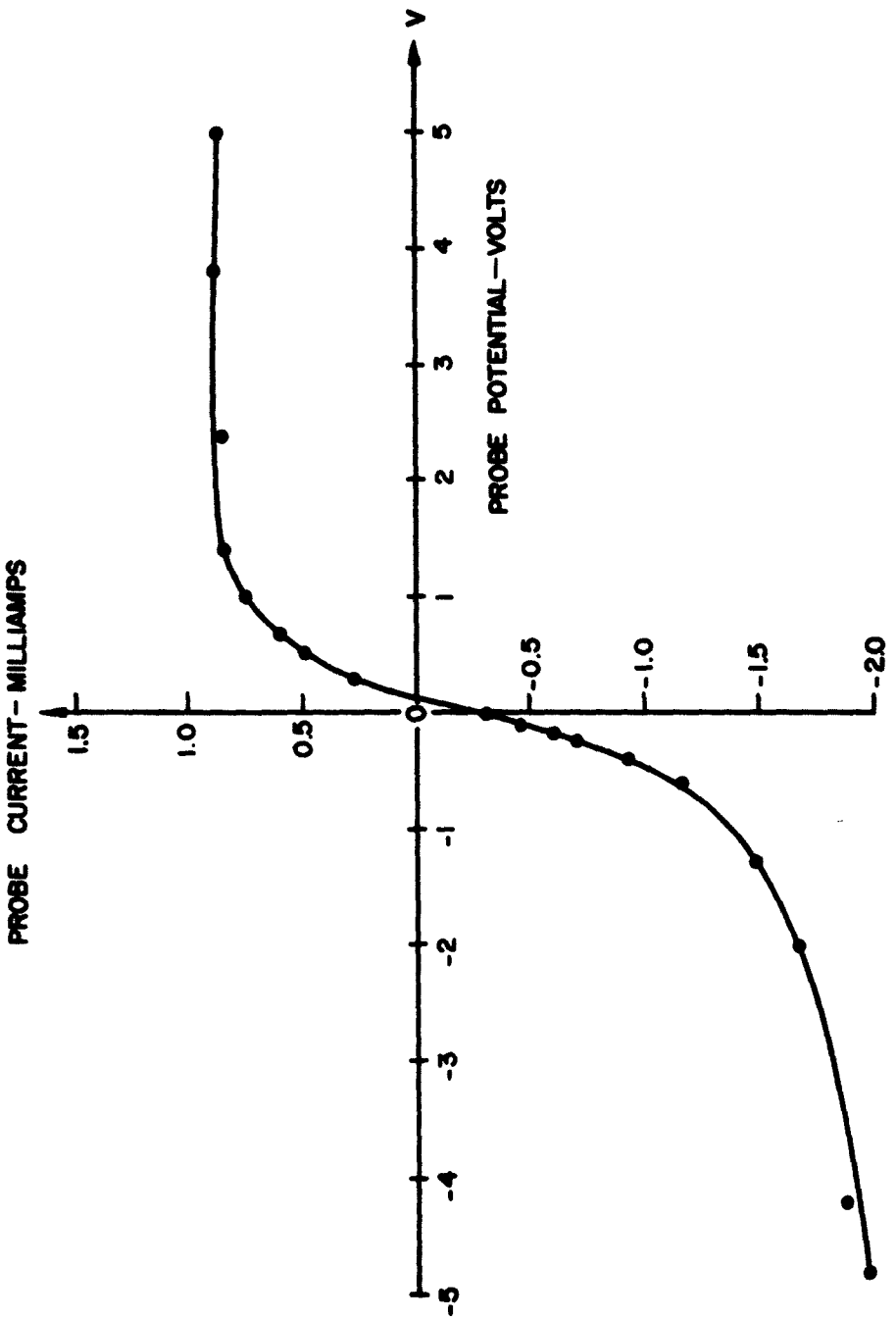

FIG. IV.C.4 PROBE CURRENT AND PROBE POTENTIAL CHARACTERISTICS AS MEASURED BY DOUBLE PROBE METHOD.

well as the plasma in order to commence a study of the electronic interaction. The major difficulty foreseen here comes in building the hot ionizing electrode into a small diameter tube without causing undue thermal strains. Should the difficulties prove insurmountable, it may be necessary to use some other method to generate the cesium plasma such as the P.I.G. discharge. Once some rough estimates of the magnitudes of various parameters have been obtained, the dispersion relations described in the previous interim report will be investigated.

D. Theory of Beam-Plasma Interaction (Y. C. Lim)

In the past six months the theoretical study of both the stationary and perturbed problems of beam-plasma interaction has reached a concluding stage as far as analytical solutions of the problems are concerned. The results will be described in detail in a forthcoming technical report. The study was made under the following assumptions:

1. The system has a low density so that only binary collisions require consideration.

2. Processes such as ionization, recombination and radiation are insignificant as a whole.

3. The plasma held between two infinitely extended parallel walls is only weakly ionized so that the short range collisions between charged particles may be neglected.

4. The interaction between a neutral gas molecule and a charged particle in their collision obeys the inverse fifth power force law.

5. The distribution functions are continuous, quadratically integrable and independent of the position variables parallel to the walls.

6. Both the externally applied d-c electric field and the internal electric field are longitudinal (i.e., perpendicular to the walls) with the former dominating the latter, while the magnetic effect is negligible.

7. The perturbation is small throughout the region of interaction.

8. The neutral gas has a Maxwellian distribution with a uniform density, a constant temperature and a zero drift velocity.

9. The nonrelativistic beam of charged particles traversing the plasma in the direction perpendicular to the walls has, at the entrance to the interaction region, a stationary distribution which is Maxwellian about its drift velocity; at each point of the interaction region it has a small axial velocity spread compared to the drift velocity.

10. The walls are perfectly reflecting to the plasma constituents.

The stationary problem, in which the beam entering the interaction region is not premodulated, was solved by the method of eigenfunctions. In the application of this method three infinite sets of eigenvalues corresponding to the three complete sets of eigenfunctions of the respective collision integral operators were obtained in the technical report mentioned above. In terms of these eigenvalues, the densities of the various constituents, the d-c electric field and the entrance data, the averages of eigenfunctions were obtained with the help of a general recurrence formula derived from the Boltzmann equation. These averages after multiplication by a proper constant give the coefficients of expansions of the stationary distribution functions in the corresponding eigenfunctions. Thus the solutions of the stationary problem as well as all the macroscopic properties of the system were obtained in terms of the eigenvalues, the d-c electric field, the entrance data and the densities of the various components of the system. All of these quantities are

known, except the densities. The determination of the densities was achieved in two different ways. For the charged particles of the beam the density $n_3(z)$ was obtained as the solution of an Abel differential equation derived from the Boltzmann equation as a consequence of assumption 9. For the charged particles of the plasma constituents the densities $n_i(z)$, $(i = 1,2)$, were approximated by properly truncated power series obtained from the solution of a finite closed algebraic system which includes a subsystem extracted from the boundary equations.

The perturbed problem was solved by the simultaneous application of the method of characteristics on both the stationary and the perturbed Boltzmann equations, thus by-passing the complicated calculation necessary in the evaluation of the effect of collision on perturbation and giving simply the perturbed distribution functions f_{i1} in terms of the perturbed electric field $E(z)$. Substitution of the f_{i1} so expressed into the Poisson equation yielded an integral equation in $E(z)$ solvable under suitable condition by the Neumann series. The dispersion relation and signal gain were shown to be obtainable. For the details see the technical report mentioned above.

In conclusion it must be pointed out that the thing that remains to be done in the theoretical study of the problem under the assumptions listed above is the insertion of physical constants and the actual carrying out of the numerical calculations of the dispersion relations and the signal gains of the system for some given d-c electric fields $E_d(z)$. For the evaluation of the necessary eigenvalues, the use of a high-speed digital computer will certainly be of great help.

E. Nonlinear Beam-Plasma Interactions (J. E. Rowe)

E.1 Introduction. The general nonlinear ballistics equations for a two-species particle-wave interaction system were derived in the previous progress report. The system applies to such cases as

a. Double-beam interaction including a propagating electromagnetic wave, forward- or backward-wave mode,

b. Beam-plasma interaction with input modulation of either particle type,

c. Beam-plasma interaction with an electromagnetic wave; forward- or backward-wave mode.

The details of the mathematical development have been presented and only the important system parameters are repeated here. The charge-to-mass ratios for the particle species are indicated by

$$\eta_1 = \epsilon_1 |\eta_1| \qquad \text{(IV.E.1a)}$$

and

$$\eta_2 = \epsilon_2 |\eta_2| \ , \qquad \text{(IV.E.1b)}$$

where $\epsilon_1, \epsilon_2 = \pm 1$. The particle currents are given by

$$I_{o1} = \epsilon_1 |I_{o1}| \qquad \text{(IV.E.2a)}$$

and

$$I_{o2} = \epsilon_2 |I_{o2}| \ . \qquad \text{(IV.E.2b)}$$

It is then convenient to define a relative charge-to-mass ratio and a corresponding particle current of the following form:

$$\eta' \triangleq \frac{|\eta_1| - |\eta_2|}{2\eta_o} \qquad \text{(IV.E.3)}$$

and

$$I' \triangleq \frac{|I_{o1}| - |I_{o2}|}{2I_o} , \qquad \text{(IV.E.4)}$$

where

$$\eta_o \triangleq \frac{|\eta_1| + |\eta_2|}{2} \qquad \text{(IV.E.5)}$$

and

$$I_o \triangleq \frac{|I_{o1}| + |I_{o2}|}{2} . \qquad \text{(IV.E.6)}$$

The important wave interaction parameters and relative velocity are given by

$$C \triangleq \frac{\eta_o I_o Z_o}{2u_o^2} , \qquad \text{(IV.E.7)}$$

$$D \triangleq \frac{C}{1+Cb} . \qquad \text{(IV.E.8)}$$

In the absence of a propagating electromagnetic wave the system is considered to be initially modulated by a simple velocity modulation gap and the depth of modulation is specified by $\alpha = V_g/V_o$.

At present the initial velocity of the particles is either considered uniform over each class of particles or is taken as that resulting from a simple gap modulation. At present a velocity distribution function for each particle species is being incorporated in the digital computer program.

E.2 Numerical Results. Several solutions have been obtained for each of the systems given above as a means of checking the digital computer program. So far only solutions for which $\omega_{p_1} = \omega_{p_2} = 0$ have been calculated. The space-charge field weighting functions are presently being calculated and will be incorporated in the program in the near

future along with the velocity distribution function. The following specific calculations are illustrative of the generality of the analysis.

a. Double-Beam Interaction. In such an interaction system the two beams are initially modulated by a klystron-like gap according to the following relation:

$$1 + \alpha u(X,\varphi_{oj}) = [1 + \alpha \sin \varphi(X,\varphi_{oj})]^{1/2} \quad . \qquad \text{(IV.E.9)}$$

After modulation the two are injected into a cylindrical drift tube and after drifting a distance as measured by $X = \pi\alpha N_s$ the velocity modulation is connected to density modulation and a bunched beam is then available for excitation of the output gap. The normalized position at which the various harmonic currents reach a maximum depends both on α and on the relative velocity as given by

$$b \triangleq \frac{u_{o1}-u_{o2}}{2u_o} \quad -1 < b < 1 \quad . \qquad \text{(IV.E.10)}$$

Specific results are shown in Figs. IV.E.1 and IV.E.2 for two beam systems as a function of the modulation parameter α. The r-f velocity distribution across the individual beams are shown in Figs. IV.E.3 and IV.E.4. In the above calculations it has been assumed that the charge-to-mass ratios and the currents carried by the two charge species are the same so that $\eta' = I' = 0$.

Other typical solutions for a double-beam system in the presence of an electromagnetic wave are shown in Fig. IV.E.5. The variation of r-f current in the stream and the velocity variation across the stream are shown in Figs. IV.E.6 and IV.E.7. Additional solutions are necessary before any general conclusions can be made about the efficiency of such interactions.

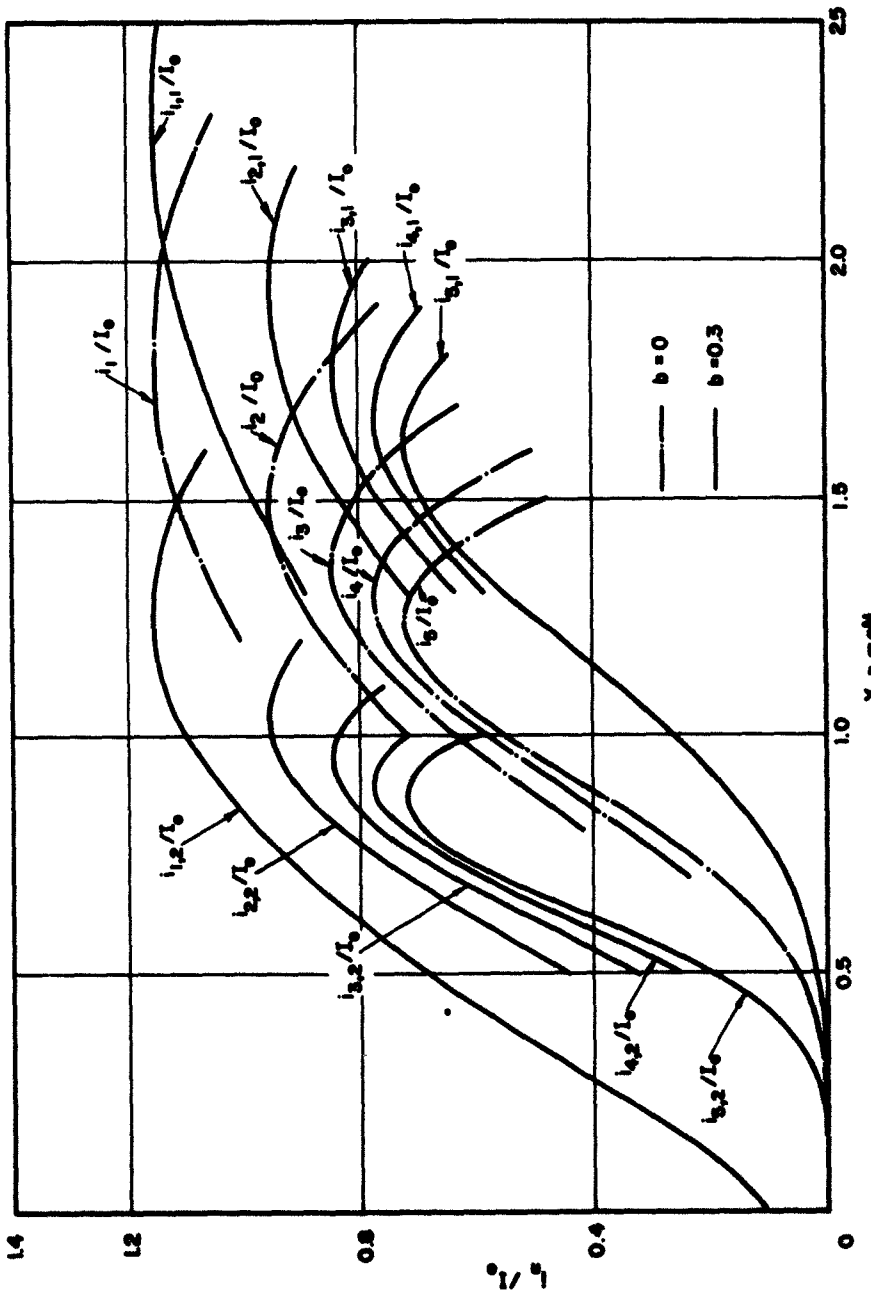

FIG. IV.E.1 HARMONIC CURRENT VS. DISTANCE FOR A DOUBLE-BEAM AMPLIFIER.

($\epsilon_1 = \epsilon_2 = \pm 1$, $\omega_{p1}/\omega = \omega_{p2}/\omega = 0$, $\alpha = 0.2$, $\eta' = I' = 0$)

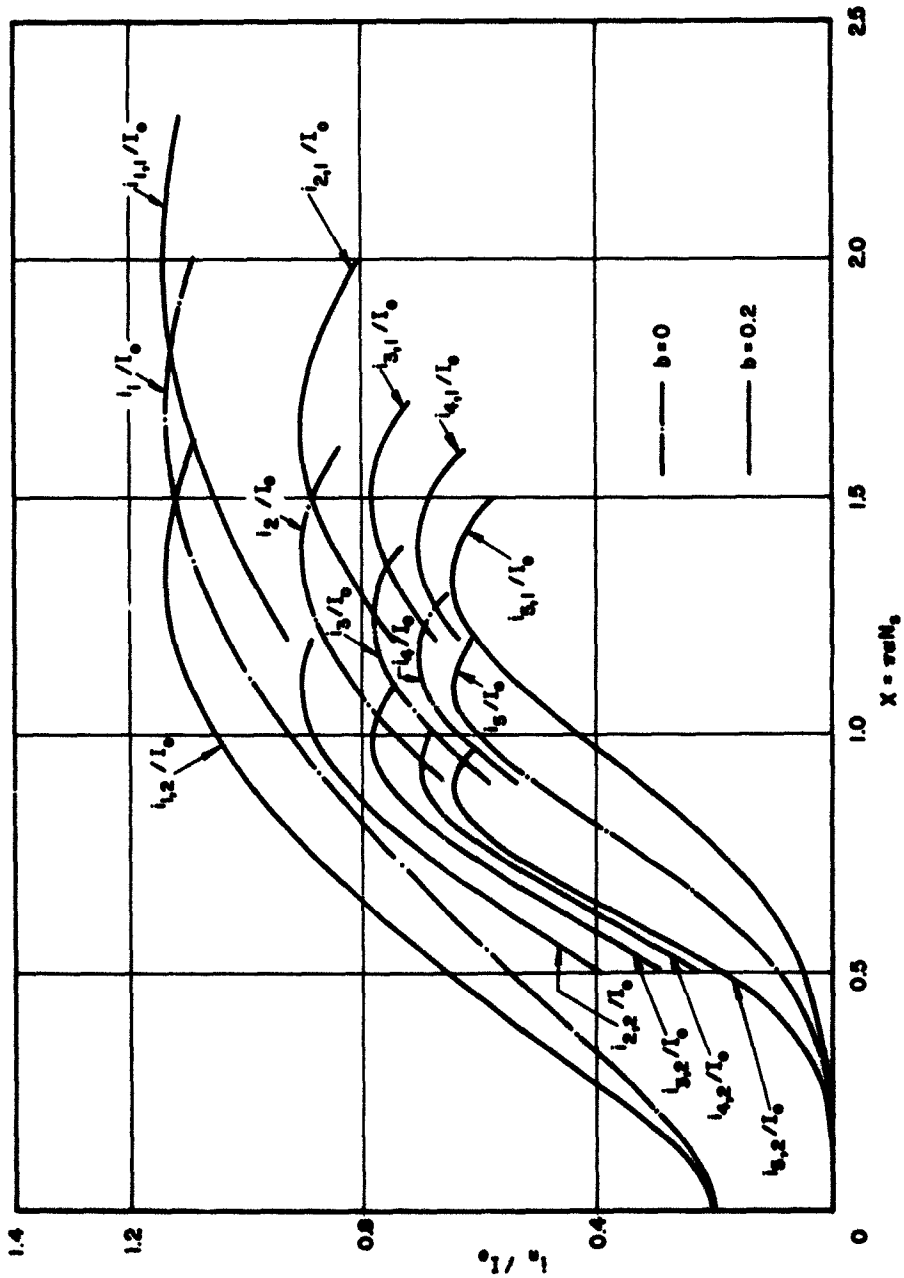

FIG. IV.E.2 HARMONIC CURRENT VS. DISTANCE FOR A DOUBLE-BEAM AMPLIFIER.

($\epsilon_1 = \epsilon_2 = \pm 1$, $\omega_{p1}/\omega = \omega_{p2}/\omega = 0$, $\alpha = 0.4$, $\eta' = \Gamma' = 0$)

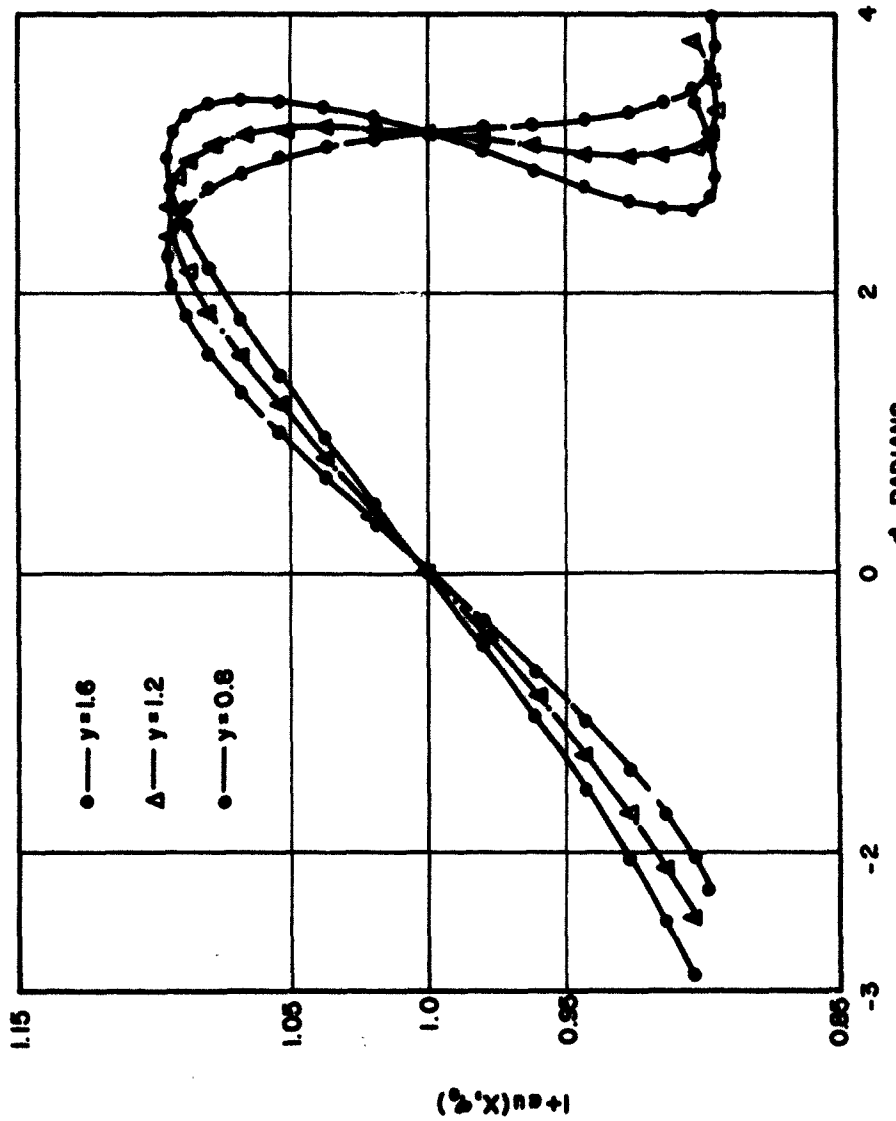

FIG. IV.E.3 VELOCITY-PHASE DIAGRAM FOR A DOUBLE-BEAM INTERACTION. ($\epsilon_1 = \epsilon_2 = \pm 1$, $\omega_{p1}/\omega = \omega_{p2}/\omega = 0$, $\alpha = 0.2$, $\eta' = \Gamma' = 0$)

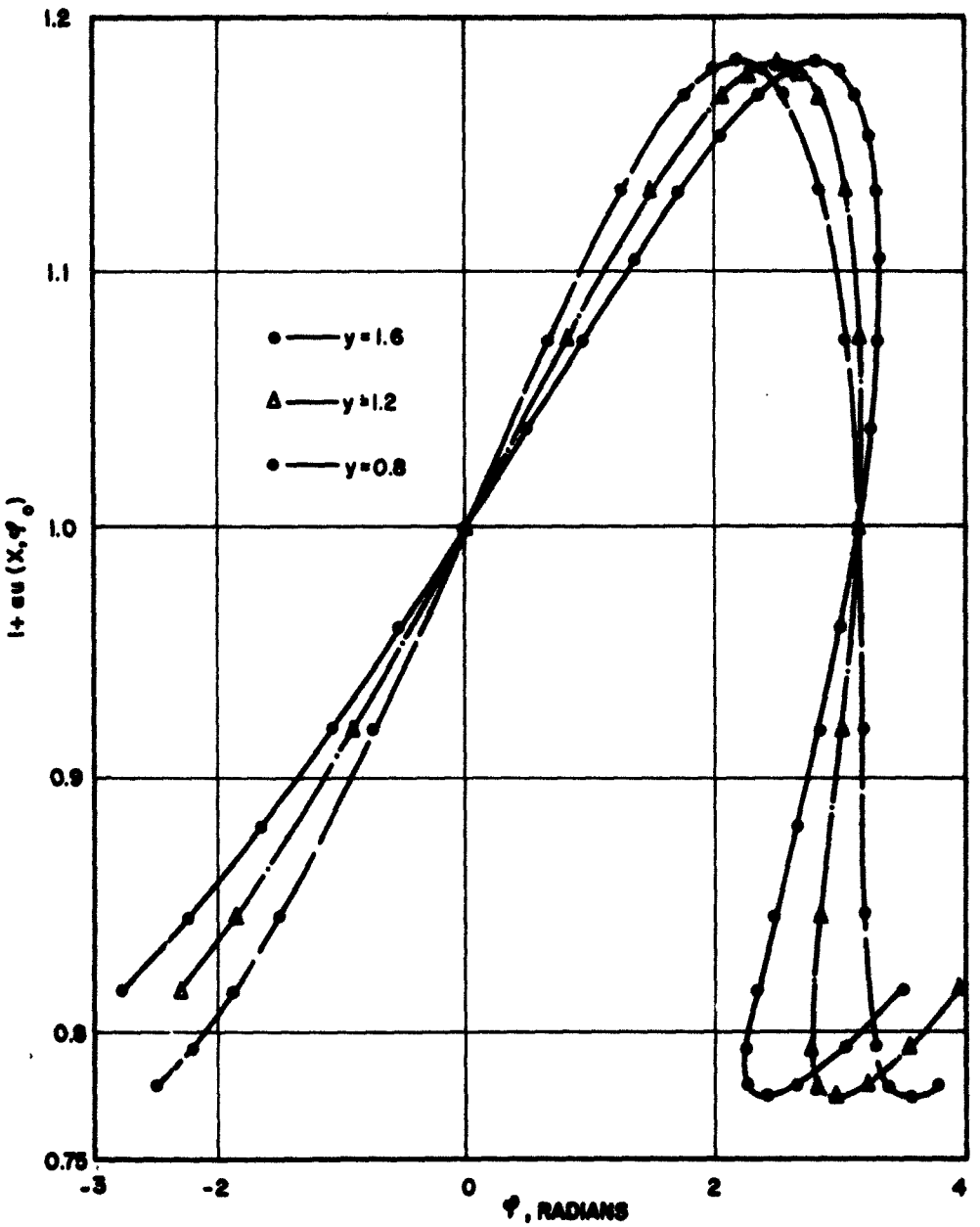

FIG. IV.E.4 VELOCITY-PHASE DIAGRAM FOR A DOUBLE-BEAM INTERACTION.

($\epsilon_1 = \epsilon_2 = \pm 1$, $\omega_{p1}/\omega = \omega_{p2}/\omega = 0$, $\alpha = 0.4$, $\eta' = I' = 0$)

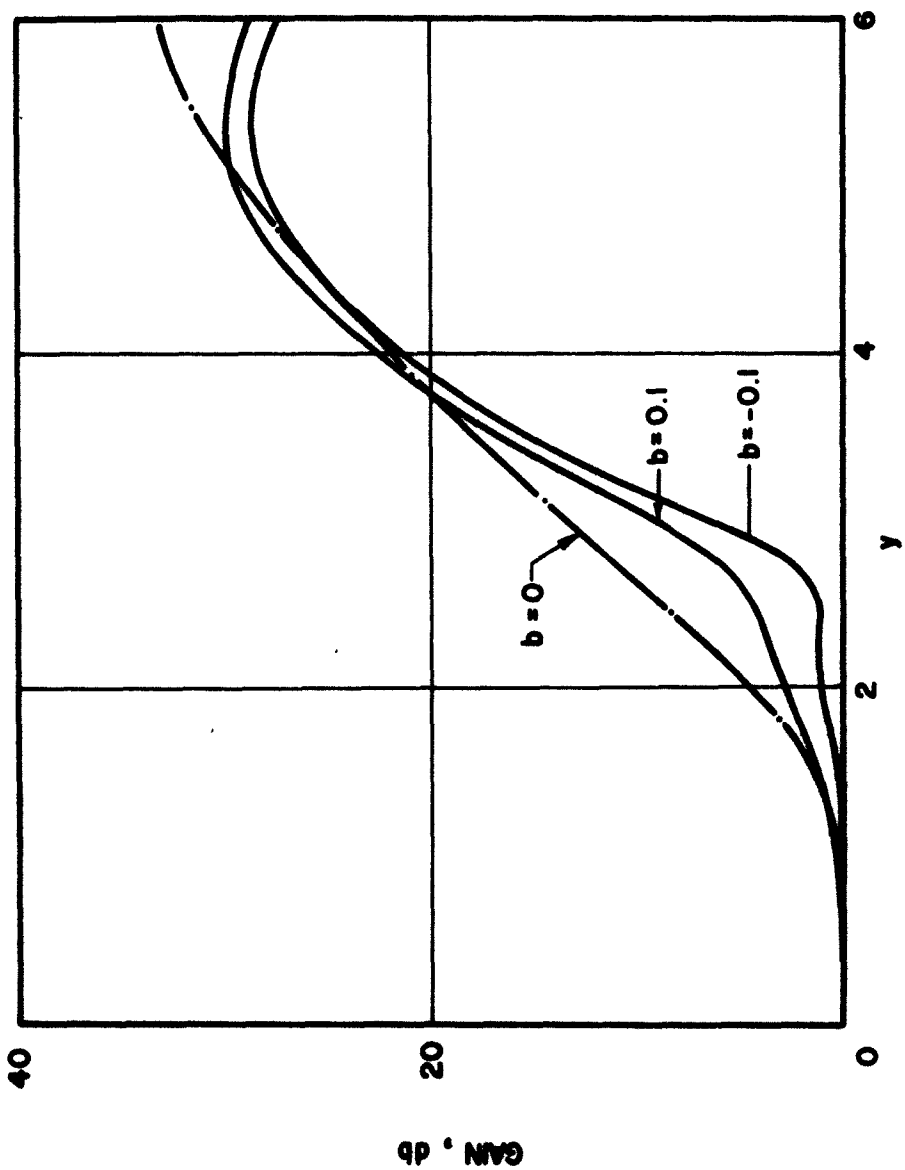

FIG. IV.E.5 GAIN VS. DISTANCE FOR A DOUBLE-BEAM INTERACTION. ($C = 0.1$, $\omega_{p1}/\omega = \omega_{p2}/\omega = 0$, $\epsilon_1 = \epsilon_2 = \pm 1$, $\eta' = \Gamma' = 0$, $\psi_o = -30$)

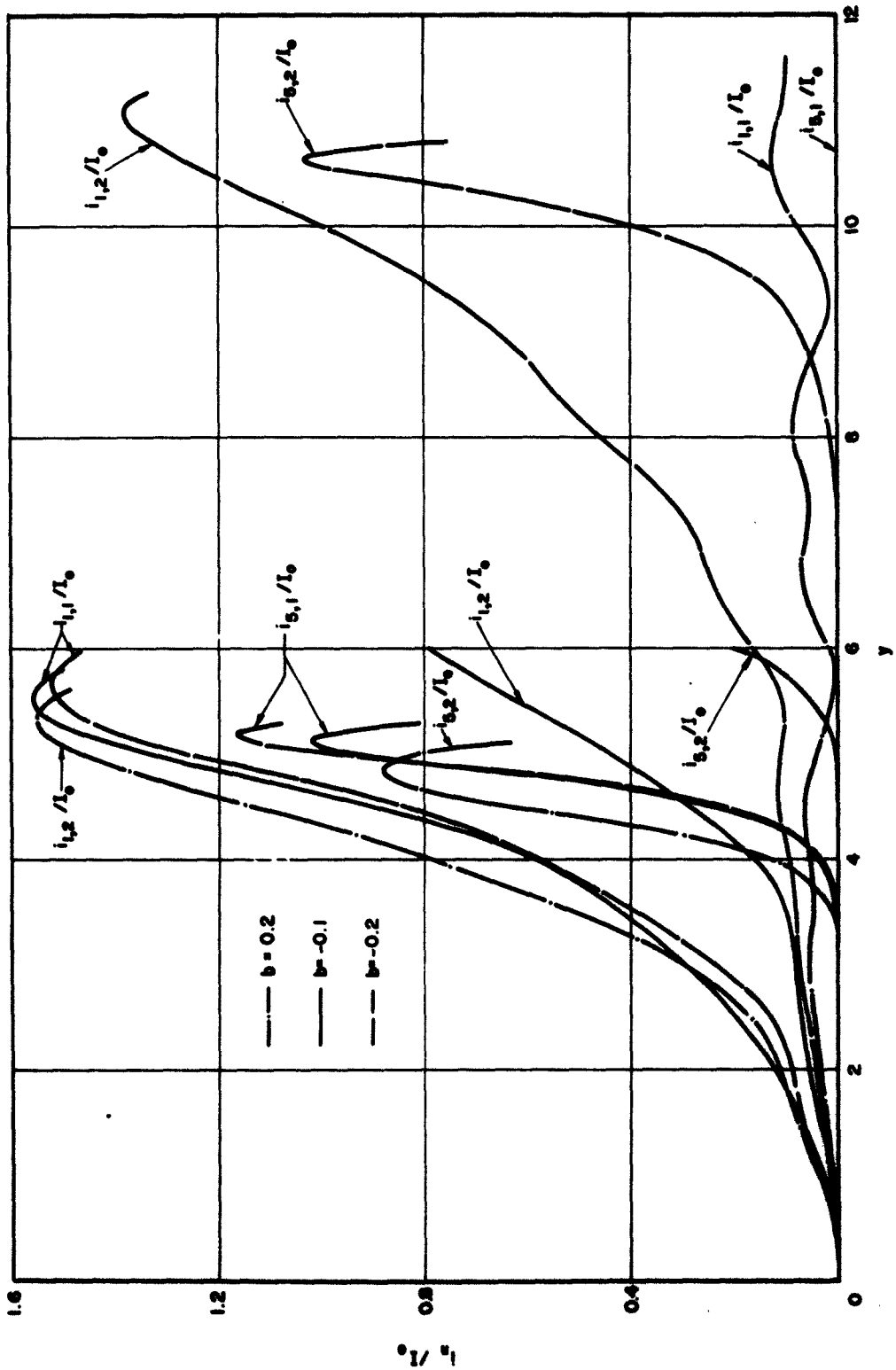

FIG. IV.E.6 HARMONIC CURRENT VS. DISTANCE IN A DOUBLE BEAM-WAVE SYSTEM. (C = 0.1, $\omega_{p1}/\omega = \omega_{p2}/\omega = 0$, $\epsilon_1 = \epsilon_2 = \pm 1$, $\eta' = \Gamma' = 0$, $\psi_o = -30$)

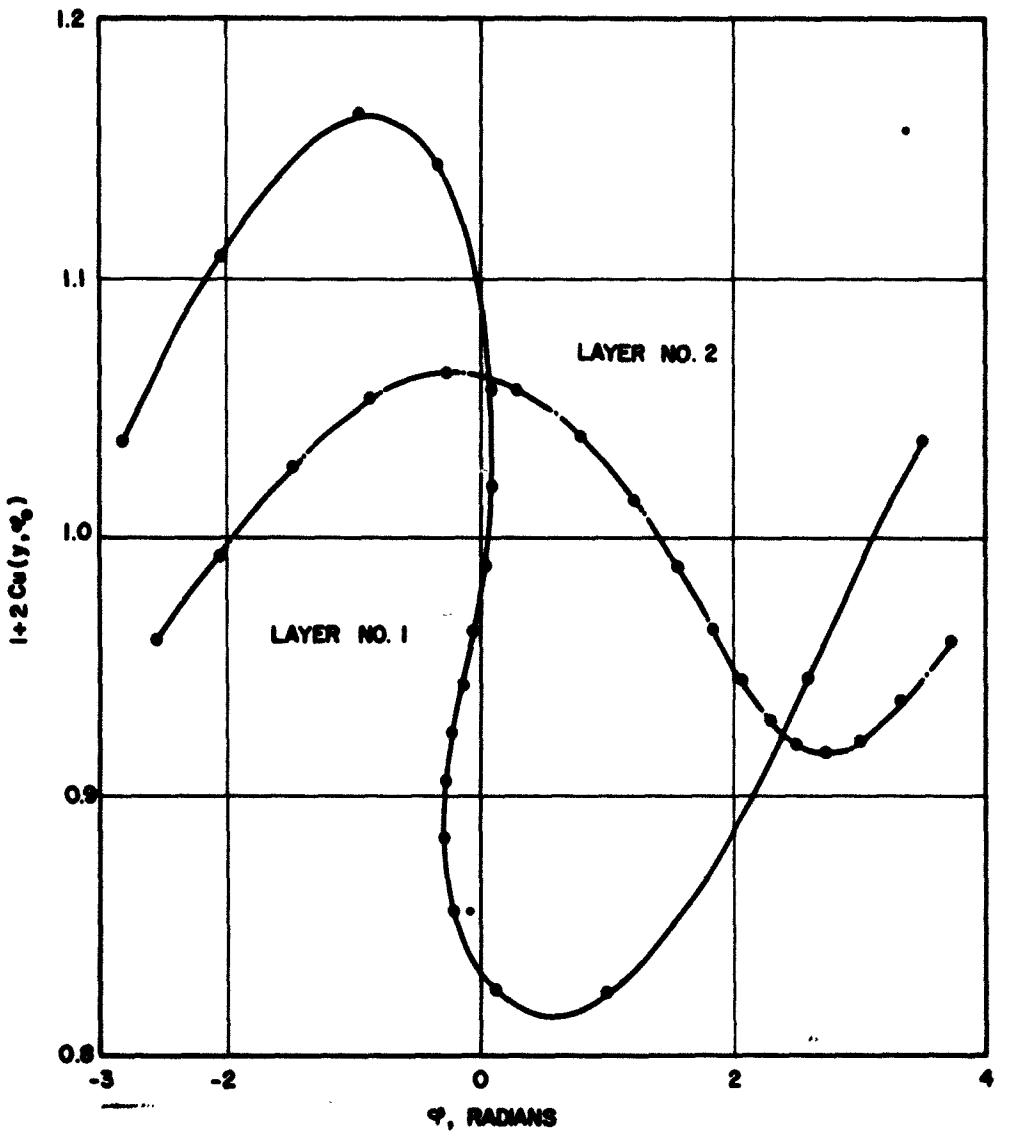

FIG. IV.E.7 VELOCITY VS. PHASE DIAGRAM FOR A DOUBLE BEAM-WAVE SYSTEM. ($C = 0.1$, $\omega_{p1}/\omega = \omega_{p2}/\omega = 0$, $\epsilon_1 = \epsilon_2 = \pm 1$, $\eta' = I' = 0$, $b = -0.1$, $\psi_0 = -30$, $y = 5.2$)

b. Beam-Plasma Interaction. To illustrate beam-plasma characteristics several solutions were obtained assuming $\epsilon_1 = -1$ and $\epsilon_2 = 1$. If space-charge forces are neglected and η' and I' are taken as zero the results will be the same as for the double-beam interaction.

E.3 Conclusions. In view of the limited computations which have been made it is impossible to form any specific conclusions at this time. The check-runs to date do indicate the validity of the theoretical formulation for both the double-beam and beam-plasma systems.

E.4 Program for the Next Period. During the next period the calculations will be generalized to include space-charge fields and velocity distributions in both the beam and the plasma. It is also planned to obtain additional specific solutions particularly for the beam-plasma system.

V. CROSSED-FIELD ELECTRON GUN STUDIES

A. Poisson Cell Investigation (N. A. Masnari)

A.1 Introduction. The Poisson cell analysis of the modified Kino gun has been continued in an attempt to generate better electron beams. The primary concern has been to increase the useful emitting area of the cathode while maintaining a reasonable convergence capability of the gun. Minor electrode configuration changes have been made and their effect on the beam analyzed.

A.2 Kino Gun Results. The most recent investigations of the Kino gun have been aimed at producing a laminar beam from a wider cathode. Previous results indicated that there was a maximum cathode width which was capable of generating a Brillouin beam for a given electron gun configuration. The particular electrode configuration being considered at

the end of the preceding period is shown in Fig. V.A.1. This figure also indicates the trajectories obtained with space-charge effects included.

Additional investigations carried out since that time have indicated that no significant improvement in the beam characteristics was possible with this particular gun. One of the major problems was the fact that the upper trajectory in the beam passed quite close to the focusing anode. Consequently any attempt to use a wider cathode resulted in the emission of electrons which were intercepted by the focusing anode.

As a result of the above observations, the focusing anode was elevated to the position shown in Fig. V.A.2. This arrangement provided more room for the beam to travel through the gun region and thus should minimize the interception by the accelerator. Figure V.A.3 illustrates the trajectories obtained for this case. The solid curves correspond to the electron paths after three iterations of the space-charge simulation process while the dashed trajectories are those obtained after the fourth iteration. Comparison between these two sets of trajectories indicates that the beam is nearly laminar and self-consistent in the cathode region. However, the beam obviously becomes nonlaminar as it approaches the entrance plane of the anode-sole region. It was also discovered after further investigation that nothing could be done to prevent the various electrons from crossing in the anode-sole region. These results lend support to the theory that attempts to produce laminar beams from excessively wide cathodes are unlikely to be successful.

Consideration of the results obtained from the various modifications of this Kino gun has resulted in the conclusion that further investigation is not worthwhile. The results indicate that no significant

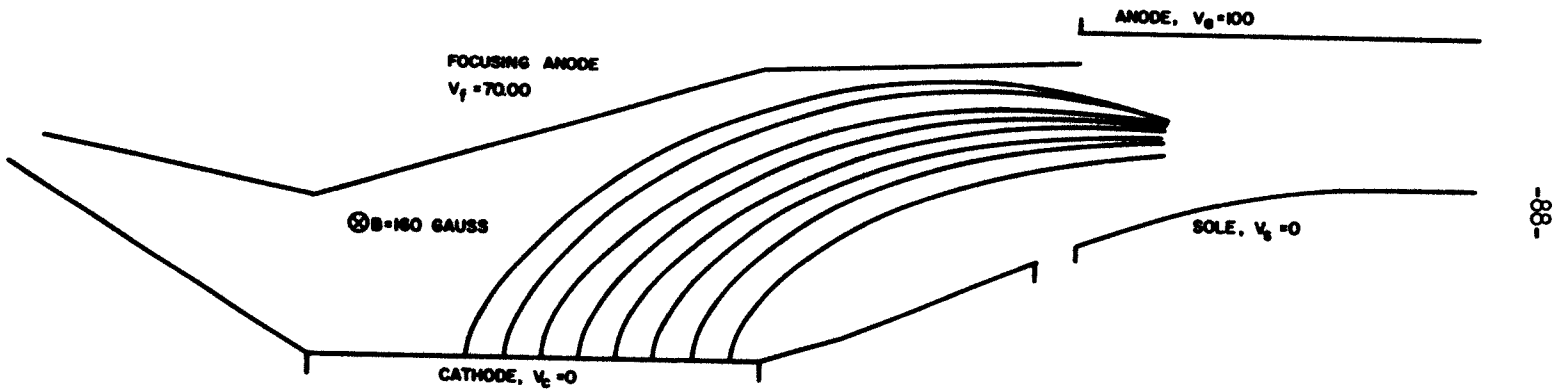

FIG. V.A.1 ELECTRON TRAJECTORIES FOR A GUN CONFIGURATION WITH A MODIFIED ANODE-SOLE REGION.

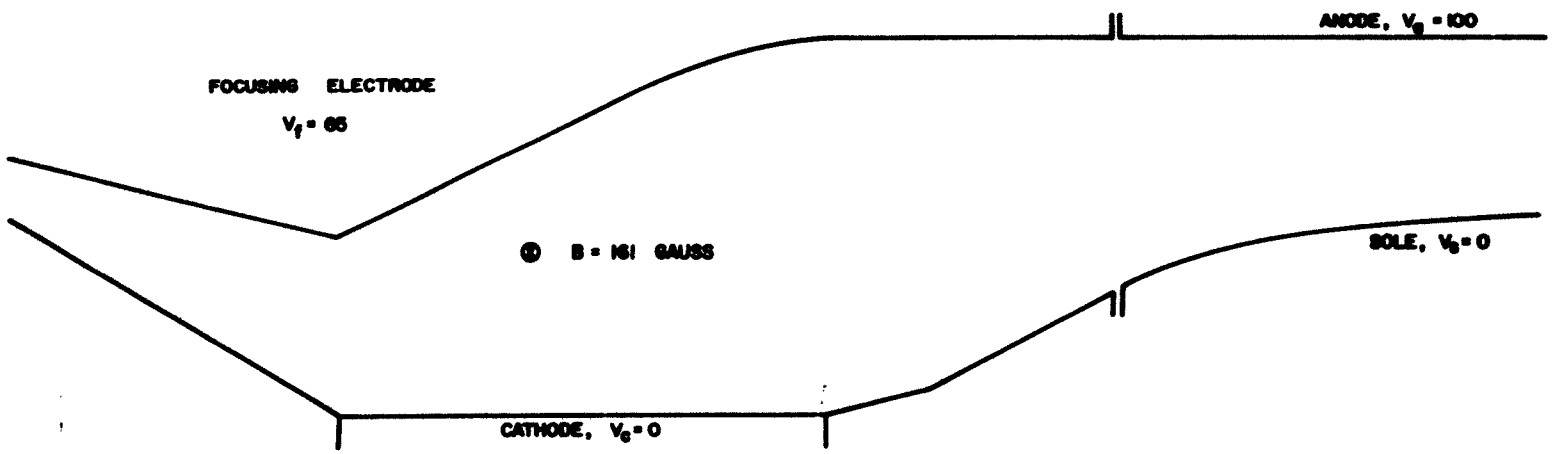

FIG. V.A.2 THE MOST RECENT KINO GUN CONFIGURATION TO BE ANALYZED.

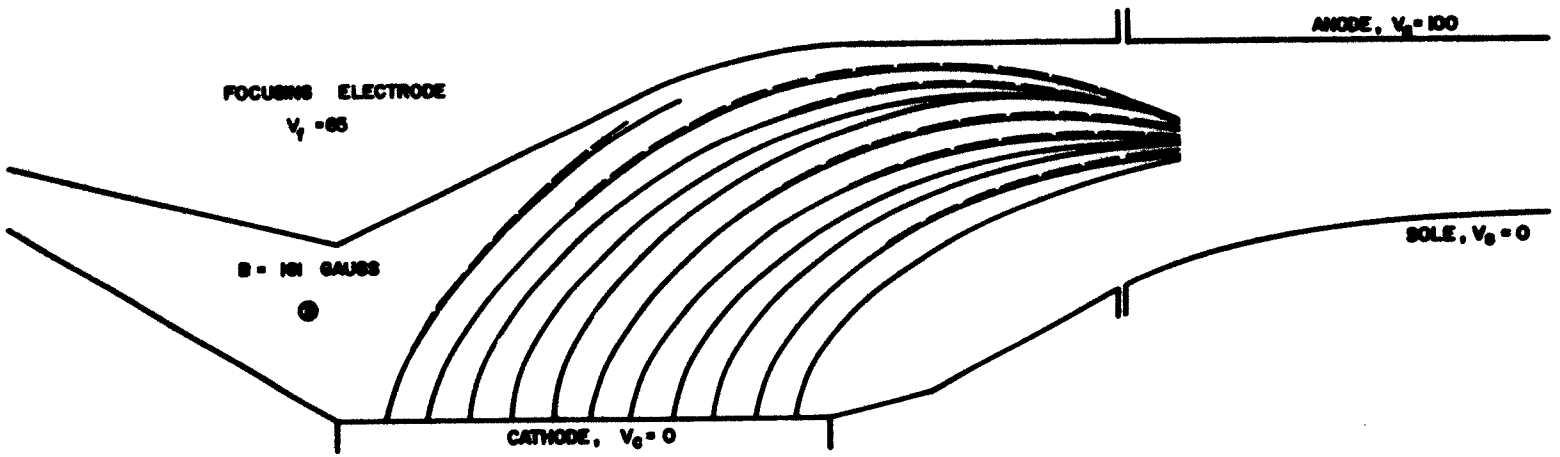

FIG. V.A.3 ELECTRON TRAJECTORIES AFTER THIRD (SOLID CURVES) AND FOURTH (DASHED CURVES) ITERATIONS OF SPACE-CHARGE SIMULATION PROCESS.

improvement in the beam characteristics can be obtained without appreciably changing the entire gun.

The Poisson cell is now being modified to simulate the same gun configuration which has been investigated in the crossed-field beam analyzer. The situation is shown in Fig. V.A.4 from which it is apparent that the basic gun is again of the Kino type. However, the cathode area is greatly reduced and the electrons must travel a relatively greater distance in moving from the cathode to the anode-sole entrance plane. The motivation behind this study is to provide some correlation between the experimental beam analyzer results and the Poisson cell investigation. In this capacity the cell results should be quite helpful in explaining the beam behavior as observed in the analyzer studies.

A.3 Conclusions. The analyses on the original Kino short gun and the various modified versions of the gun have been completed. The results indicate that a Kino gun can generate a laminar beam of limited convergence if the cathode width does not exceed some maximum value. The investigation also implies that such limitations are not restricted to Kino guns, but rather are characteristic of crossed-field electron guns in general.

A.4 Program for the Next Period. The Poisson cell analog of the crossed-field beam analyzer electron gun will be investigated under various conditions to observe the effect of certain parameters on the characteristics of the beam. In particular, the magnetic field, focusing anode voltage and anode voltage will be varied and the results compared with the analyzer studies. This comparison should be quite helpful in providing a better understanding of the behavior of electrons in crossed-field devices.

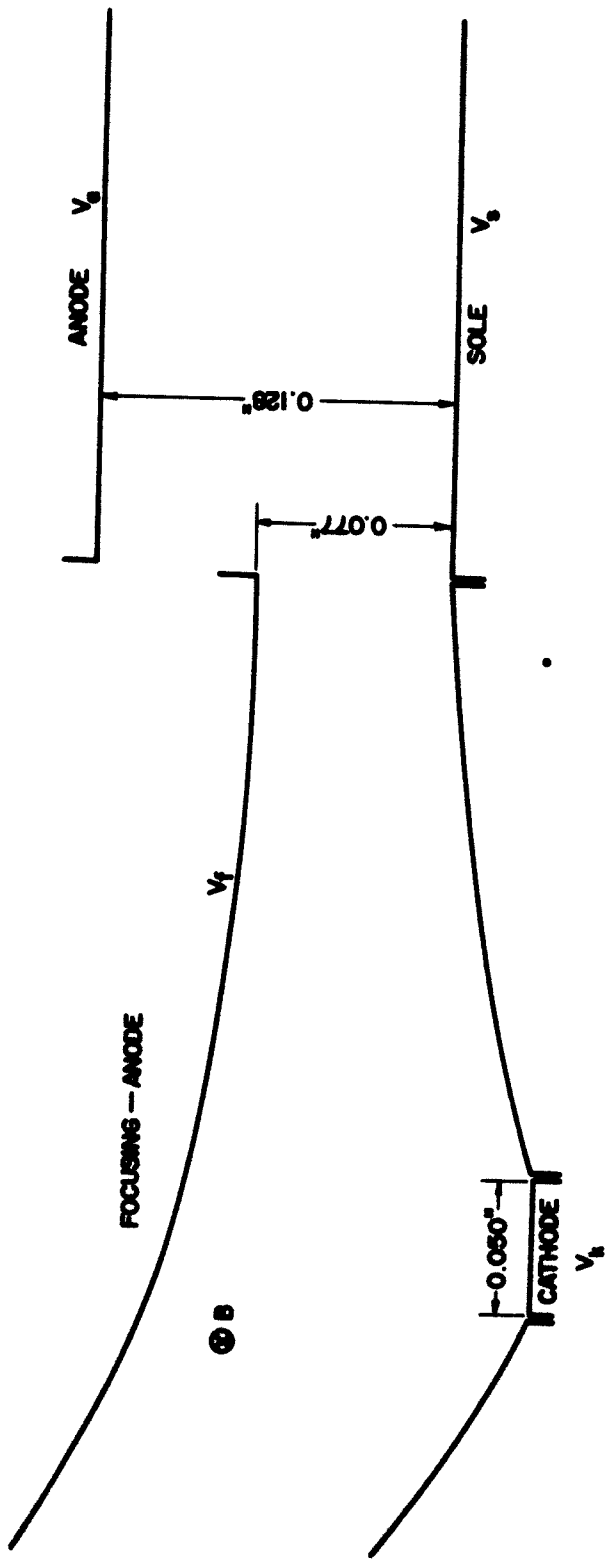

FIG. V.A.4 BEAM ANALYZER KEMO GUN WHICH IS BEING SET UP FOR POISSON CELL INVESTIGATION.

B. Crossed-Field Beam Analyzer (N. A. Masnari)

B.1 Introduction. The data from the original experiments on the crossed-field beam analyzer described in the previous report indicated that the transmission to the collector was very poor. The implication of the results was that the beam spread laterally and moved out of the anode-sole region shortly after passing the gun exit plane and grid of wires. For this reason it was decided to incorporate end hats on the sole structure to confine the beam in the interaction region. These hats were in the form of two rails spaced 0.680 inch apart and situated along the entire length of the sole. The height of the hats was 0.020 inch in the region where the grid wires moved and 0.060 inch everywhere else. This modification was quite successful in increasing the amount of current reaching the collector.

Other problems which were encountered during the first run have also been solved. These included the elimination of shorts between various grid wires and the short between anode and collector. The grid problem was solved by welding the lead-in wire near the end of the grid-wire and clipping off the excess wire extending beyond the weld point.

There have been essentially two separate investigations carried out following the work described in the previous report. The first analysis was performed without including the ten grid wires in the anode-sole region. The data obtained from this investigation provided information concerning the basic transmission capability of the device and its dependence on the magnetic field and electrode voltages. The grid wires were then inserted across the interaction region and experiments similar to those described previously were performed. This allowed an evaluation of the effect of the grid on the transmission and other

characteristics of the beam. It also provided more detailed information than was previously available since there were no longer any shorts between various grid wires. In general, the results substantiated the conclusions reached after the first investigation.

B.2 Experimental Results.

a. Investigation with Grid Wires Omitted. The experiments were initiated by analyzing the basic transmission characteristics of the device without the grid wires. The results indicated that it was quite possible to obtain better than 90 percent transmission to the collector for certain values of V_c (cathode voltage), V_f (focusing-anode voltage), and B (magnetic field). Figure V.B.1 illustrates the basic geometry and the voltages applied to the various electrodes.

The start of the investigation was concerned with the variation of currents with magnetic field. Figure V.B.2 illustrates the cathode current (I_k), focusing anode current (I_f), anode current (I_a), and collector current (I_c) as the magnetic field is varied with fixed values of V_f = - 500 volts and V_c = - 1430 volts. I_k behaves in the usual manner by decreasing as the magnetic field is increased. I_f is observed to be fairly constant until the cutoff magnetic field is reached at which point it decreases very rapidly. In other words, as B is increased it eventually becomes large enough to curve the beam away from the focusing anode and into the interaction space. When this cutoff point is reached, I_f decreases rapidly and I_c rises abruptly as shown in the figure. It seems reasonable that I_c should rise to a maximum value and then decrease gradually just as I_k does. Such a behavior is observed for I_c except for a slight depression which occurs shortly after the maximum value of I_c has been reached. For the above case, this dip occurs at about B = 350 gauss.

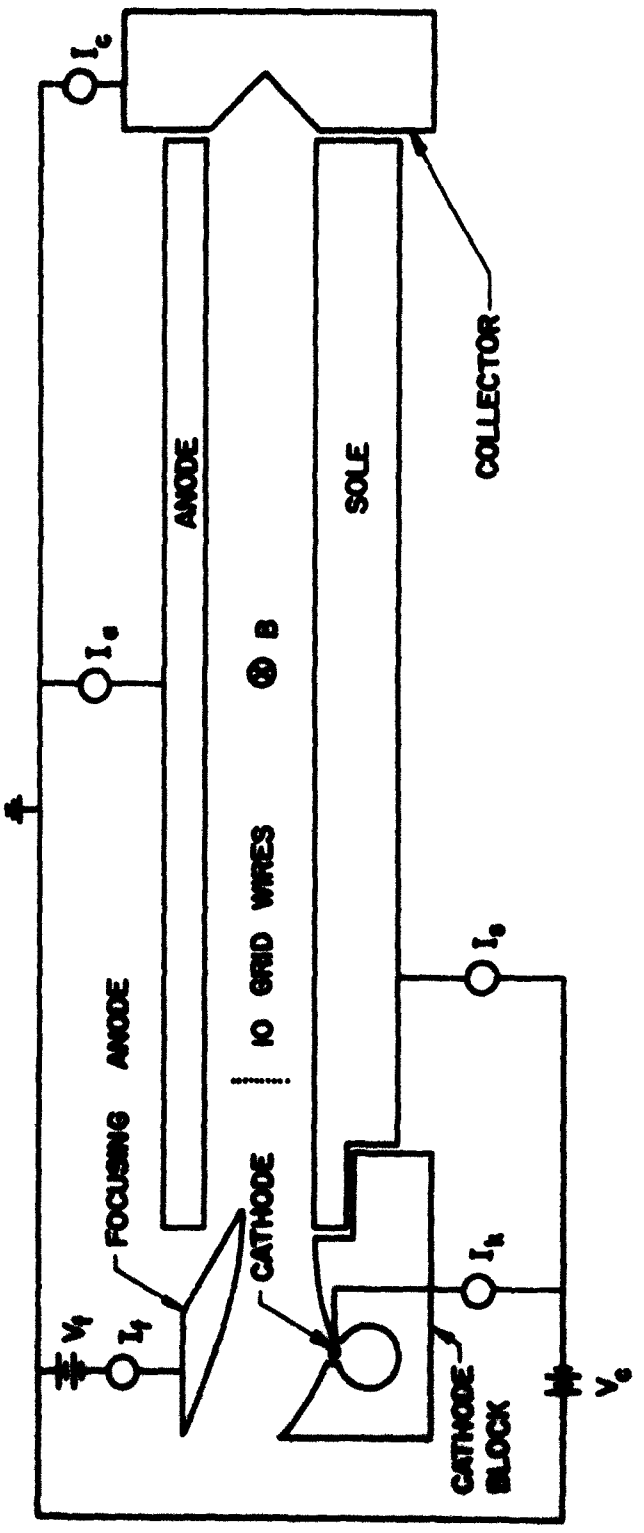

FIG. V.B.1 CIRCUIT DIAGRAM OF THE CROSSED-FIELD BEAM ANALYZER TUBE.

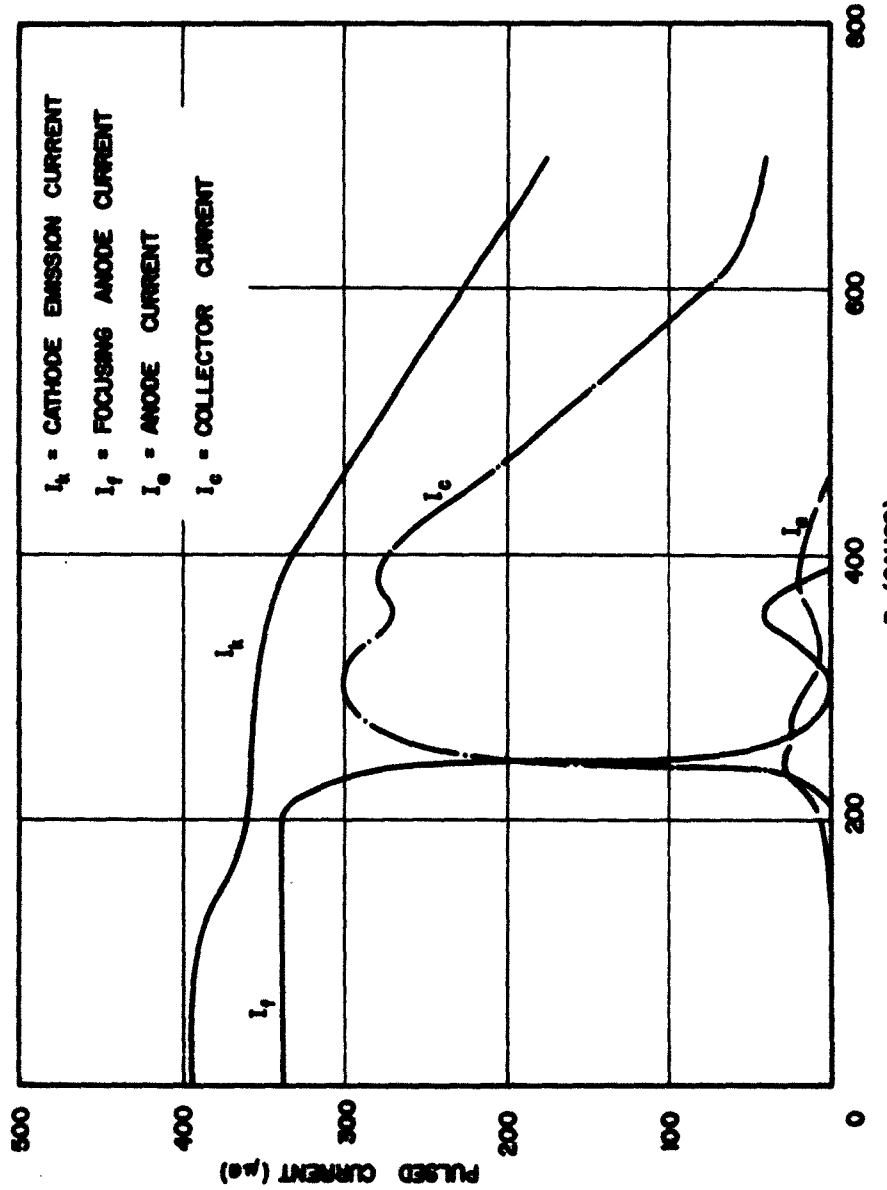

FIG. V.B.2 VARIATION OF CURRENTS WITH MAGNETIC FIELD. NO GRID WIRES IN ANODE-SOLE REGION. (V_c = - 1430, V_f = - 500)

At this same point I_f rises suddenly to assume a relative maximum before dropping off again with increasing B. This strange behavior might be passed over as an experimental error except that it was observed for other values of V_c and V_f.

One explanation for the phenomenon is concerned with the cycloidal type of motion experienced by the electrons in the gun region. As B increases, the curvature of the motion of the electrons becomes greater until eventually their upward trajectories following the first cycloidal minimum causes a portion of the beam to strike the focusing anode. This produces the observed peak in I_f while at the same time it causes I_c to decrease since part of the previously transmitted beam is now being intercepted by the focusing anode.

Figure V.B.3 illustrates the variation of currents with B for V_f = - 750 volts and V_c = - 2010 volts. The results are similar to those described above except that this is one of those cases in which there seems to be no dip in I_c. However, the small peak in I_f is still present for values of B just beyond the maximum I_c point. One reason for the absence of the I_c dip might be the fact that the data points are widely spaced in the vicinity of where the dip should occur. In any case, the results are not sufficiently accurate to determine whether the dip actually exists.

The results for V_f = - 900 volts and V_c = - 2400 volts are shown in Fig. V.B.4 where once again the dip in I_c is present along with the corresponding relative maximum in I_f.

The dependence of various currents on V_c is shown in Figs. V.B.5, V.B.6, and V.B.7 where each case corresponds to different values of V_f and B. The cathode current apparently varies with the square of the

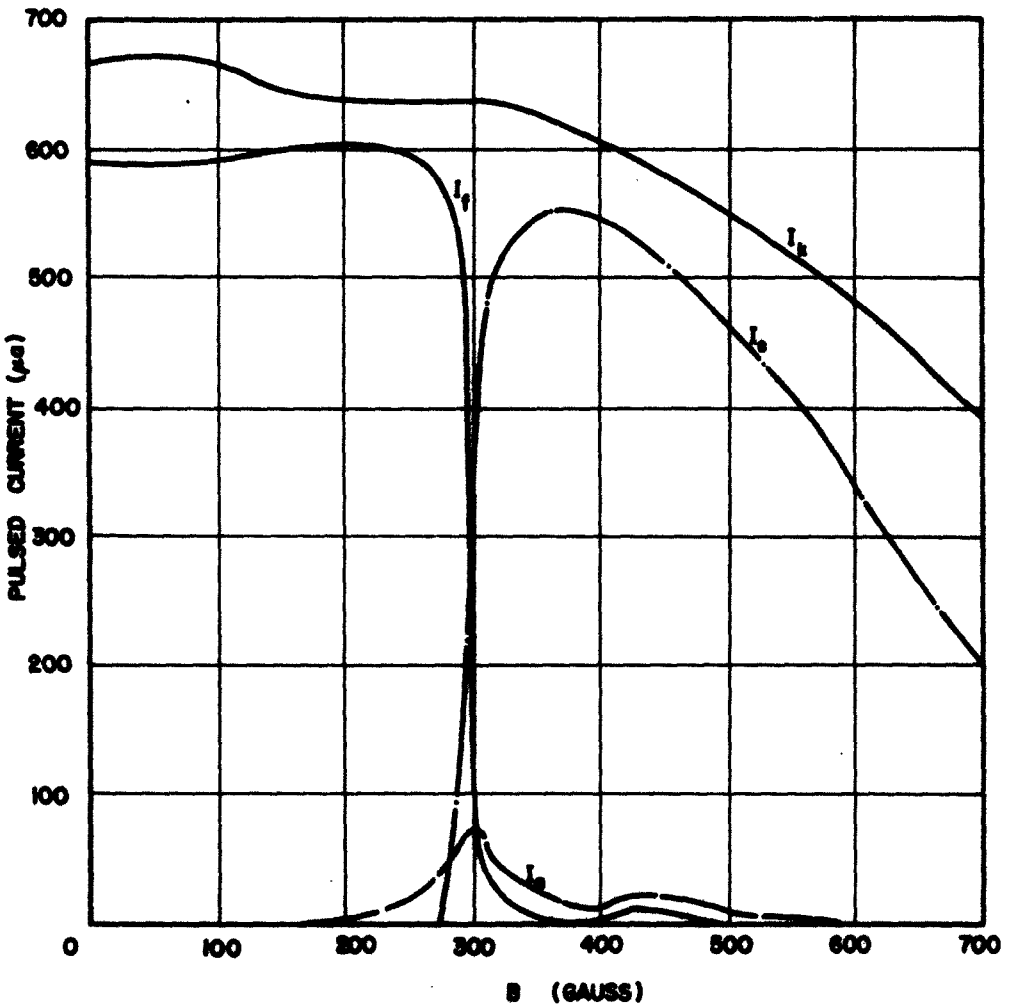

FIG. V.B.3 VARIATION OF CURRENTS WITH MAGNETIC FIELD.

NO GRID WIRES. (V_c = - 2010, V_f = - 750)

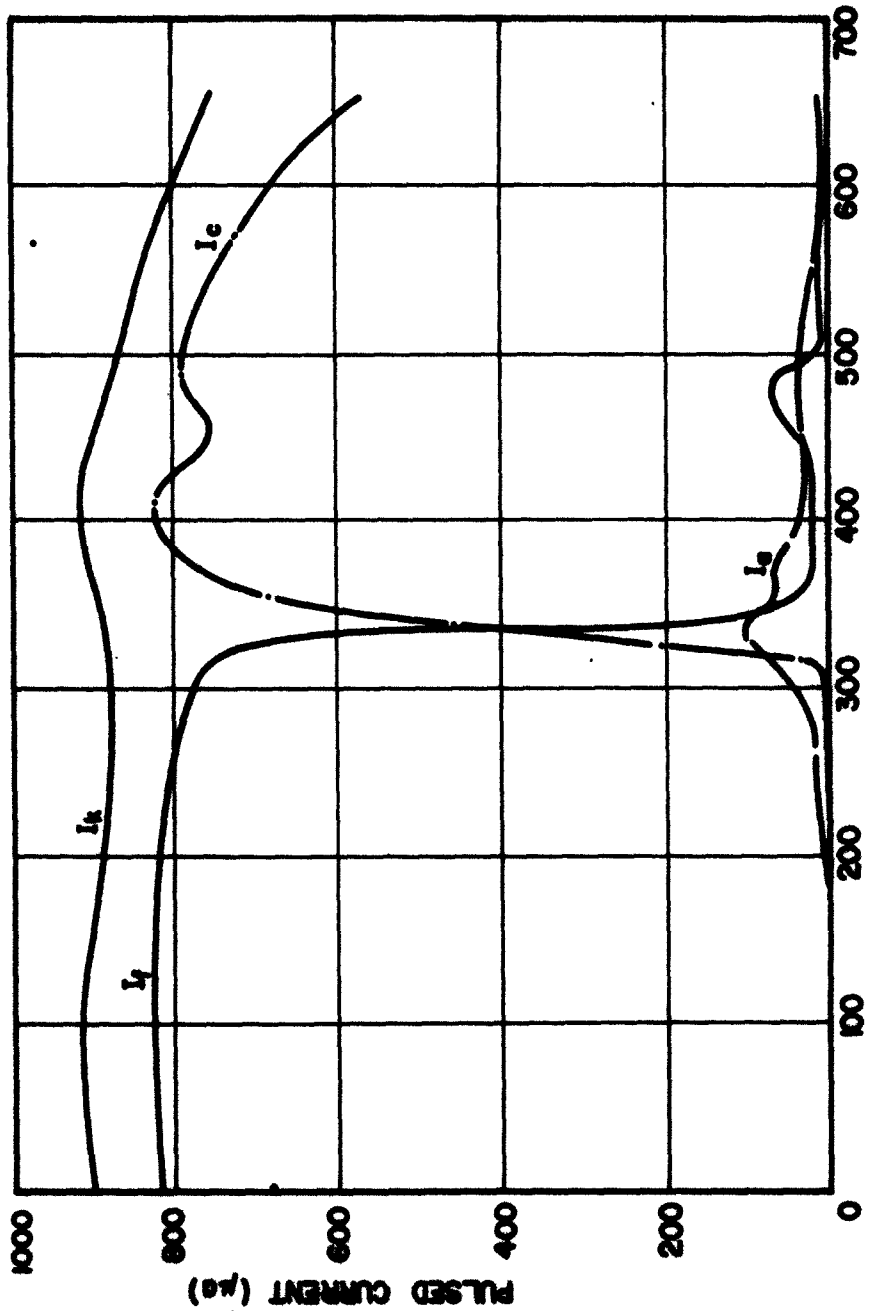

FIG. V.B.4 VARIATION OF CURRENTS WITH MAGNETIC FIELD.

NO GRID WIRES. (V_c = - 2400, V_f = - 900)

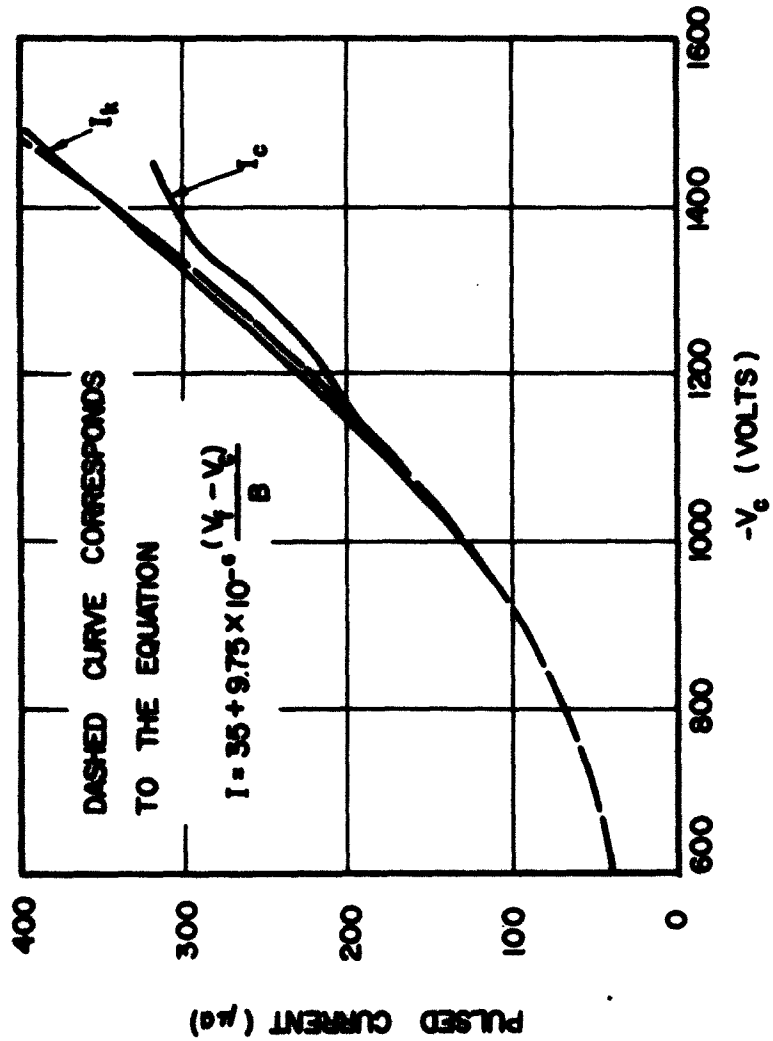

FIG. V.B.5 VARIATION OF CURRENTS WITH V_c. NO GRID WIRES. (V_f = - 500, B = 256 GAUSS)

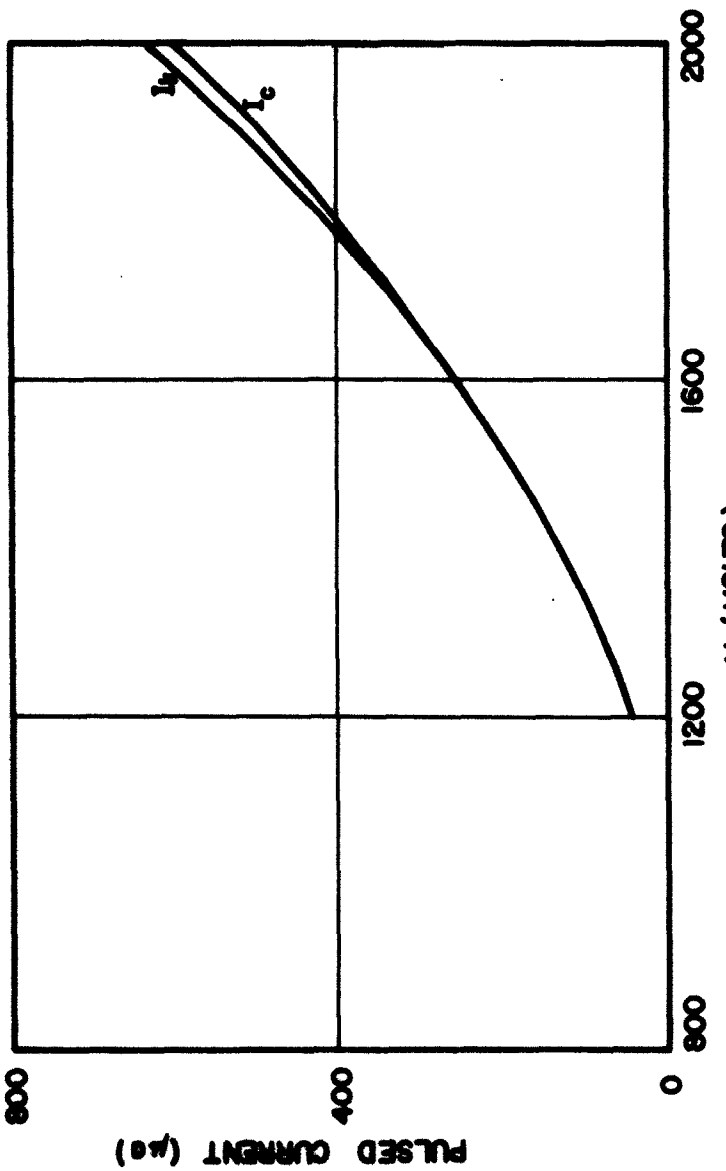

FIG. V.B.6 VARIATION OF CURRENTS WITH V_c. NO GRID WIRES. (V_f = - 750, B = 419)

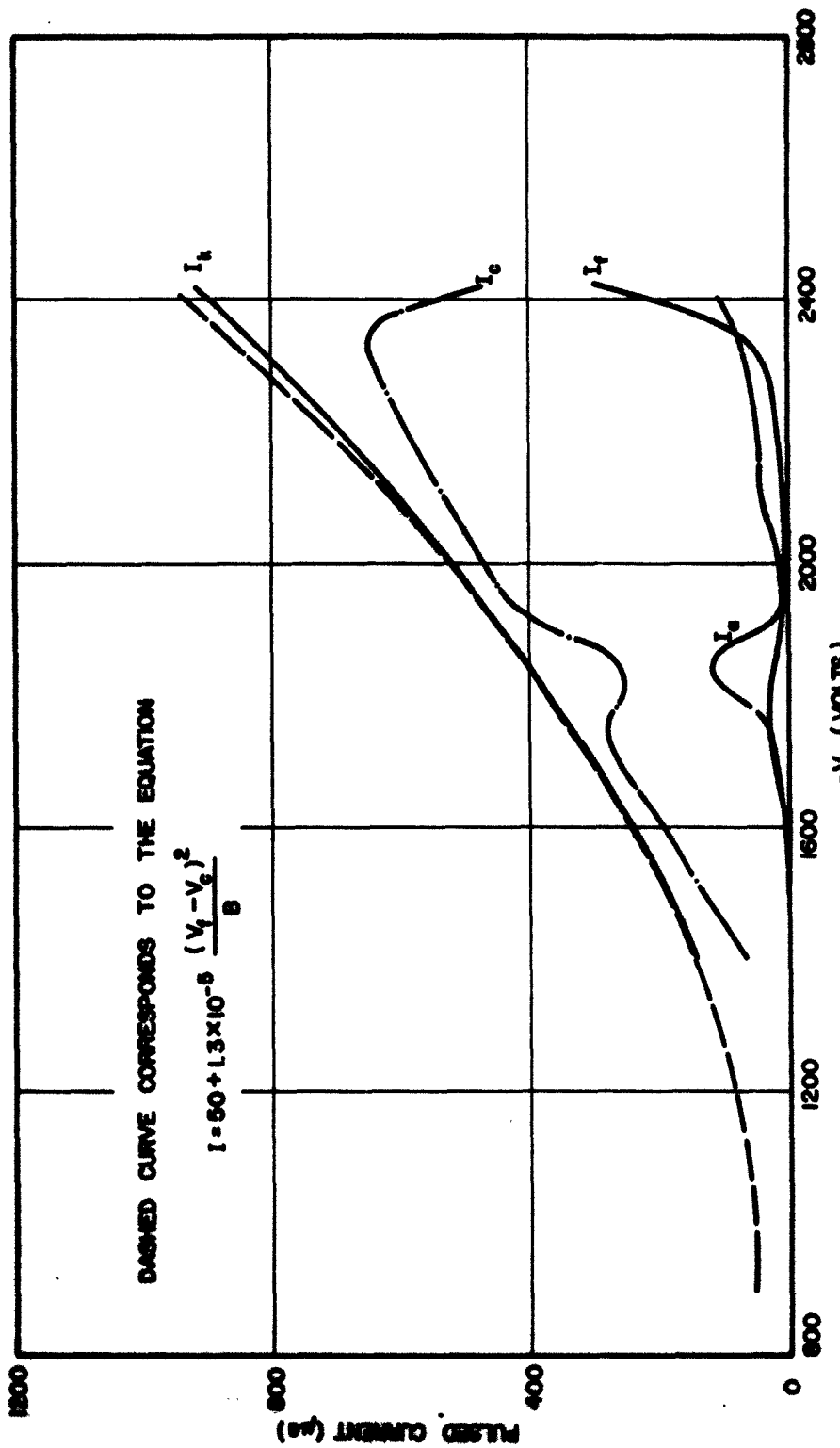

FIG. V.B.7 VARIATION OF CURRENTS WITH MAGNETIC FIELD.

NO GRID WIRES. (V_f = - 900, B = 335)

voltage difference between the cathode and focusing anode. This is illustrated in Figs. V.B.5 and V.B.7 where parabolic curves (dashed curves) have been plotted according to the evaluation

$$I = C + K\frac{(V_f-V_c)^2}{B} \qquad \text{(V.B.1)}$$

with C and K as constants. This type of variation agrees with that observed by other experimenters[1,2] using simpler types of electron guns. Midford[3] at Stanford has stated that I_k varies linearly with (V_f-V_c) for the Kino short gun, but this variation is valid only in the vicinity of the design value of (V_f-V_c). On the other hand, he shows that the long gun has a $(V_f-V_c)^2/B$ variation for the cathode current.

There has been no attempt to critically evaluate the constants (C and K) appearing in Eq. V.B.1 and in fact different values were used in plotting the two parabolic curves mentioned above. However, Fig. V.B.8 illustrates a situation similar to Fig. V.B.5 except for an increase in B to 315 gauss. The equation used to plot the parabola of Fig. V.B.5 was also used to obtain the curve illustrated in Fig. V.B.8. Once again the agreement between experimental points and the theoretical parabola is reasonably good. This suggests that the cathode current varies with $(V_f-V_c)^2/B$ over a fairly wide range of voltages.

---

1. Miller, M. H., "Study of High Temperature Electrons Originating in Streams Flowing in Crossed D-c Electric and Magnetic Fields", Tech. Rpt. No. 26, Electron Tube Laboratory, The University of Michigan; July, 1958.

2. Epstein, B., "Effects de la Charge D'espace sun les Faisceaux Electroniques Minces", Ph.D. thesis, University of Paris; 1957.

3. Midford, T. A., "Some Experiments with New Types of Crossed-Field Electron Guns", Scientific Report No. 36, Stanford University; February, 1962.

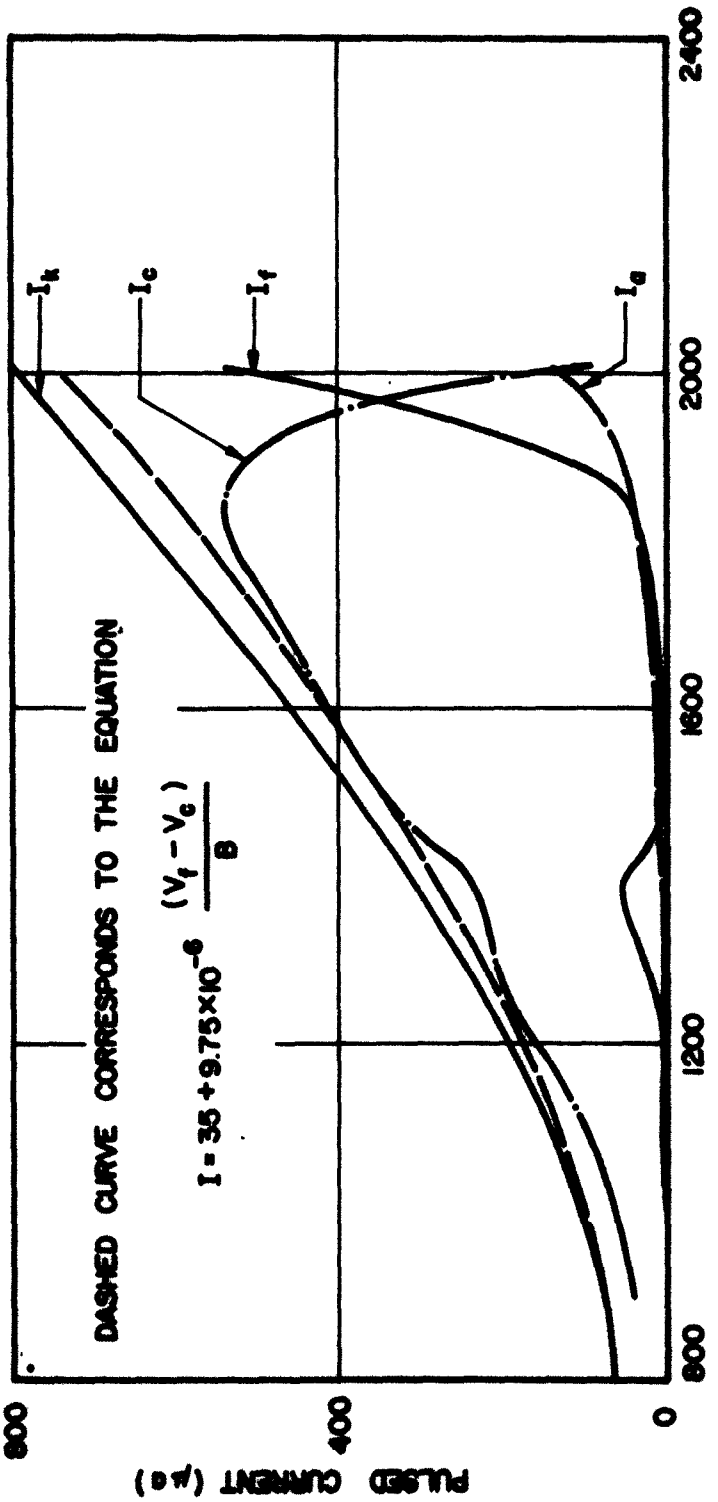

FIG. V.B.8 VARIATION OF CURRENTS WITH V_c, NO GRID WIRES. (V_f = - 500, B = 315)

b. Investigation with Grid Wires in the Interaction Region. Following the above tests, the grid wire assembly was mounted in place and several experiments were performed to more fully evaluate the distortion caused by the wires. The first data was obtained with the grid assembly located at a distance of z = 0.025 inch from the gun exit plane and with V_f = - 500 volts and V_c = - 1450 volts. The cathode current, collector current and total grid wire currents were plotted as the magnetic field was varied. The solid curves of Fig. V.B.9 illustrate the variations of I_k and I_t where I_t is defined as the sum of the collector current and all of the grid wire currents. I_t should provide a reasonable comparison with the current going to the collector (I_c) when there are no grid wires present (as in Section a above). The dashed curves correspond to the case with no grids present. For B < 350 gauss, the general variation of I_c and I_t are quite similar, at least as good as could be expected in view of the fact that the cathode block had to be removed to allow insertion of the grid wires. Obviously, it is impossible to relocate the block in exactly the same position as it previously occupied and hence it is difficult to obtain identical results. In a like manner it is difficult to explain the smaller values of I_k after the grid assembly was placed in the interaction region.

Figures V.B.10 and V.B.11 show similar results for different V_f and V_c. The I_t and I_c curves seem to differ more than they did in Fig. V.B.9, but much of this can be attributed to greater derivations in the corresponding I_k curves. A more realistic comparison of the various situations are shown in Figs. V.B.12, V.B.13, and V.B.14 which contain plots of percent transmission (i.e., $I_c \times 100/I_k$ or $I_t \times 100/I_k$) against B. These figures indicate that the various curves are more similar, at

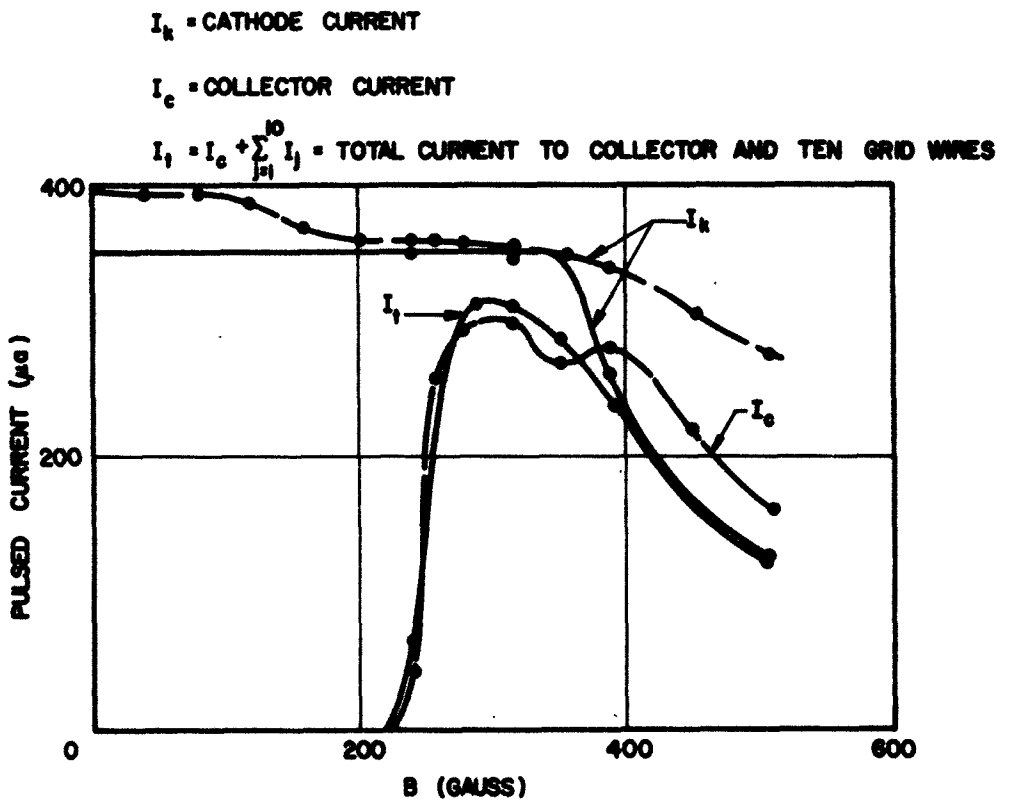

FIG. V.B.9 COMPARISON OF THE CURRENT VARIATIONS WITH MAGNETIC FIELD. DASHED AND SOLID CURVES CORRESPOND RESPECTIVELY TO THE ABSENCE AND PRESENCE OF GRID WIRES. (V_f = - 500, V_c = - 1450)

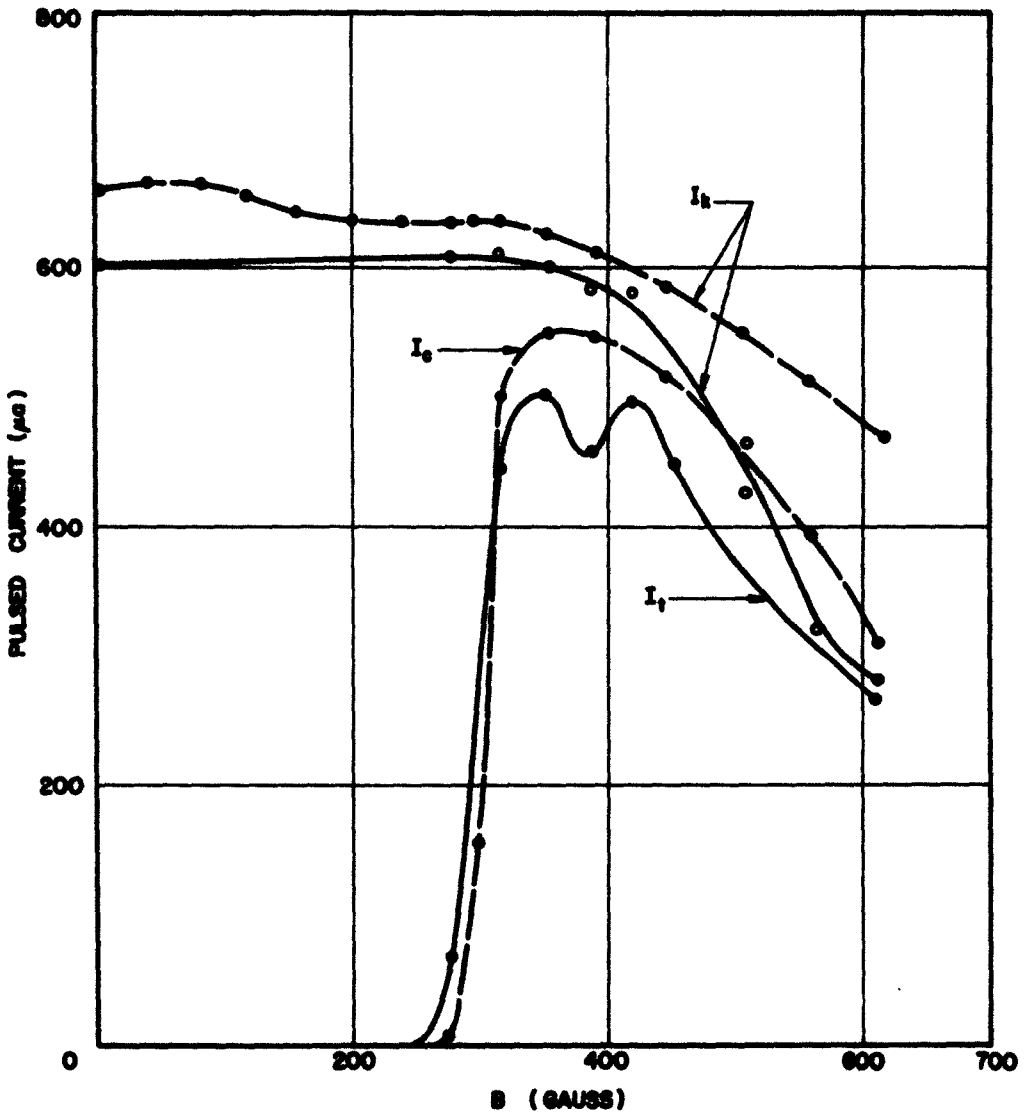

FIG. V.B.10 COMPARISON OF CURRENT VARIATION. DASHED AND SOLID CURVES CORRESPOND RESPECTIVELY TO ABSENCE AND PRESENCE OF GRID WIRES. (V_f = - 750, V_c = - 2010)

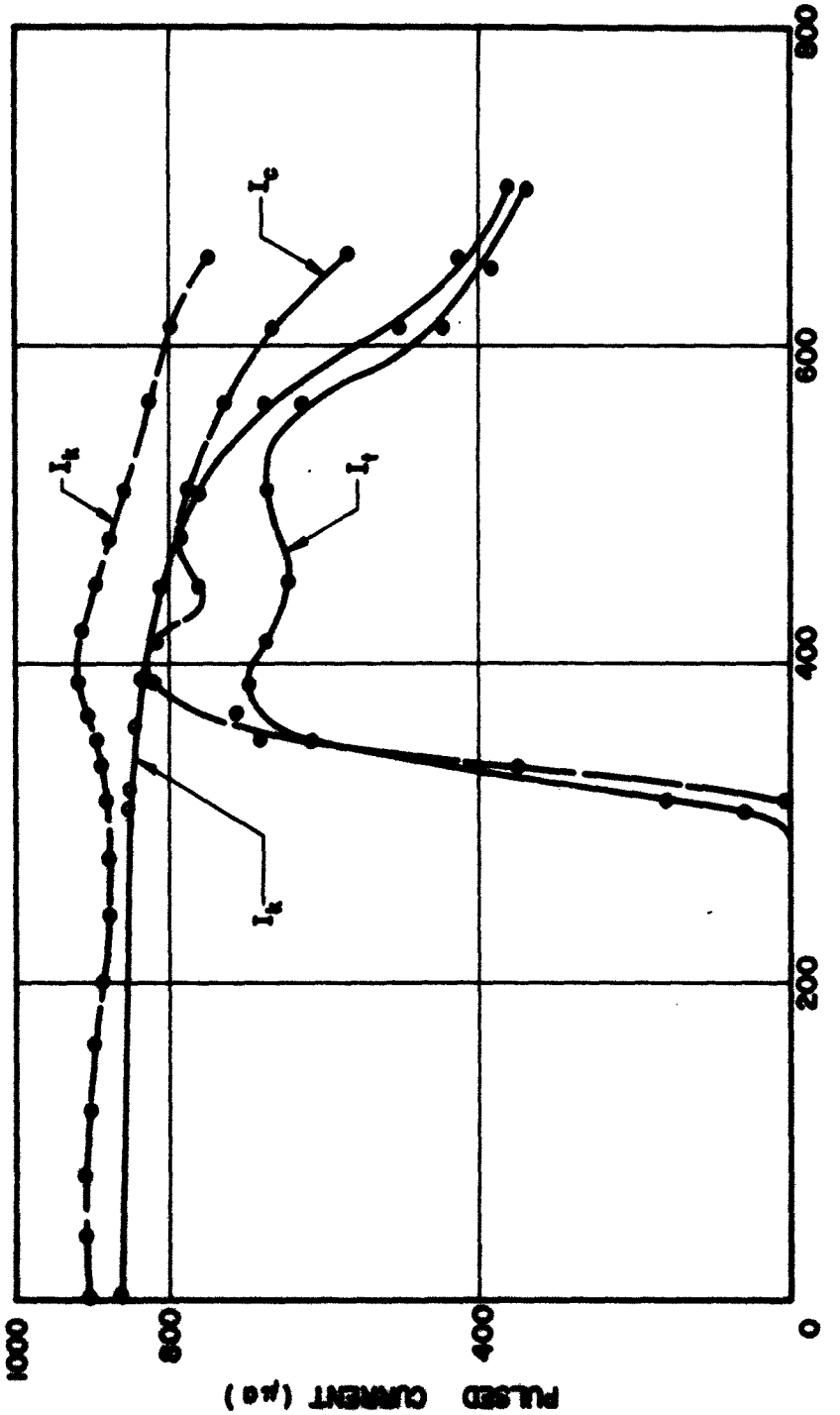

FIG. V.B.11 COMPARISON OF CURRENT VARIATIONS, DASHED AND SOLID CURVES CORRESPOND RESPECTIVELY TO ABSENCE AND PRESENCE OF GRID WIRES. (V_f = - 900, V_c = - 2400)

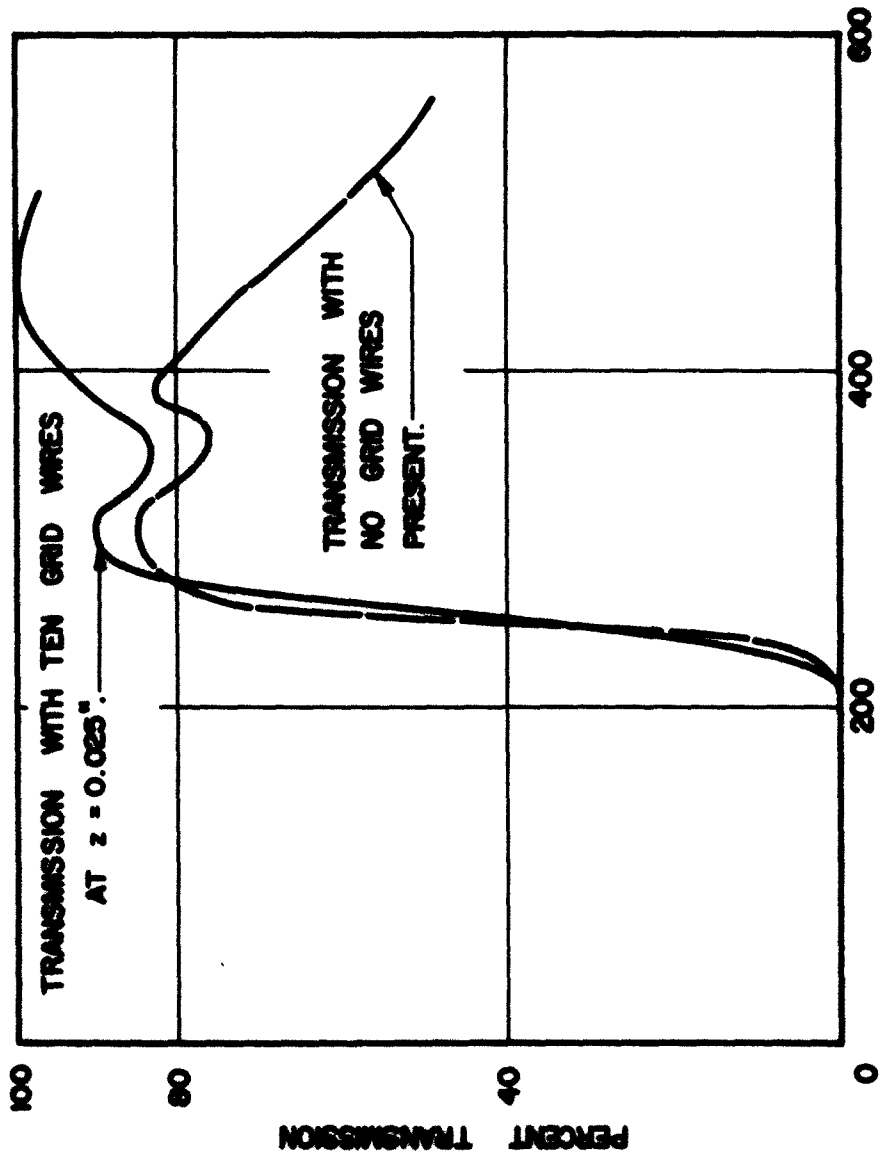

FIG. V.B.12 COMPARISON OF TRANSMISSION WHEN MAGNETIC FIELD IS VARIED.

(V_f = - 500, V_f = - 1430)

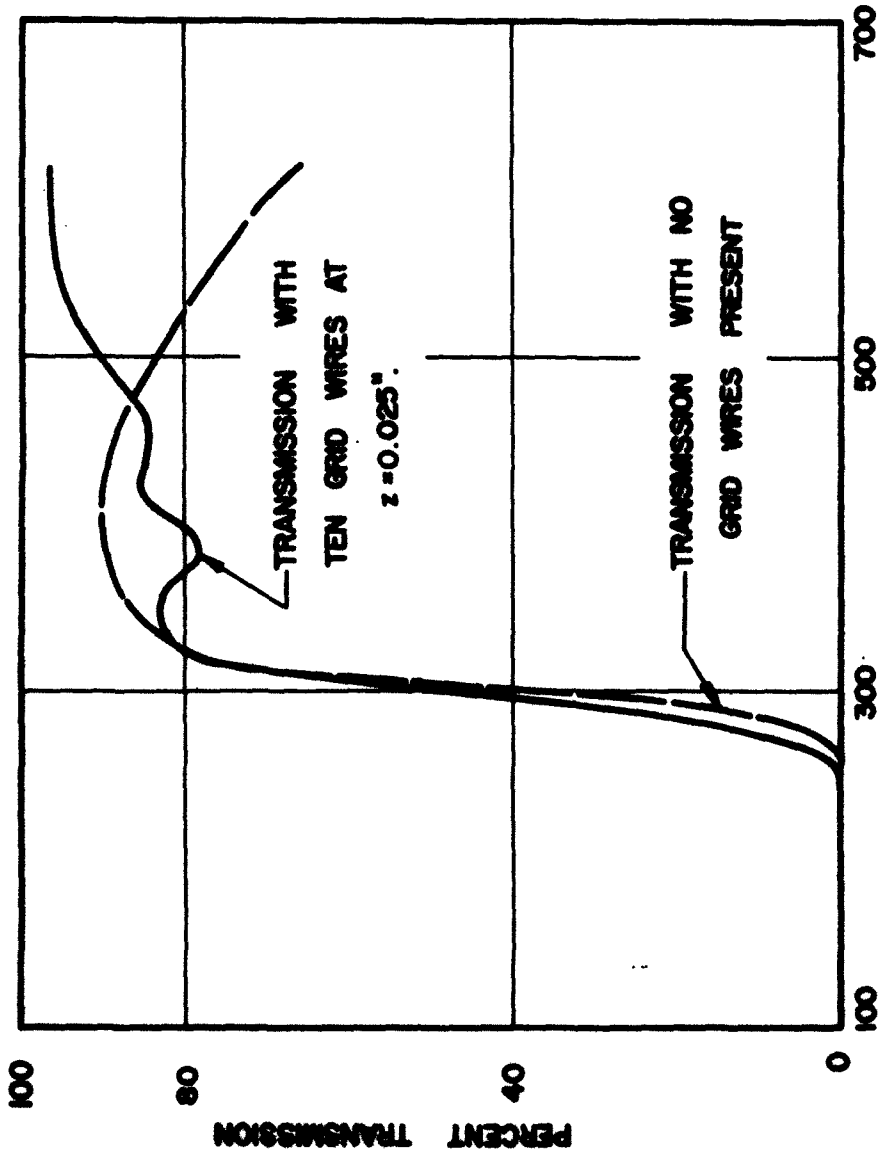

FIG. V.B.13 COMPARISON OF TRANSMISSION CHARACTERISTICS.

(V_f = - 750, V_c = - 2010)

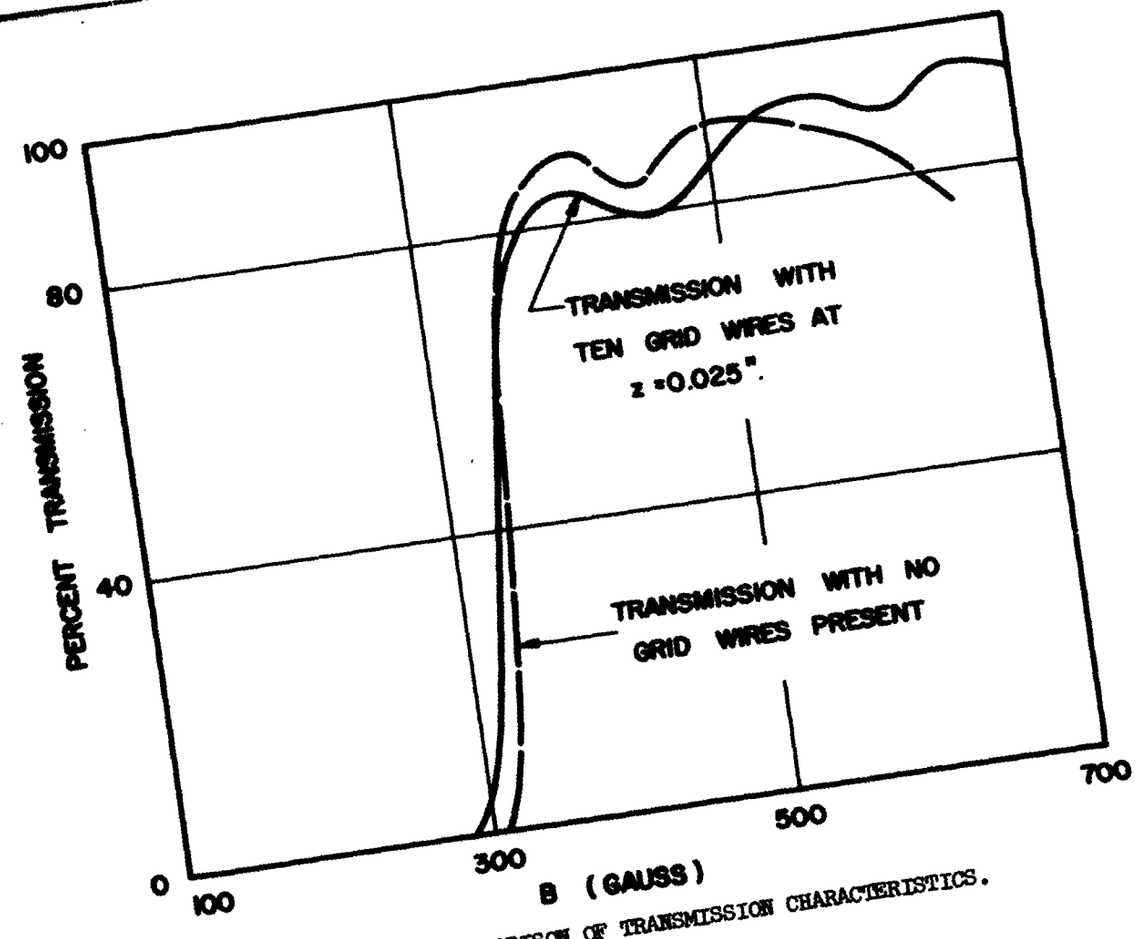

FIG. V.B.14 COMPARISON OF TRANSMISSION CHARACTERISTICS.

(V_f = - 900, V_c = - 2400)

least for lower values of magnetic field. However, at higher B values the results definitely do not agree, indicating that high magnetic field conditions are not conductive to accurate measurements by the grid system. Nevertheless, values of B near which maximum transmission is produced lead to reasonable agreement in the two situations. It is also interesting to observe that the previously mentioned dip in the I_c vs. B plot still occurs when the grid wires are intercepting the beam.

The beam profiles illustrated in the previous report were obtained under conditions where wires 1 and 2 were shorted to the sole and wire 4 was shorted to wire 5. These problems were corrected and additional tests have been performed to investigate the current intercepting characteristics of the grid structure. Figure V.B.15a shows the profile at various z locations along the anode-sole region for V_c = - 1890 volts and B = 409 gauss. The solid curves are for V_f = - 1100 volts and the dashed ones for V_f = - 1000 volts. Part b of this figure illustrates the y-location of the maximum current interception at each z-position of the grid structure. The theoretical cycloidal length for this case is

$$L_{th} = 0.486 \text{ inch} ,$$

which agrees closely with the experimental values of 0.482 and 0.495 inch indicated on the figure. The change in focusing anode voltage from - 1100 to - 1000 volts apparently was responsible for making the beam more laminar as indicated by the reduced amplitude of the maximum current interception curve.

The results for V_f = - 850 volts, V_c = - 2210 volts, and B = 590 gauss are shown in Figs. V.B.16 a and b. The application of such a high magnetic field caused the beam to travel closer to the sole as attested by the fact that the maximum current in the beam was generally located

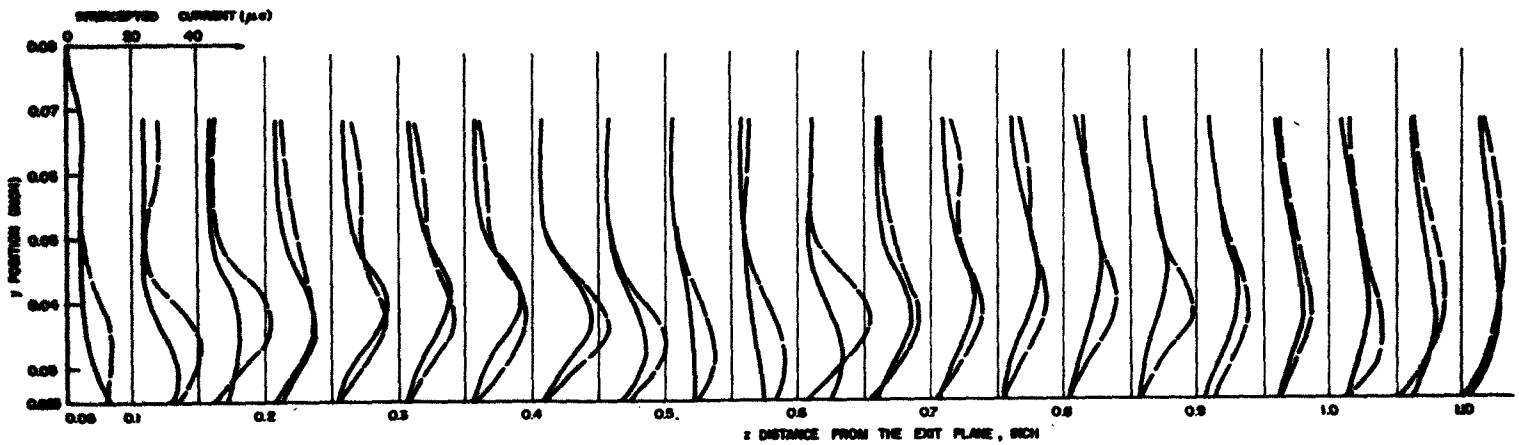

FIG. V.B.15a CURRENTS INTERCEPTED BY THE GRID WIRES AT VARIOUS CROSS SECTIONS IN THE INTERACTION REGION. (V_c = - 1890, B = 409 GAUSS)

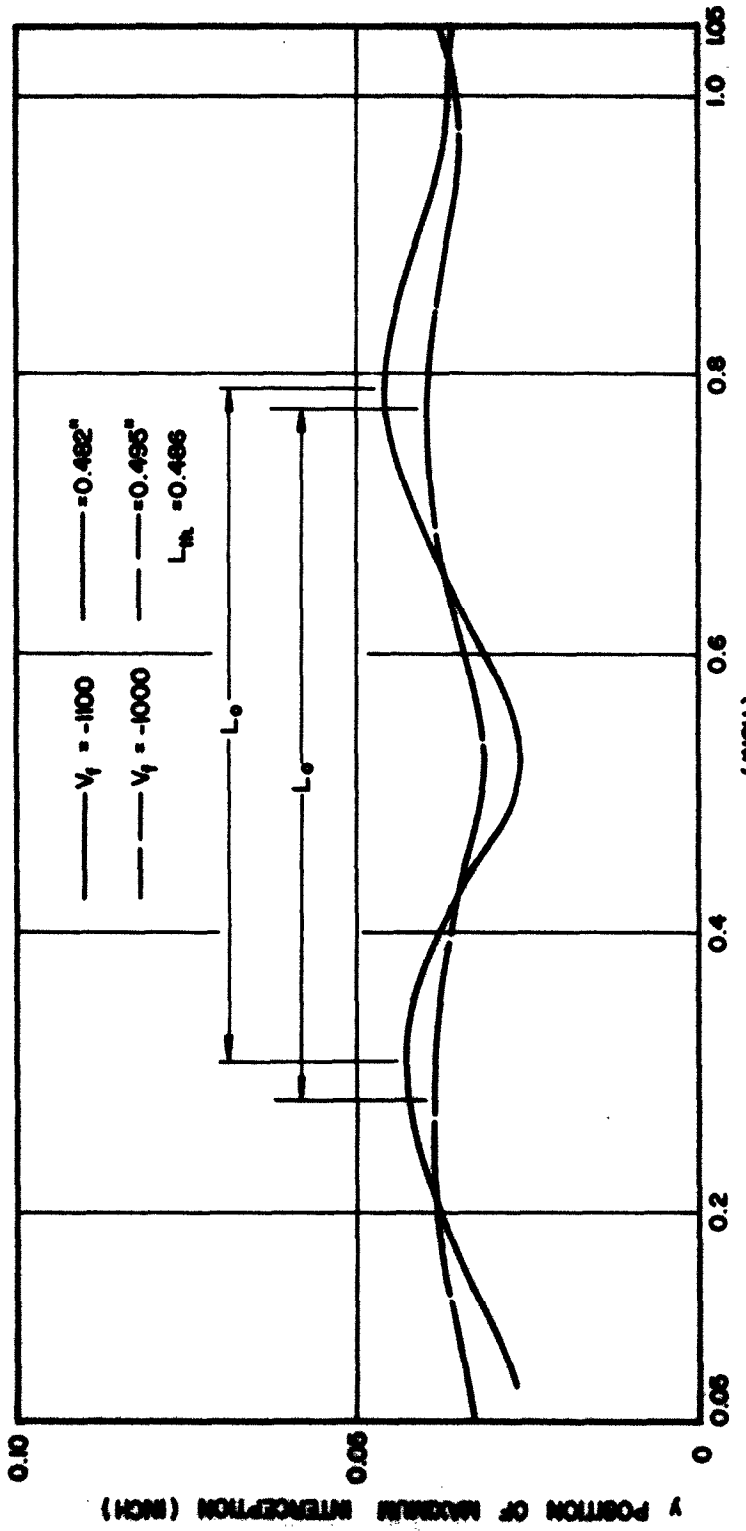

FIG. V.B.15b LOCATION OF MAXIMUM CURRENT INTERCEPTION AT VARIOUS z POSITIONS. (V_c = - 1890, B = 409 GAUSS)

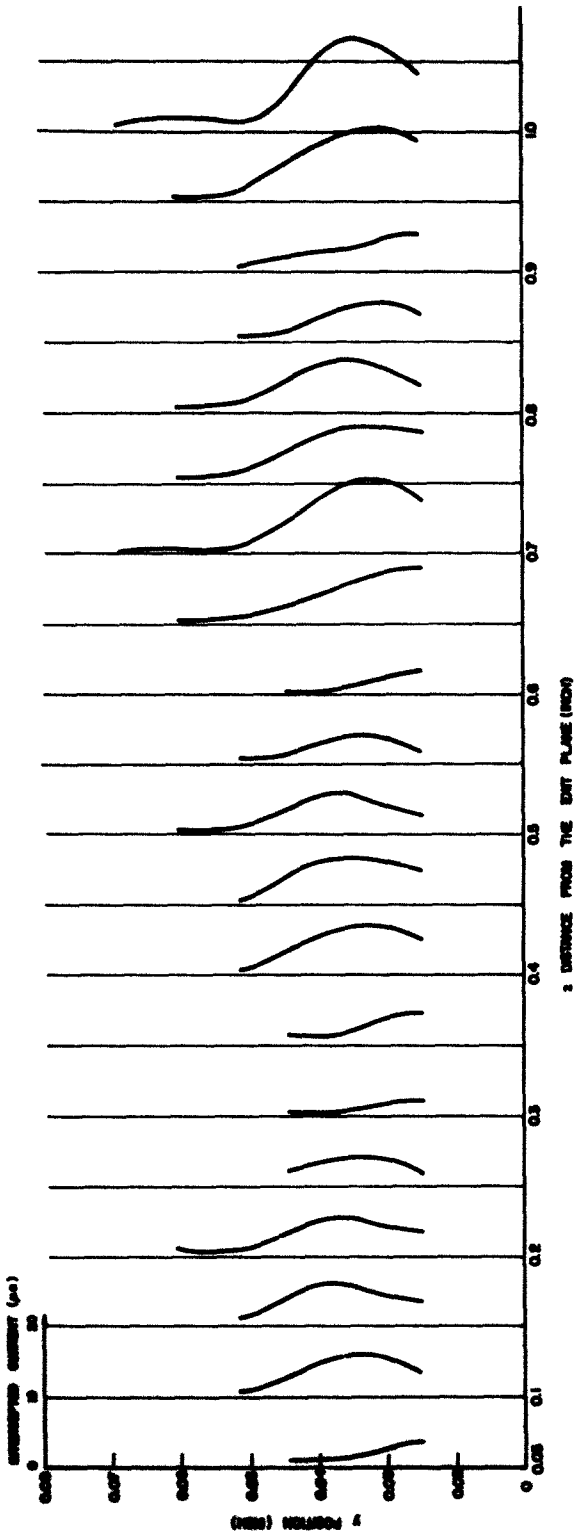

FIG. V.B.16a CURRENTS INTERCEPTED BY THE GRID WIRES AT VARIOUS CROSS SECTIONS IN THE INTERACTION REGION. (V_c = - 220, V_f = - 850, B = 590 GAUSS)

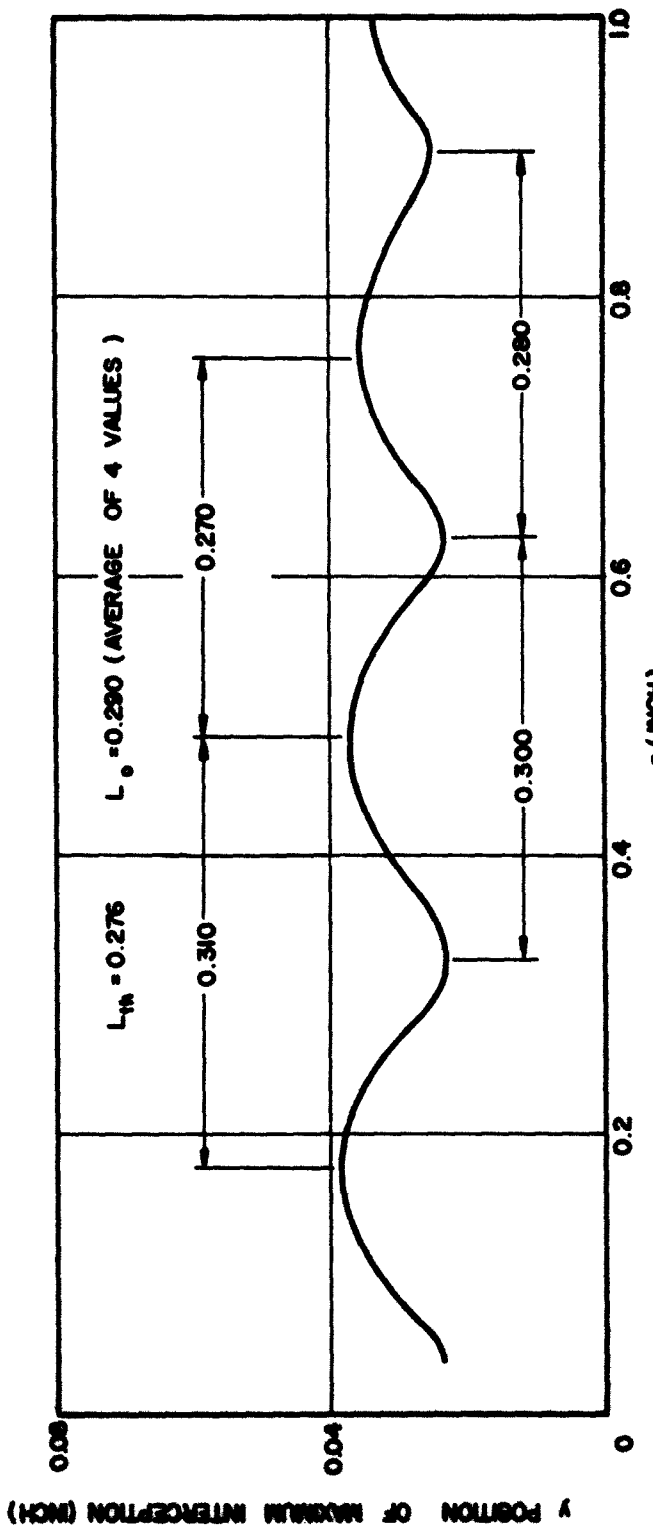

FIG. V.B.16b LOCATION OF MAXIMUM CURRENT INTERCEPTION AT VARIOUS z POSITIONS. (V_c = - 2210, V_f = -850, B = 590 GAUSS)

in the vicinity of the bottom two wires (wires 1 and 2). Four ways of measuring the cycloidal length are shown in part b and the average of these measurements gives L_o = 0.290 inch which agrees quite well with L_{th} = 0.276 inch.

An attempt was made to evaluate the effect of electrically removing nine of the wires from external voltages and monitoring the current to the remaining grid wire, number 4. However, as the beam started passing through the grid, the wires began to vibrate rapidly and eventually their motion became great enough to cause arcing between adjacent members. The breakdown was apparently caused by the accumulation of surface charge on the wires as the pulsed beam passed through the grid. The induced charge then reacted to the charge on the other wires and in the beam. The mutual repulsion of the charges caused the wires to start vibrating and as the motion continued the wires came close enough together to allow breakdown to occur. After the beam was first transmitted into the interaction region it was observed that the time required to initiate the arcing depended on the value of V_c and hence on the total current passing through the wires. This is in agreement with the theory that the mutual repulsion of induced charges causes the vibration. Thus increasing the beam current causes a faster accumulation of charge on the wires and this leads to faster arcing between wires.

Although nine grid wires could not simultaneously be removed from the circuit, it was possible to observe the effects of isolating one wire. Figures V.B.17 a and b illustrate the beam profile and maximum interception variation for V_f = - 500 volts, V_c = - 1425 volts, B = 352 gauss and all ten grid wires in the circuit. These results can be compared with those of Figs. V.B.18 a and b wherein V_c has been increased to - 1490

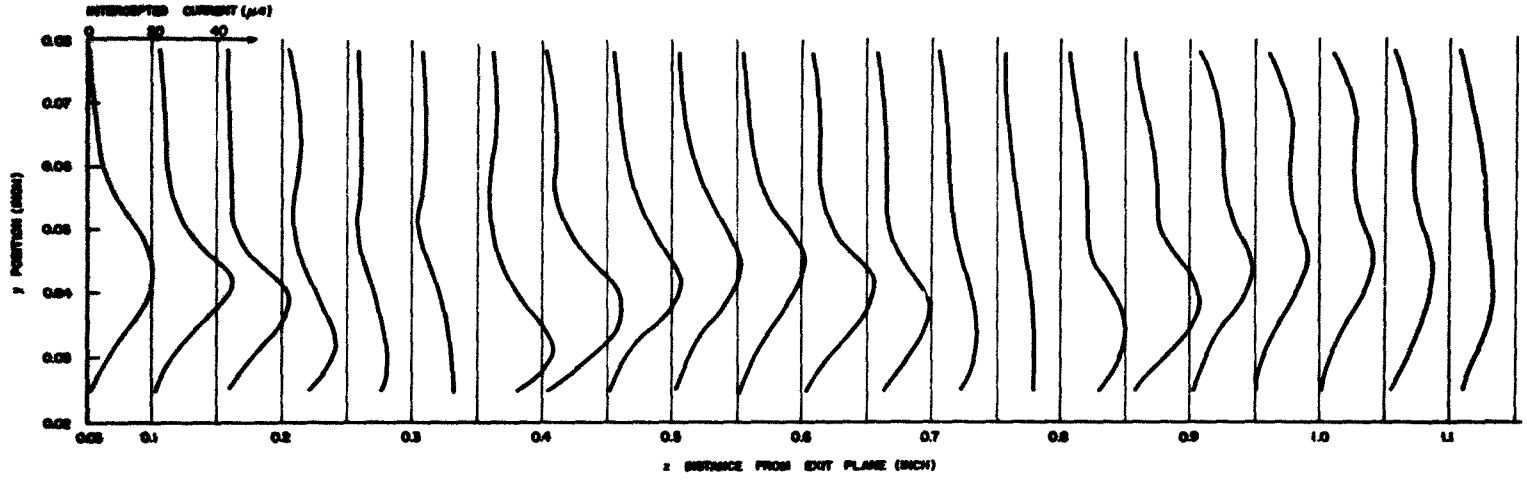

FIG. V.B.17a CURRENTS INTERCEPTED BY THE GRID WIRES AT VARIOUS CROSS SECTIONS IN THE INTERACTION REGION. (V_c = - 1425, V_f = - 500, B = 352 GAUSS)

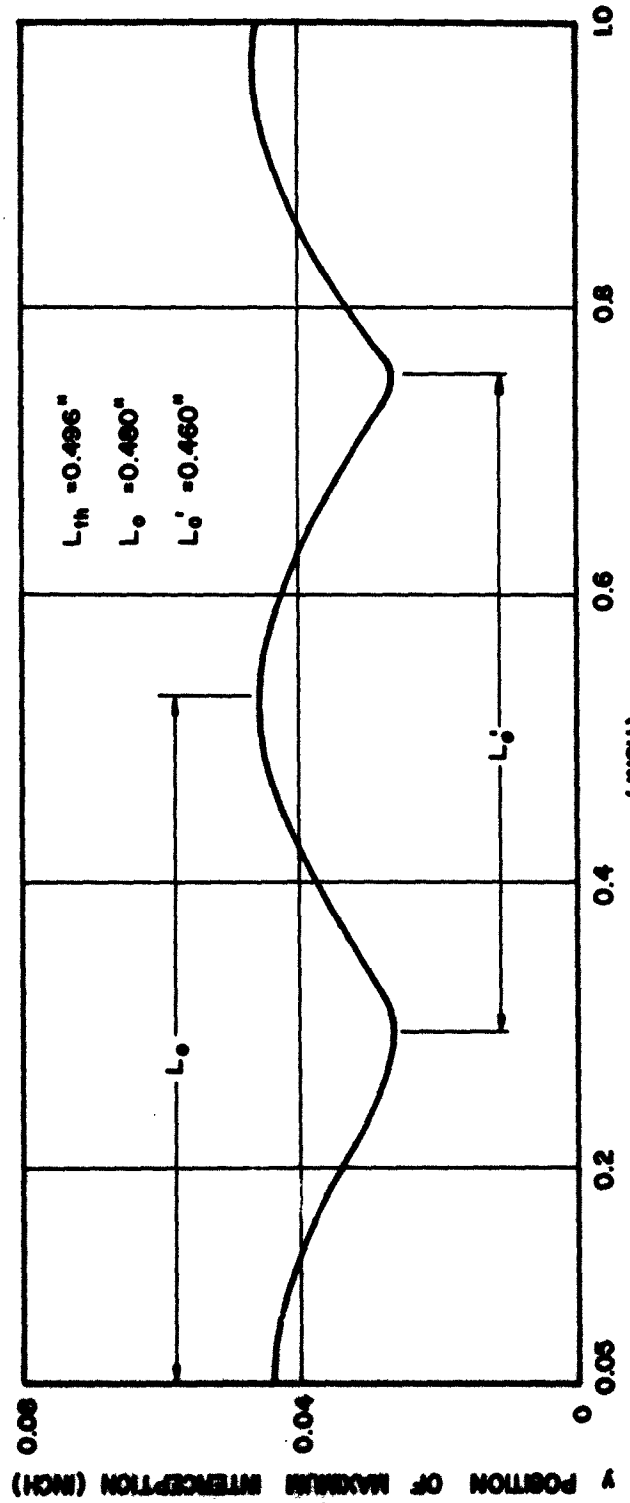

FIG. V.B.17b LOCATION OF MAXIMUM CURRENT INTERCEPTION AT VARIOUS z POSITIONS. (V_c = - 1425, V_f = - 500, B = 352 GAUSS)

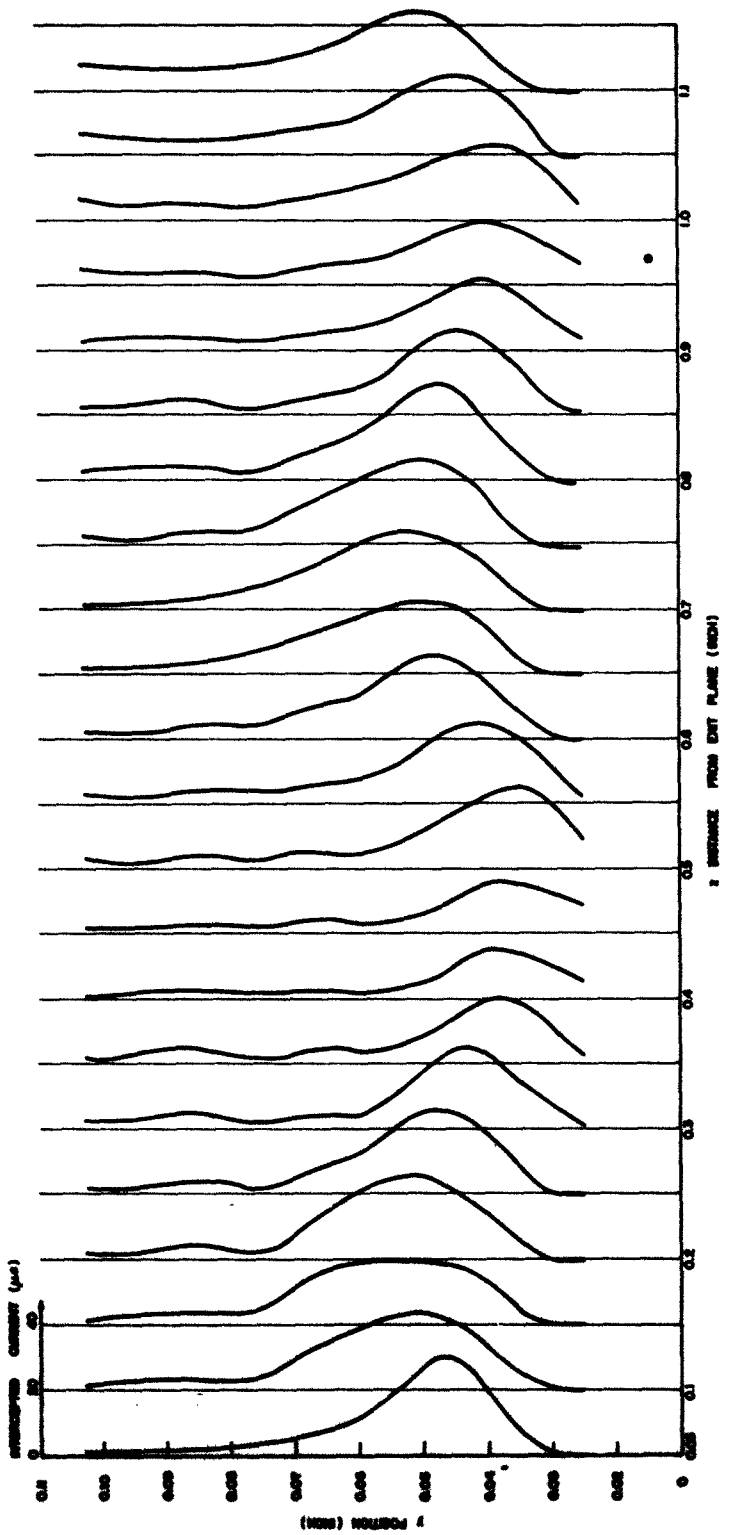

FIG. V.B.18a. CURRENTS INTERCEPTED BY THE GRID WIRES AT VARIOUS CROSS SECTIONS OF THE INTERACTION REGION WITH WIRE NO. 4 DISCONNECTED. (V_c = - 1490, V_f = - 500, B = 352 GAUSS)

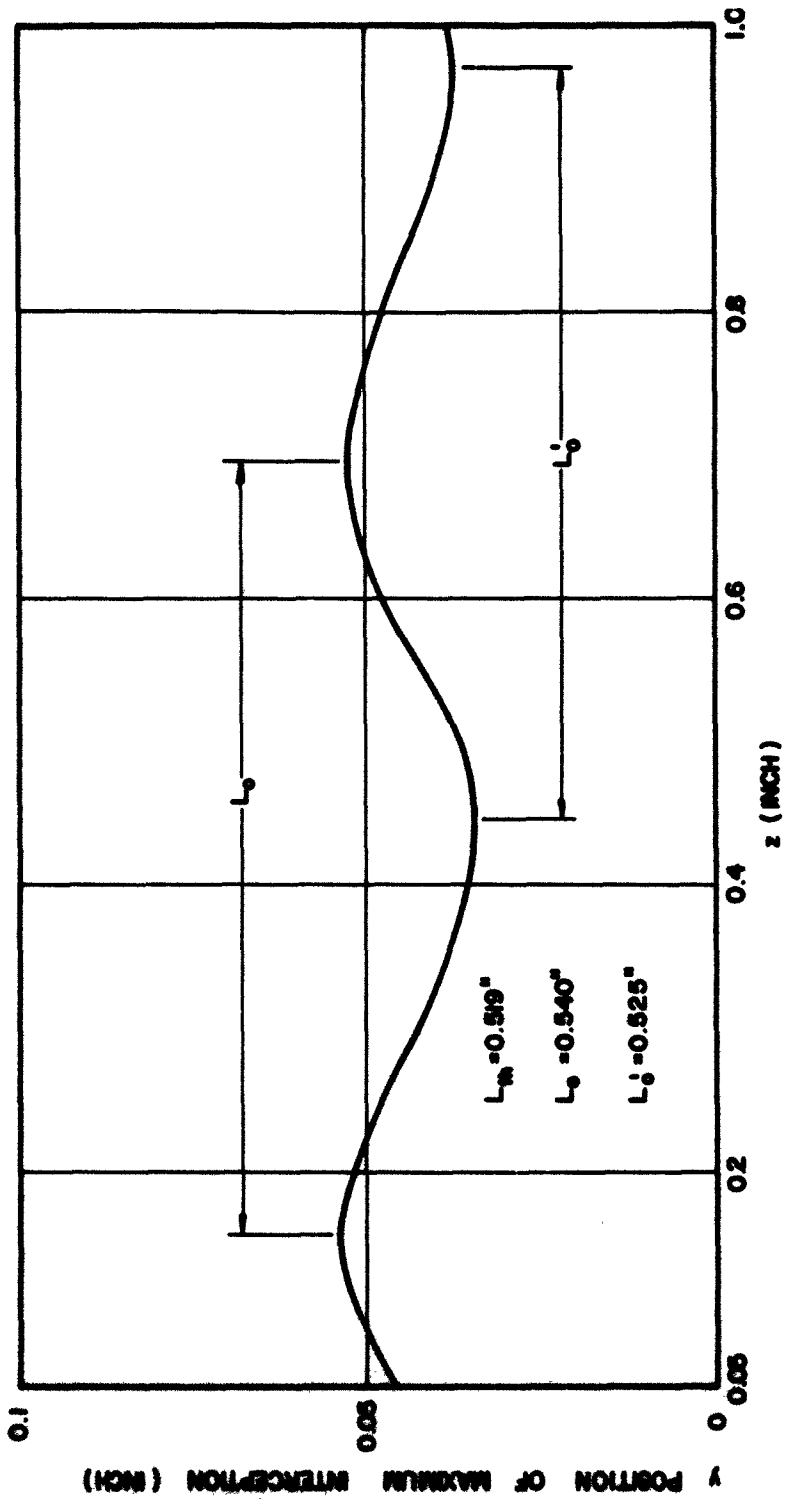

FIG. V.B.18b LOCATION OF MAXIMUM CURRENT INTERCEPTION AT VARIOUS z POSITIONS WITH WIRE NO. 4 DISCONNECTED. (V_c = - 1490, V_f = - 500, B = 352)

volts and wire 4 has been disconnected. The net effect of these two changes is to cause wire 3 to receive more current and to raise the y-location of the maximum current in the beam. Once again the theoretical and experimental cycloidal lengths agree quite well in both cases.

Figure V.B.19 shows a more detailed investigation of the current intercepted by grid wire 3 (I_3) both in the presence and absence of wire 4. The experimental points were obtained by moving the grid along the z-axis in increments of 0.01 inch and reading I_3 at each point. Interestingly enough, the variation of I_3 for each case is the same except that the magnitude of the intercepted current is greater when the fourth wire is disconnected. The experimental value of the cycloidal length is obtained by measuring the distance between alternate peaks rather than adjacent peaks of the intercepted current. The fact that L_o must be measured in this fashion can be easily explained by considering the peak of the beam profile to be located at wire 3 when the grid assembly is at z_o. As the grid moves along the z-axis the peak moves below wire 3, and I_3 decreases. Eventually the peak reaches a minimum y-location and moves back up until reaching wire 3 at which time I_3 again becomes a maximum. However, this z travel has not constituted a complete cycloid. Moving the grid further in the z-direction causes the maximum point in the beam to rise above wire 3, reach a maximum y-location and then return until reaching 3 again. This now is a complete cycloid and continued z travel of the grid would reproduce the above I_3 variation. Figure V.B.20 graphically illustrates the above discussion. The cycloidal curve describes the variation of the maximum profile point along the z-axis with the shaded area representing the rest of the beam. The straight line represents the motion of the third wire as the grid is moved. Thus it is

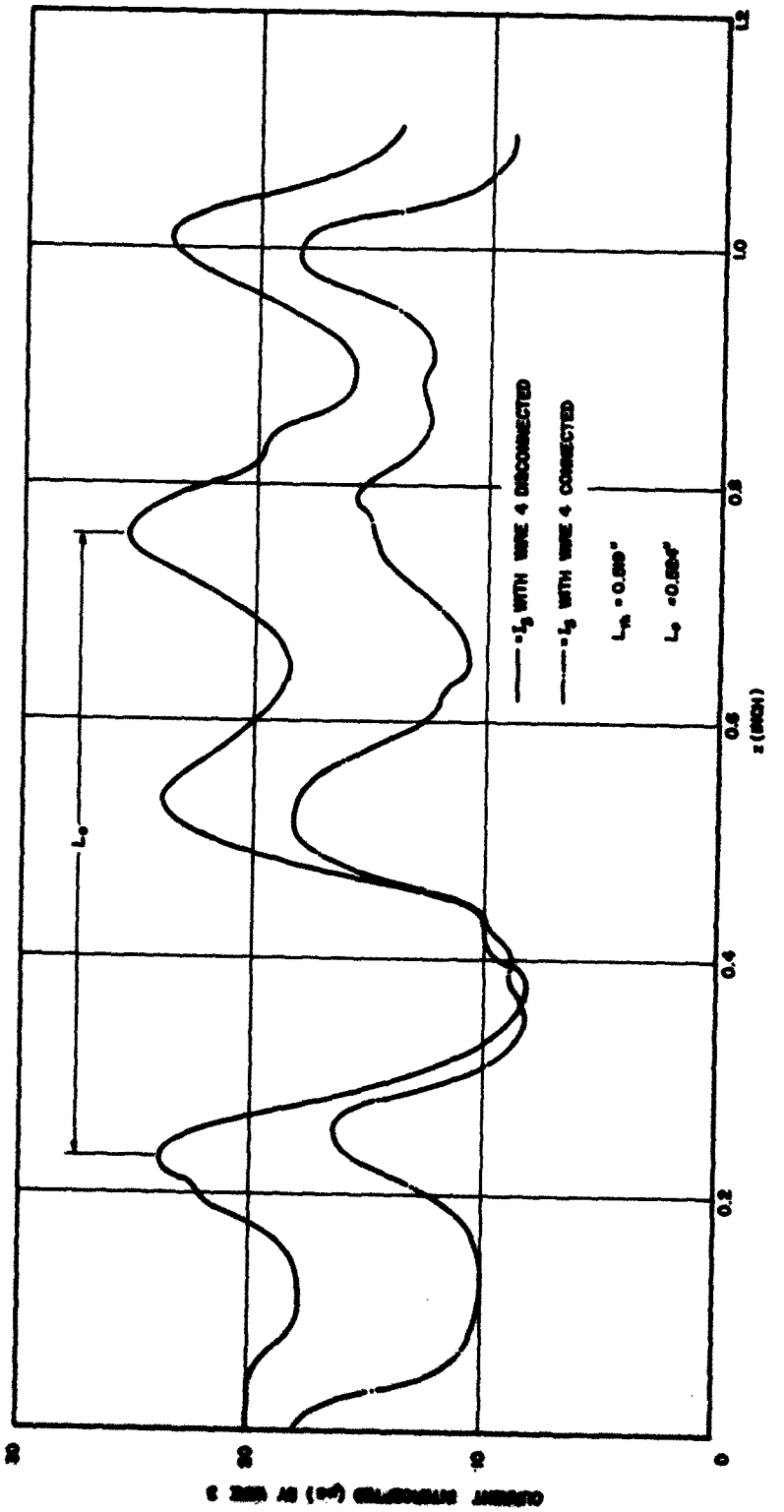

FIG. V.B.19 COMPARISON OF THE CURRENTS INTERCEPTED BY WIRE 3 WHEN WIRE 4 IS CONNECTED AND DISCONNECTED. (V_c = - 1490, V_f = - 500, B = 352 GAUSS)

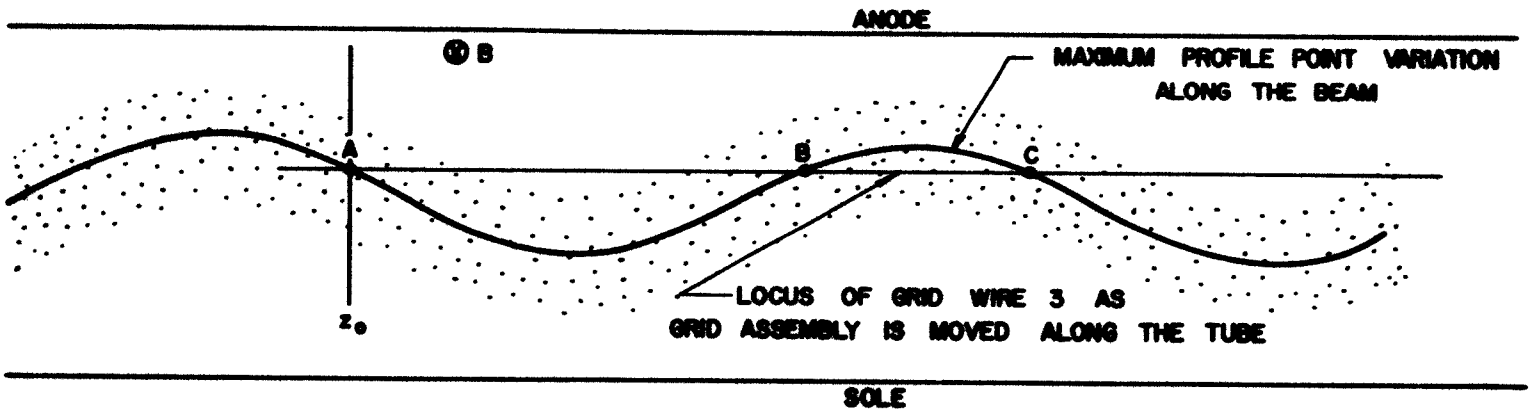

FIG. V.B.20 ILLUSTRATION OF THE MANNER IN WHICH A GRID WIRE INTERCEPTS VARIOUS PARTS OF A CYCLOIDING BEAM AS THE GRID ASSEMBLY IS MOVED IN THE z-DIRECTION. THE DISTANCE FROM A TO C CORRESPONDS TO ONE PERIOD OF THE BEAM VARIATION.

obvious that the cycloidal length is that distance from A to C although relative maximums of I_g occur at three points, A, B and C. This type of behavior always occurs as long as the maximum point passes through the wire in question. However, if the maximum profile point does not cross a certain wire, the existence of two consecutive maximum current interceptions by that wire should describe an approximate measure of the cycloidal length.

Figure V.B.21 shows the detailed characteristics of the currents intercepted by wires 2, 3, 4, 5 and 6 for the case V_f = - 850 volts, V_c = - 2200 volts, and B = 387 gauss. The theoretical cycloidal length is 0.635 inch and the appropriate measurements of the peaks of some of the intercepted currents gives distances which are in good agreement with this value. On the other hand, some of the current variations defy all attempts to obtain reasonable cycloidal lengths.

B.3 Analysis of Intercepted Currents. In the last report some rough calculations of the current density in the beam were made from the experimental data. This analysis was based on the assumption that each wire in the beam intercepted the amount of current contained within the shadow of the wire. That is, the electrons were assumed to be unaffected by the presence of the wires and would travel in their usual trajectory either striking one of the wires or passing between them. This method indicated current densities which were usually less than the cathode value and hence implied gun convergence ratios of less than one. Obviously this is a very crude way of determining the current densities in the beam.

Various efforts have been introduced to evaluate the densities in the beam more accurately. One investigation was based on the theory that

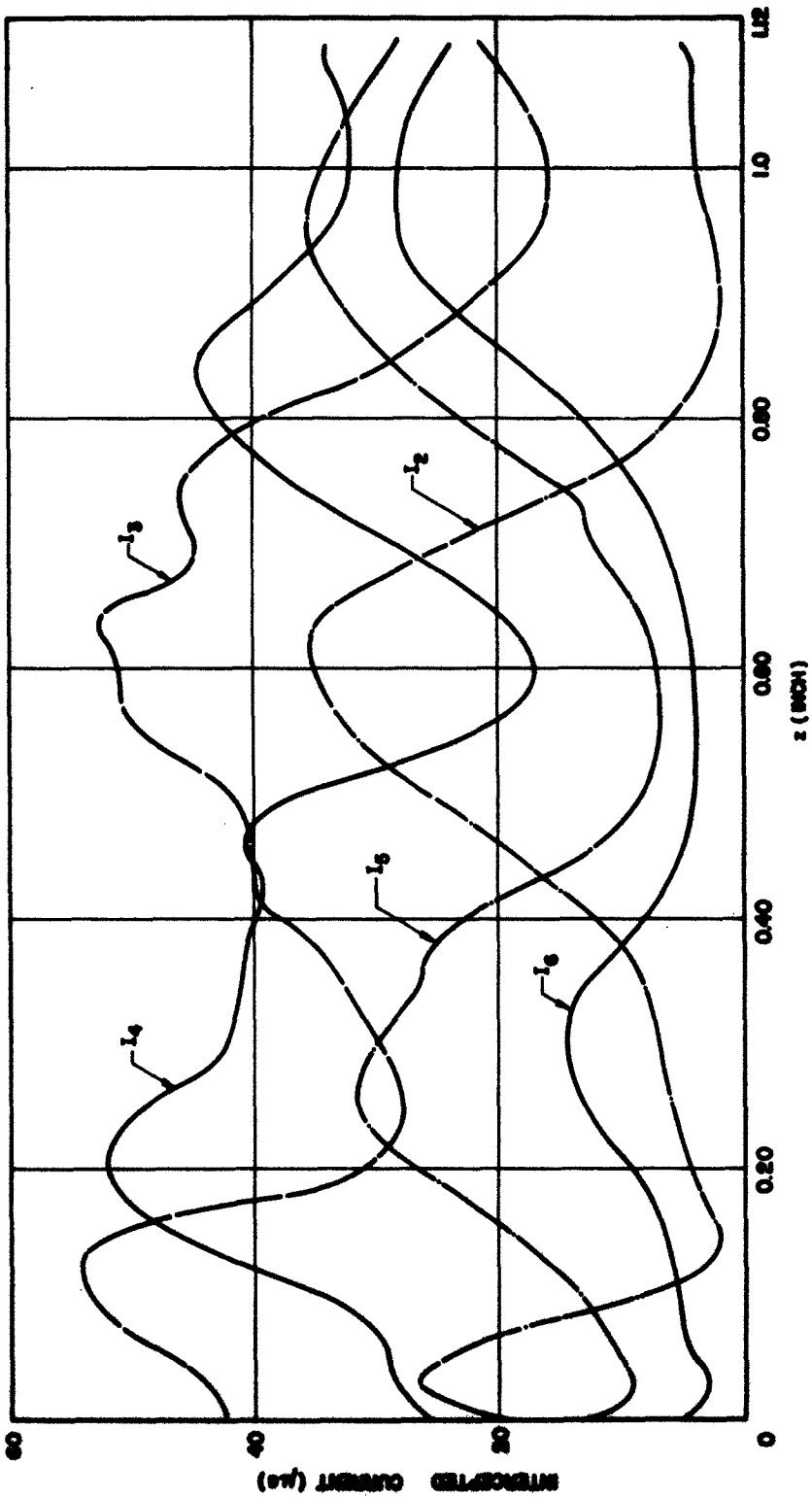

FIG. V.B.21 CURRENTS INTERCEPTED BY THE GRID WIRES AT VARIOUS z LOCATIONS. (V_c = - 2200, V_f = - 850, B = 387 GAUSS)

each wire intercepts electrons in the proper proportion to produce the necessary voltage distribution in the beam. For a Brillouin beam this means that the voltages at the various wires in the beam should vary as y^2 (y is measured from the bottom of the beam). Figure V.B.22 shows a laminar beam passing through the grid and is similar to the situation which might exist in the beam analyzer. The bottom electrons are located in the plane of the first wire (2.5d/14 above the sole) and the voltage in the beam must satisfy[4]

$$V = \frac{\eta B^2}{2}\left(y + \frac{5d}{14}\right)^2 \quad . \qquad \text{(V.B.2)}$$

Evaluation of this system results in the following currents:

$$I_o = \frac{5\eta\, B^2 d^2}{196\, R} \quad , \qquad \text{(V.B.3)}$$

$$I_1 = \frac{\eta\, B^2 d^2}{392 R} \qquad \text{(V.B.4)}$$

and

$$I_2 = I_3 = I_4 = I_5 = \frac{2\eta\, B^2 d^2}{392\, R} \quad . \qquad \text{(V.B.5)}$$

Thus the first wire in the beam should take exactly half as much current as each of the other wires in the beam. Those which are located outside of the beam, of course, will not intercept any current. Notice that these results are valid only for Brillouin flow and the particular resistance network shown in Fig. V.B.22. The magnitudes of the intercepted currents are observed to depend on the magnetic field, anode-sole

---

4. Masnari, N. A., et al, "Research on Crossed-Field Electron Devices", Final Report, Contract No. DA-36-039 sc-78260, Electron Physics Laboratory, The University of Michigan; December, 1962. (This report describes the conditions which must be fulfilled to allow a Brillouin beam to exist in a planar region.)

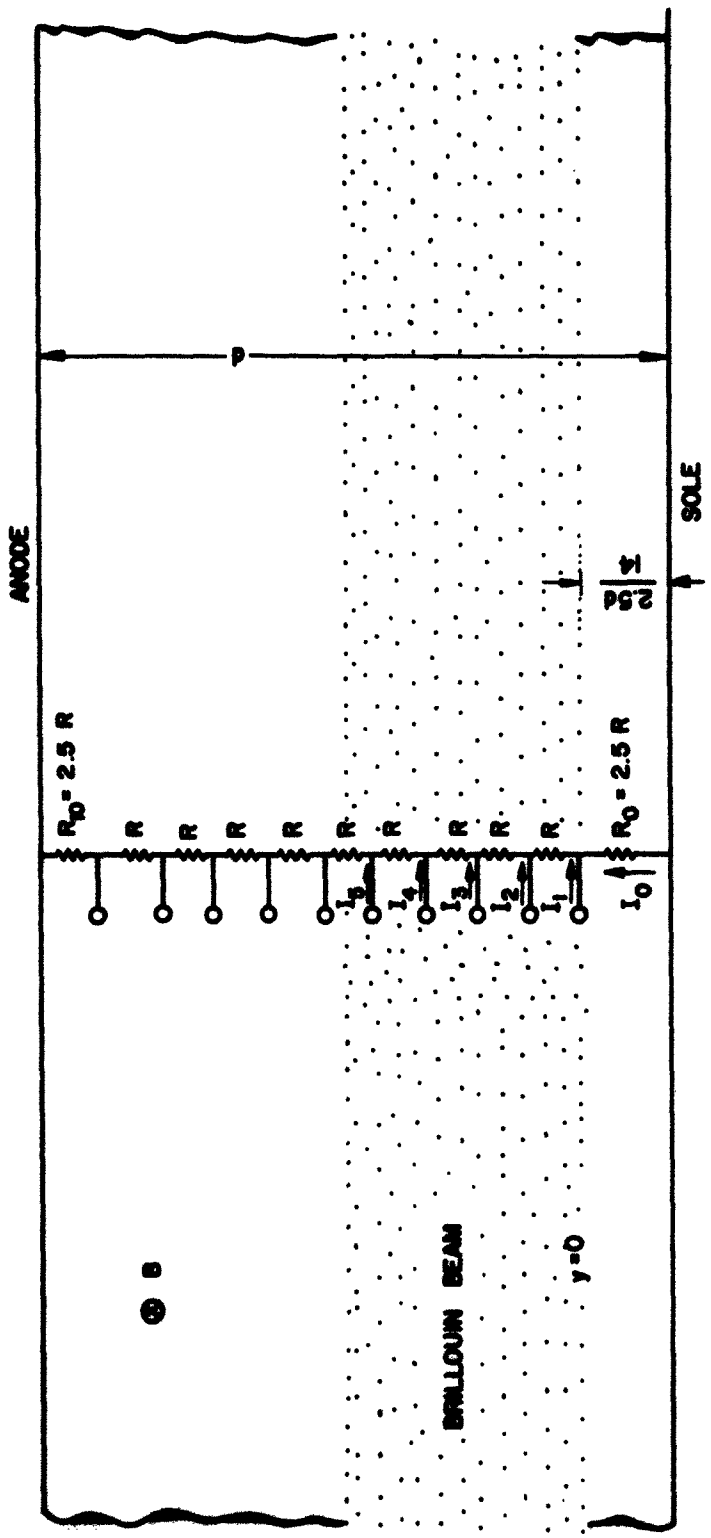

FIG. V.B.22 BRILLOUIN BEAM PASSING THROUGH THE GRID WIRE ASSEMBLY. (WIRE SPACING IS d/14)

spacing, and resistance between wires. Consequently, the intercepted currents should increase as B increases, provided the beam is laminar. In general, the magnetic field varied between 200 and 700 gauss which would produce minimum and maximum intercepted currents of

$$I_{min.} = 4 \text{ microamps}$$

and

$$I_{max.} = 49 \text{ microamps.}$$

These are the average values of the intercepted pulse currents and the peak values would be 100 times these results. For these calculations, R_L was chosen as 10,000 ohms which is approximately the value used in the experimental investigation.

The results from the beam analyzer indicated that the intercepted currents were generally in the range described above. This is not suggesting that the beams obtained during the investigation were laminar. In fact there is substantial evidence to indicate that the exact conditions of Brillouin flow were never realized. Nevertheless, the results show that the maximum currents intercepted by the wires were consistent with those predicted for a Brillouin beam. There are still too many questions to be answered before more significant conclusions can be reached regarding the experimental results. In particular, the finite diameter of the wires and the unequal resistance values separating the wires will modify the intercepted currents from the values predicted by Eqs. V.B.4 and V.B.5.

B.4 Conclusions. The various problems encountered in the initial experiments have been successfully solved and additional investigations have been performed. The Kino gun crossed-field device was first tested without the grid structure after which the wires were inserted and the

investigation repeated. This allowed comparison of the basic transmission characteristics of the gun in the two cases. The results indicated that reasonable agreement was achieved as long as the magnetic field was not extremely large. The inference is that insertion of the grid wires does not greatly distort the gross characteristics of the beam for reasonable values of B.

Investigation of the cathode current variation with voltage and magnetic field indicated that it satisfies the equation

$$I = C + K\frac{(V_f - V_c)^2}{B} \quad .$$

The nature of the constants C and K were not considered here but may well be a worthwhile future exploration.

Analysis of the beam profile variation along the z-axis generally substantiated the results described in the previous report. In particular, the location of the maximum profile point was observed to trace out a cycloidal path whose experimental period was usually in good agreement with the theory.

Detailed analyses of the variation of individual intercepted currents also provided information resulting in the evaluation of the cycloidal length of the beam undulations. The results were better for some cases than others.

The currents intercepted by a particular wire under normal conditions were compared to the values when an adjacent wire was disconnected from the external circuit (see Fig. V.B.19). The variations of the intercepted current as the grid was moved along the tube were nearly the same in each case with the exception that the magnitude of the current was greater with the adjacent wire disconnected. In both situations, the

resultant plots of I_3 against z allowed accurate measurement of the cycloidal length.

An analysis was started on the currents which would be intercepted by the wires when placed in a Brillouin beam. The theory is based on the assumption that the wires intercept current in the right proportion to produce the parabolic Brillouin potential distribution across the beam. The results indicate that the intercepted currents should depend on the magnetic field, anode-sole spacing and resistance values between wires. A detailed comparison between the theoretical and experimental results has not yet been made.

B.5 Program for the Next Period. The future crossed-field beam analyzer investigations will be similar to those described in this report. More effort will be directed toward obtaining a more detailed picture of the dependence of the various currents on the magnetic field, gun voltage, etc.

The analyses will also be concerned with obtaining a better understanding of the disturbances caused by the presence of the grid wires. This investigation will be accompanied by additional theoretical work involving electron beams passing through the grid of wires.

However, the primary objective for the next period will be the incorporation of the aperture system into the analyzer. The system will be placed directly behind the grid wires and its function will be to intercept and analyze minute portions of the beam. Hopefully this system will provide a microscopic picture of the beam characteristics as contrasted to the macroscopic view obtained from the present grid wire analysis. The ultimate goal is to obtain information which will allow the evaluation of current density, space-charge density, electron

velocity, and electron direction in the beam. The various components comprising the aperture system are presently being fabricated and, barring unforeseen difficulties, should be available in the near future.

C. Multi-Electrode Crossed-Field Gun (N. A. Masnari)

C.1 Introduction. The transmission characteristics of the multi-electrode crossed-field gun have been investigated. The initial experiments were concerned with only one of the proposed two cathodes and its associated gun electrodes. The investigation was carried out in two steps. Information was first obtained on the capability of the system to transmit the beam without any applied magnetic field. The magnetic field was then introduced and its effect on the beam was determined. This allowed an evaluation of the effectiveness of the shield in preventing magnetic flux from passing through the gun region.

C.2 Experimental Results. Damage to the ceramic spacers which support the various electrodes made assembly of both gun systems impossible and hence only one section was analyzed in this preliminary investigation. Figure V.C.1 illustrates the particular configuration which was investigated. It is similar to that described in the previous report except that the heater was changed from an uncoated to an oxide coated filament. This was necessitated by the continual shorting of the uncoated heater to the cathode block as operating temperatures were reached.

The initial investigation consisted of the collector at ground potential and the cathode at a negative voltage V_c. The other electrode voltages were obtained by connecting to various points of a resistor network which was placed across the power supply. Unfortunately, this method of biasing the various anodes did not provide good transmission to

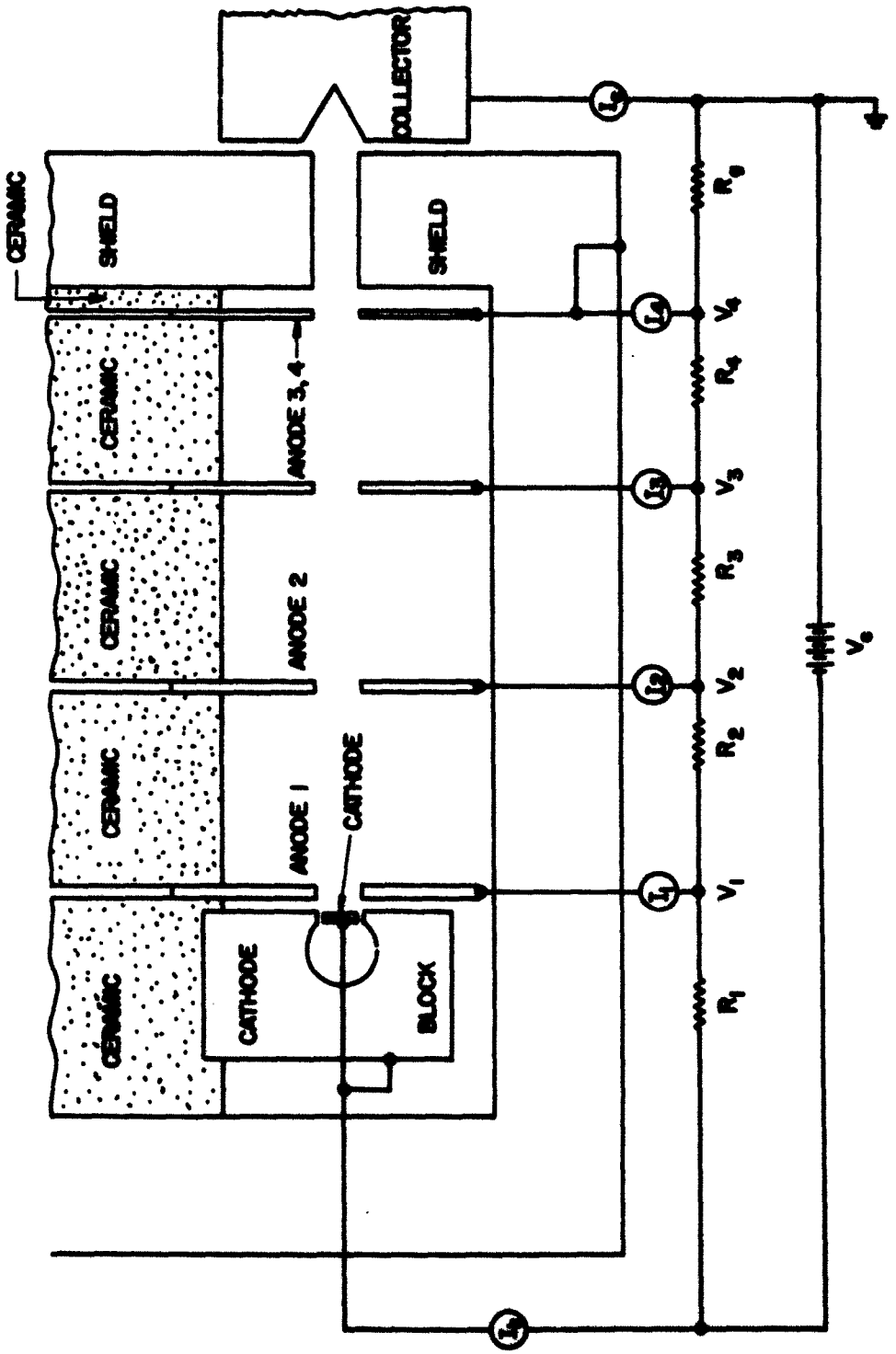

FIG. V.C.1 MULTI-ANODE CROSSED-FIELD GUN CONFIGURATION WITH ELECTRODE VOLTAGES PROVIDED BY A RESISTANCE NETWORK.

the collector. In fact the maximum transmission was less than 30 percent even for the most favorable conditions. The interdependence of the various anode voltages was apparently responsible for the poor transmission. In other words, as V_c was varied all of the electrode voltages varied proportionally depending on their connections to the resistance network. This made it impossible to vary one anode voltage independently of the others and consequently made it difficult to obtain good transmission to the collector.

The provision for independent variation of certain electrode voltages was obtained by reconnecting the circuit as shown in Fig. V.C.2. In this case three separate supplies were provided and the increased flexibility of such an arrangement resulted in transmission figures of better than 99 percent in certain low emission cases. The controlling factor in the cathode emission was found to be the voltage V_1 on the first anode which was consistent with the fact that this electrode was located only 0.020 inch from the cathode. For any given V_1 value, the other voltages (V_4 and V_c) could be varied to provide maximum transmission. However, if V_1 became too large, most of the current was intercepted by the first anode.

The introduction of a magnetic field was found to greatly influence the beam. This indicated that the magnetic shield was not performing satisfactorily and required certain modifications. In particular, the two holes in opposite sides of the shield which provided access to the heater and cathode leads were especially troublesome. These holes will be plugged and provision will be made to bring the leads out through the bottom of the shield.

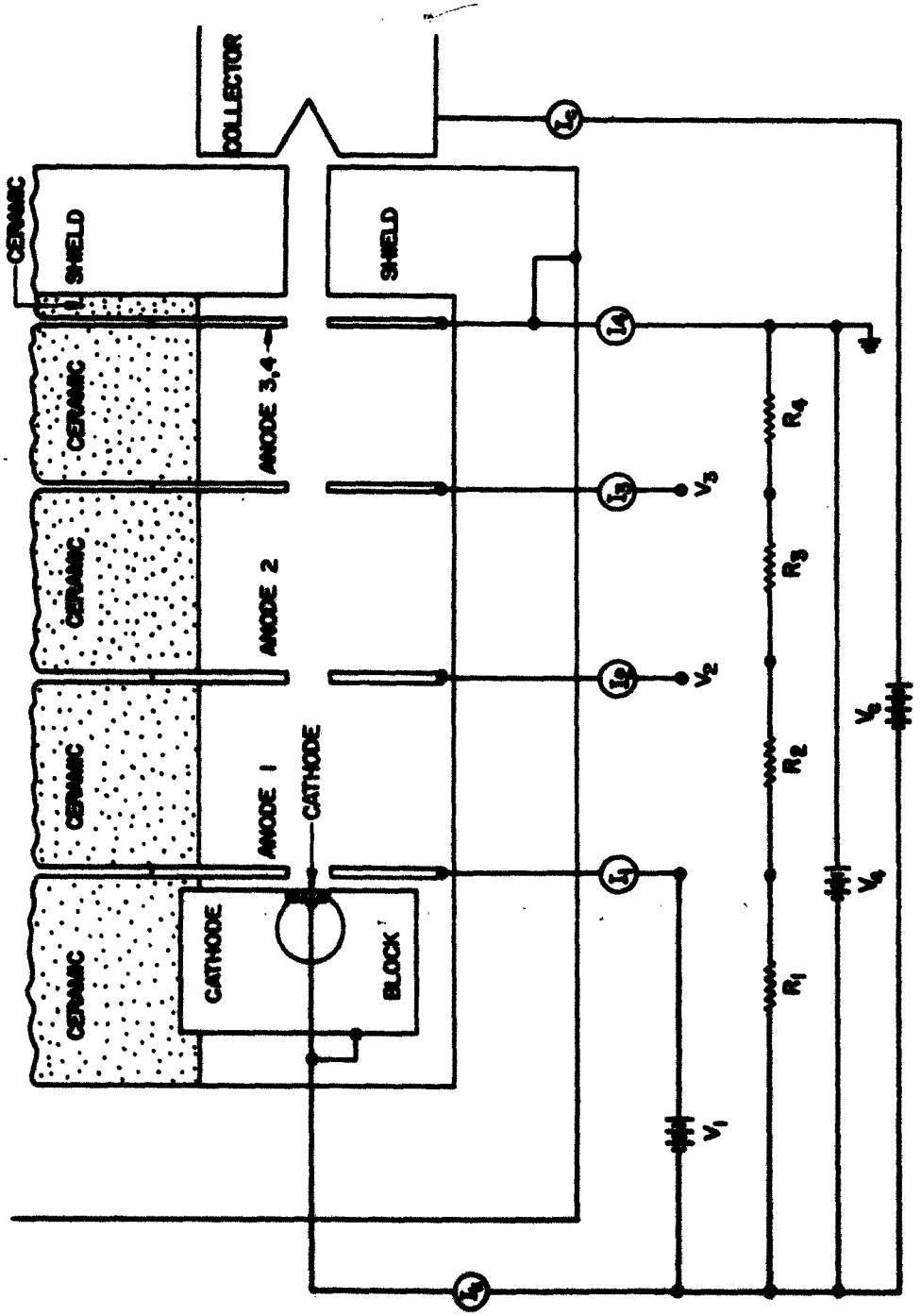

FIG. V.C.2 MULTI-ANODE GUN WITH BIAS VOLTAGES PROVIDED BY THREE SEPARATE SUPPLIES.

During the experiment it was also noticed that as the magnetic field was increased, the collector current first increased and then dropped off rapidly. This initial rise in the collector current was not consistent with theory and suggested further examination. Consequently the magnetic field was reversed and the collector current was observed to decrease continuously as the field was increased. This is the behavior which should occur regardless of the direction of magnetic field and thus indicated that either the anode apertures were not perfectly aligned with respect to the cathode or the cathode itself was tilted slightly. In either case, the line normal to the center of the cathode does not coincide with the axis of the aperture system. Thus with the magnetic field in the usual direction, increasing its value would move the center of the beam toward the aperture axis. When the beam axis and aperture axis coincided, the collector current became maximum. Further increases in B would cause the current to decrease as was observed in the experiment. On the other hand, with a reversed field an increase in B would always move the beam away from the aperture axis and hence the collector current would always decrease. This particular behavior is illustrated in Fig. V.C.3 where I_k (cathode current) and I_c (collector current) are plotted against magnetic field.

Figure V.C.4 shows the variation of I_c and I_k when the shield voltage (V_4) was varied and all other voltages held constant. V_1 (first anode voltage) was held fixed at 1.5 volt and the collector voltage was V_c = 700 volts. The third and fourth anodes were at the same potential as the shield ($V_3 = V_4$) and the second anode was biased at $V_2 = V_4/4$. The magnetic field was B = 30 gauss. The curves show that the collector current was zero until V_4 exceeded 60 volts after which it increased more

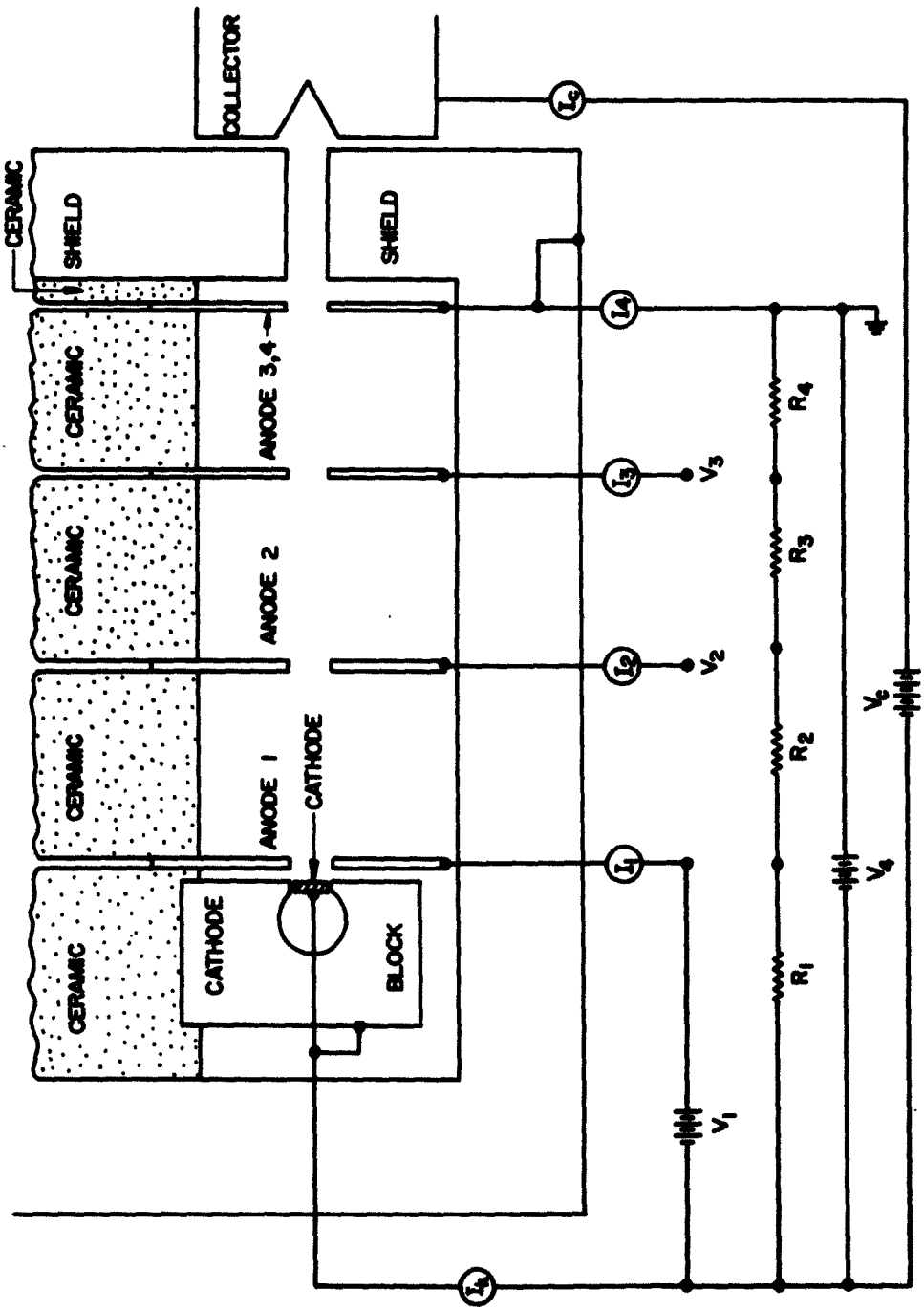

FIG. V.C.2 MULTI-ANODE GUN WITH BIAS VOLTAGES PROVIDED BY THREE SEPARATE SUPPLIES.

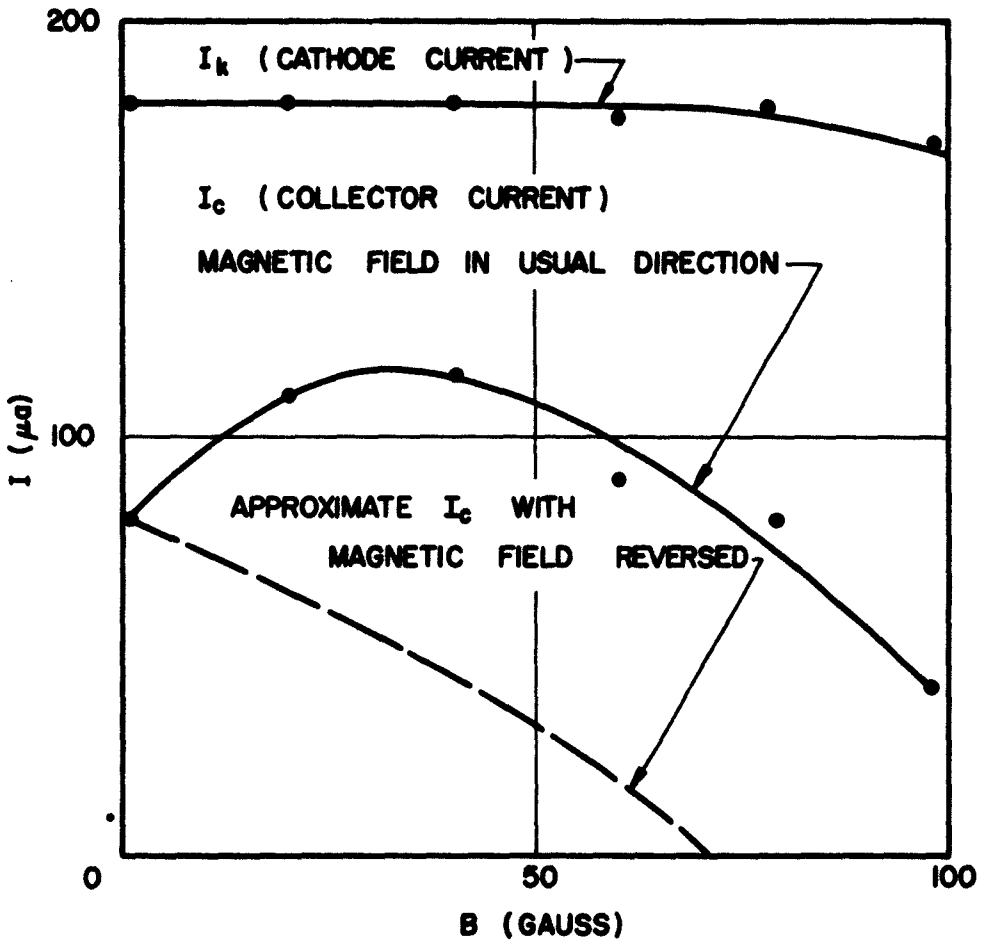

FIG. V.C.3 VARIATION OF CATHODE AND COLLECTOR CURRENTS WITH MAGNETIC FIELD. (V_1 = 1 VOLT, V_c = 700, $V_3 = V_4$ = 500, V_2 = 125)

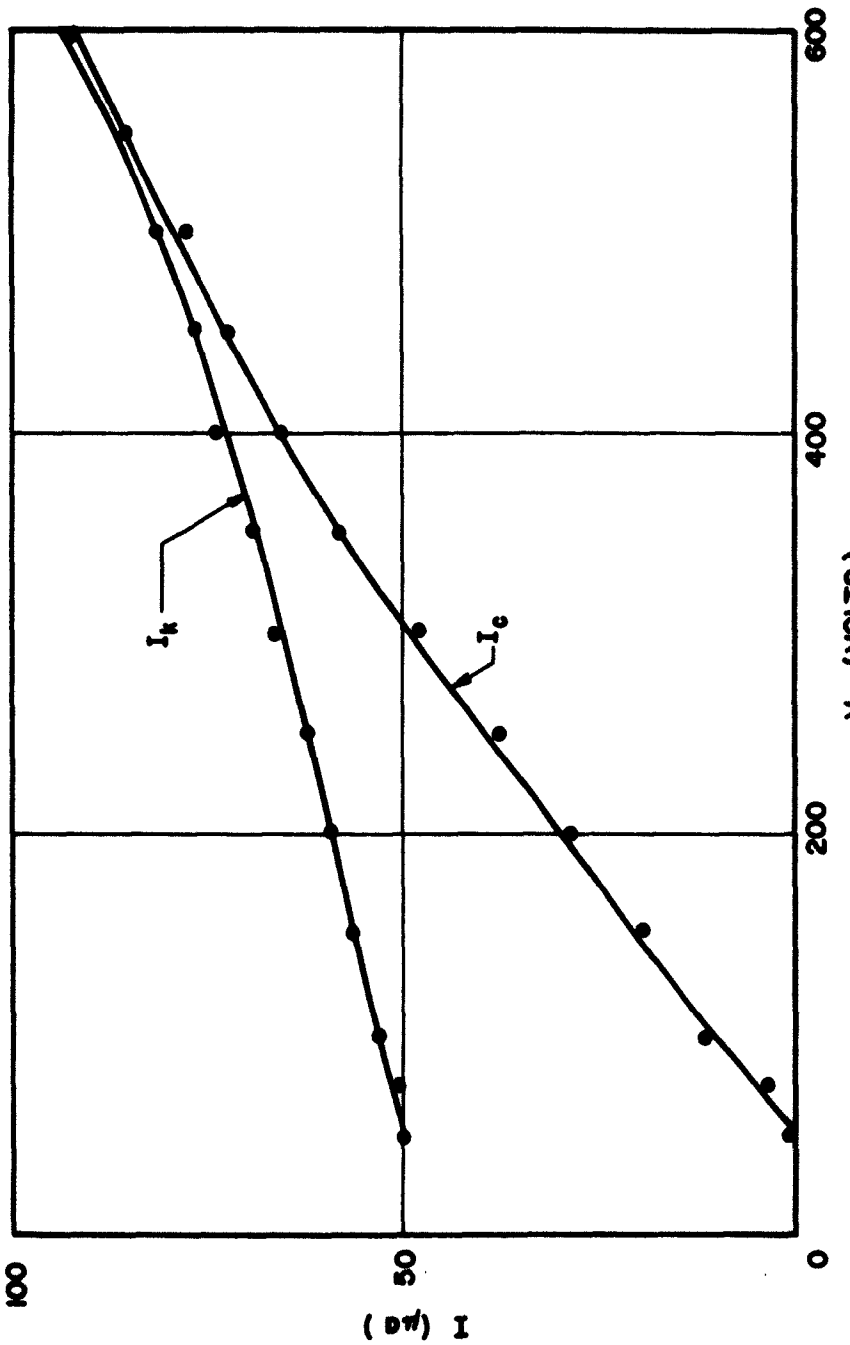

FIG. V.C.4 VARIATION OF CATHODE AND COLLECTOR CURRENTS WITH V_4. (V_1 = 1.5 VOLTS, $V_3 = V_4$, $V_2 = V_4/4$, V_c = 700, B = 30 GAUSS)

rapidly than the cathode current. As V_4 approached 600 volts (collector potential), nearly 98 percent of the cathode current reached the collector.

Figure V.C.5 illustrates a similar situation except that the collector voltage was reduced to 500 volts. The variation of I_k was nearly the same as the above case, indicating that the collector voltage exerts a negligible influence on the cathode emission. For $V_4 < 460$ volts, the I_c curves are nearly identical, indicating that the collector potential also does not affect the collector current as long as V_c is slightly larger than V_4. However, as V_4 is increased beyond 460 volts, I_c decreases quite rapidly and reaches 0 for V_4 slightly greater than V_c. Any attempt to increase V_4 beyond this point resulted in negative values of I_c indicating that each primary electron reaching the collector was causing the emission of several secondaries.

The effect of varying V_1 is illustrated in Fig. V.C.6. Obviously the first anode voltage plays a significant part in pulling electrons off the cathode. This is entirely consistent with the above mentioned observation that V_1 is the controlling factor in the amount of emission from the cathode.

Figure V.C.7 again illustrates the variation of I_k and I_c as V_4 is varied and B, V_1 and V_c are held constant. There are two sets of curves in this figure, one for $V_3 = V_2 = V_4/4$ and the other for $V_3 = V_4$, $V_2 = V_4/4$. The results indicate that both I_k and I_c are greater for $V_3 > V_2$ than for $V_3 = V_2$. This indicates that the voltage on anode No. 3 does affect the emission from the cathode, but not to the extent that the first anode voltage controls I_k.

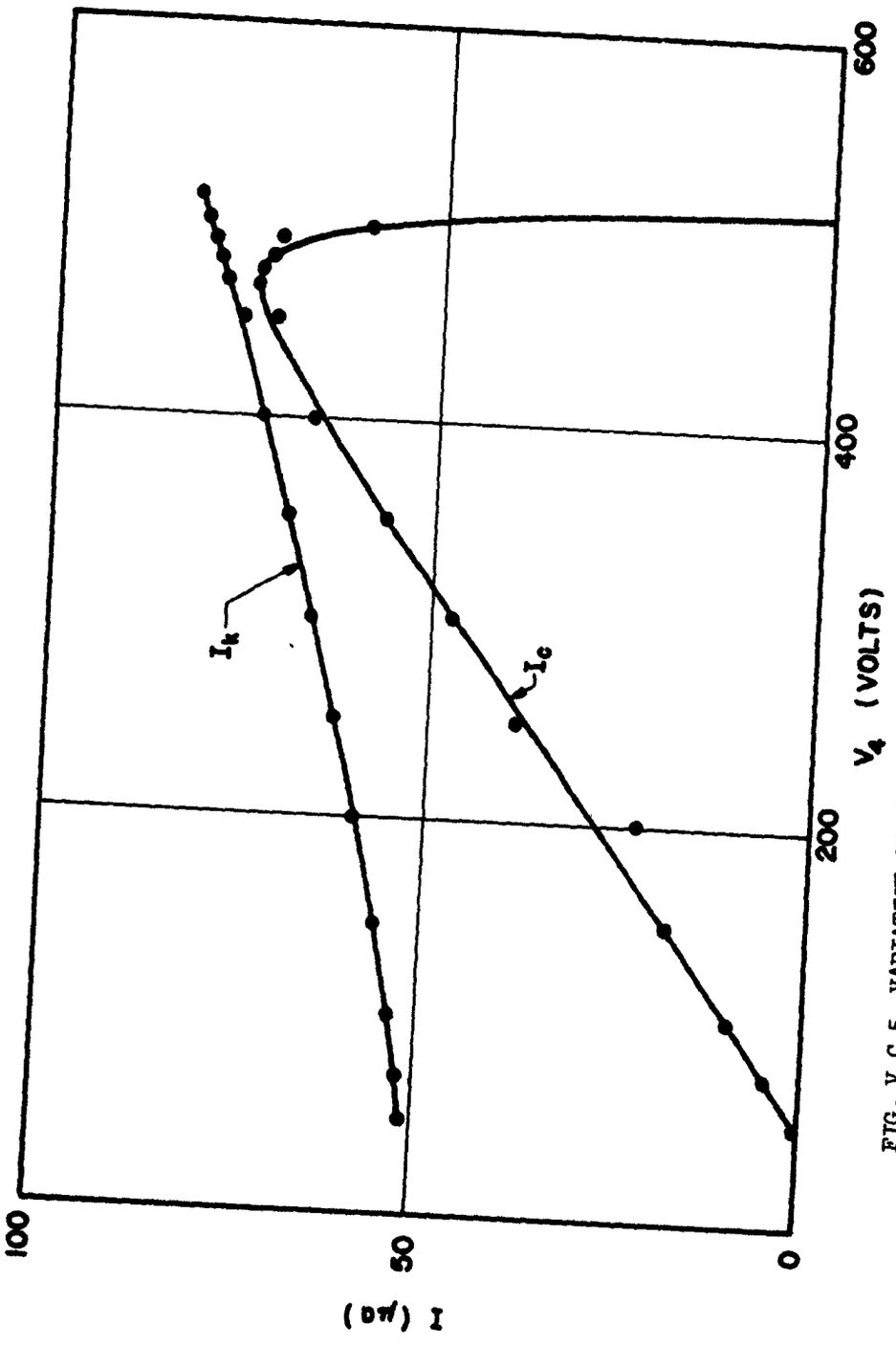

FIG. V.C.5 VARIATION OF CATHODE AND COLLECTOR CURRENTS WITH V_4. (V_1 = 1.5, $V_3 = V_4$, $V_2 = V_4/4$, V_c = 500, B = 30 GAUSS)

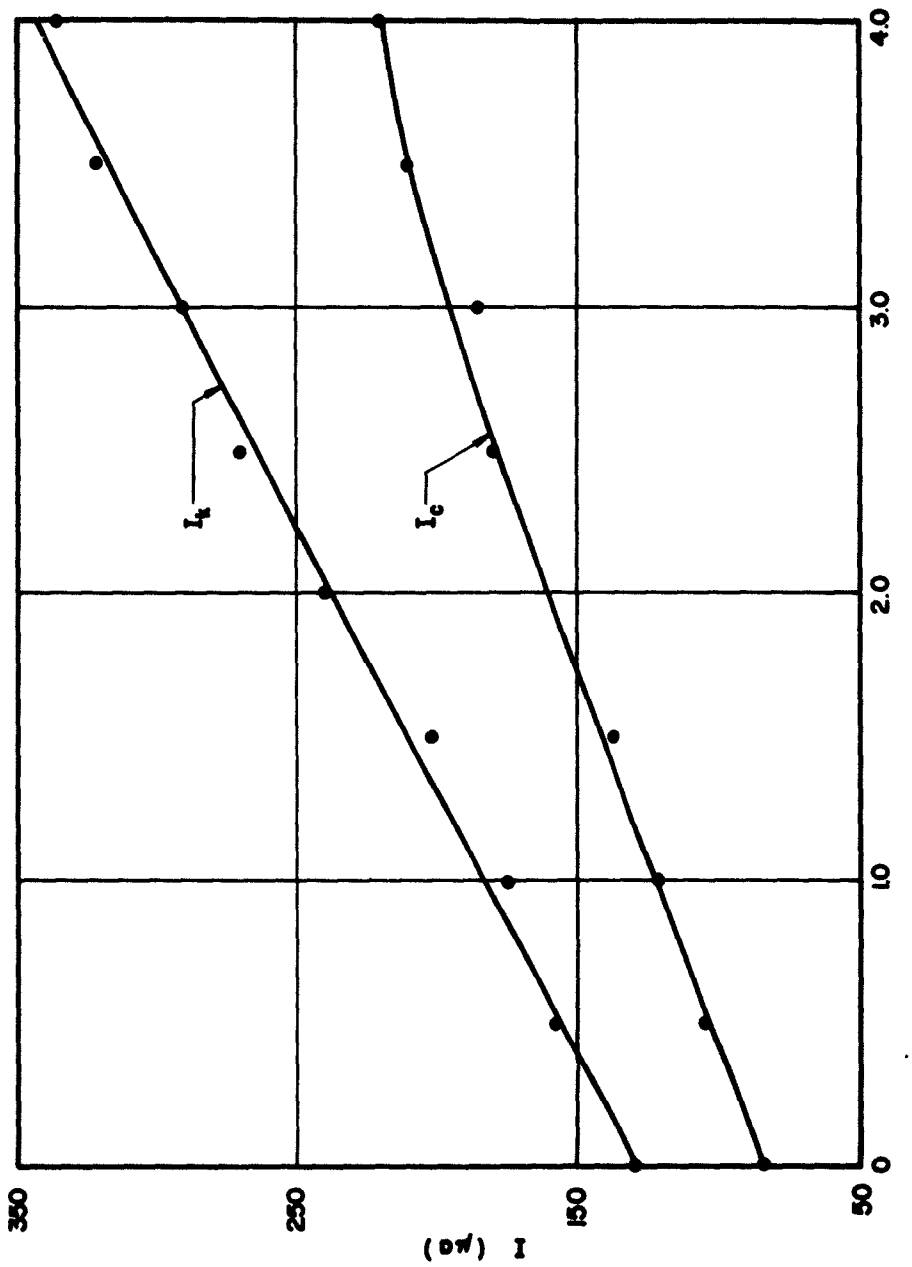

FIG. V.C.6 VARIATION OF I_c AND I_k WITH V_1. (V_2 = 125, $V_3 = V_4$ = 500, V_c = 700, B = 30 GAUSS)

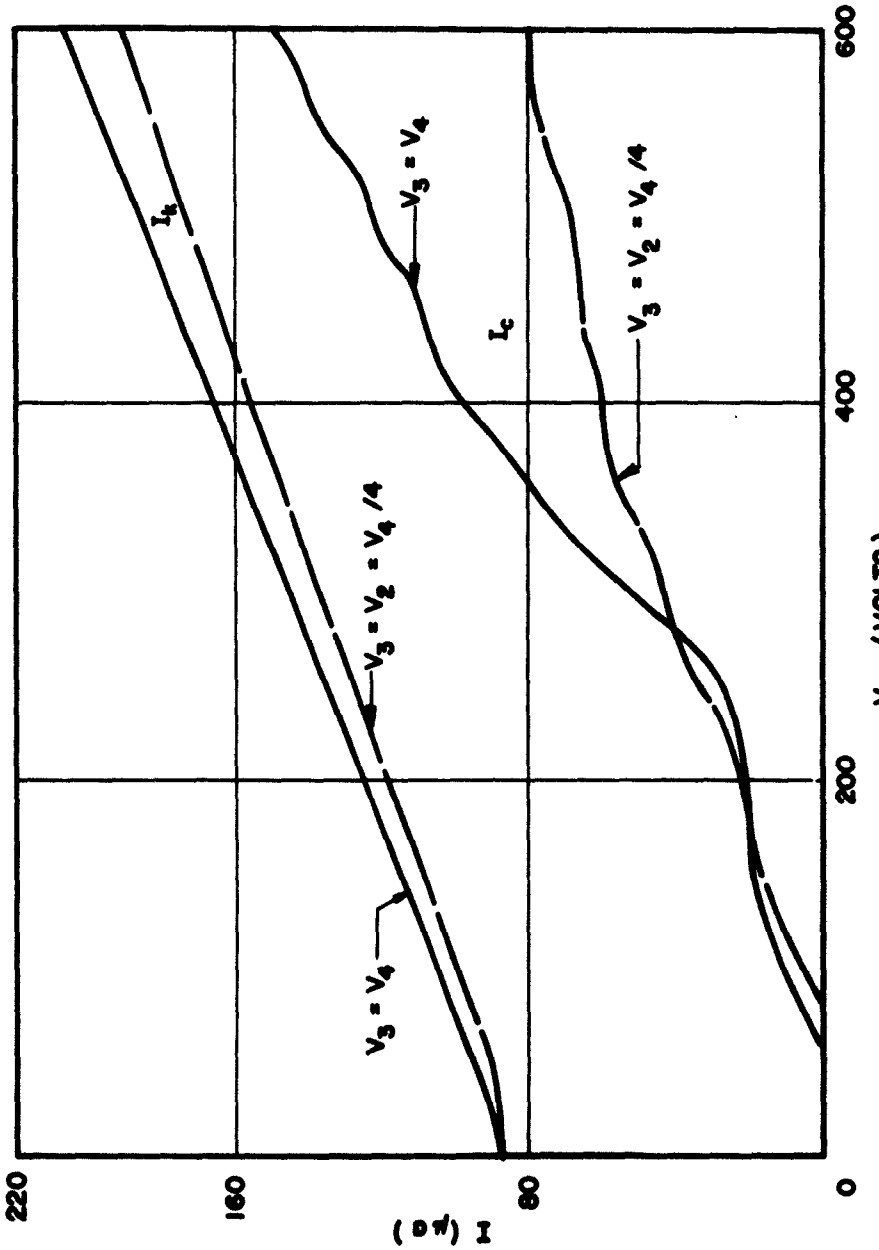

FIG. V.C.7 VARIATION OF I_K AND I_c WITH V_4 FOR DIFFERENT VALUES OF V_3.

($V_1 = 1$, $V_2 = V_4/4$, $V_c = 700$, $B = 0$)

C.3 Conclusions. The preliminary investigation of the multi-electrode crossed-field gun has indicated that reasonable transmission to the collector can be achieved at least for limited values of cathode current. The first anode voltage is the determining factor in the amount of current emitted, although other anodes have some effect. Unfortunately, the increase in I_k caused by increasing V_1 results in more current being intercepted by the first anode and less transmission to the collector. On the other hand, the collector voltage seems to have no effect on the emission, at least not for the values of V_c investigated above.

As the shield voltage (V_4) is increased, I_c becomes larger until V_4 approaches V_c, at which time the collector current drops rapidly. For values of V_4 slightly greater than V_c, I_c becomes negative as a result of the large number of secondary electrons emitted as a result of the impinging primaries.

The magnetic shielding was found to be unsuccessful and the transmitted current dropped off rapidly as B was increased. The application of the magnetic field also revealed an apparent asymmetry in the alignment of the apertures of the various anodes with respect to the cathode.

C.4 Program for the Next Period. The magnetic shield will be redesigned in an attempt to minimize the field which is capable of penetrating into the gun region. The major change will be to run the cathode and heater leads through the bottom of the shield.

The alignment of the anode apertures will be checked to determine their correctness. The cathode will also be investigated for correct location.

Further effort will be directed toward increasing the emission from the cathode without sacrificing transmission to the collector. This

may require the design and incorporation of focusing electrodes between the cathode and first anode. In other words, large values of I_k can be obtained if V_1 is made sufficiently large. However, when V_1 becomes too large, the first anode starts intercepting a greater percentage of the emitted current. Thus the use of focusing electrodes in this region may allow greater values of V_1 and hence I_k, while still maintaining reasonably good transmission.

D. Hybrid Crossed-Field Electron Guns (J. E. Boers)

D.1 Introduction. The hybrid gun is an attempt to take advantage of the large circulating current found in a cylindrical magnetron diode operated near its cutoff potential to produce a high current pulse in an M-type structure. The gun consists of a cylindrical magnetron diode blended into a rectilinear M-type geometry. A "gate" electrode, which is biased to the anode potential during the beam-off time, maintains the voltage distribution in the cylindrical magnetron. When this gate is biased near or below the cathode potential, a potential well is created across the magnetron and the circulating current should be focused out into the rectilinear region, the gate now serving as the first section of the sole. Thus a very high current density pulse should flow for a time approximately equal to the period of electron motion around the cathode.

D.2 Experimental Results. The results of d-c testing of the hybrid gun were reported earlier[1] but it was impossible to obtain significant data under pulsed conditions due to the lack of properly designed

1. Boers, J. E., et al, "Applied Research on Crossed-Field Electron Guns", TDR Rpt. No. ASD-TDR-62-757, Final Report, Contract No. AF 33(616)-8111, Electron Physics Laboratory, The University of Michigan; November, 1962.

connections to the electrodes. The peak output current pulse is extremely short (the order of millimicroseconds) and with the d-c connections available it was impossible to detect this with available equipment.

It was decided to add coaxial probes to the sole-anode drift space and to the cylindrical magnetron region of the gun. After considerable difficulty with internal shorts caused by sputtering from the cathode, the gun was reassembled and some tests have been carried out.

Several interesting and as yet not completely explained effects have been observed. In the d-c, off condition a 1000 gauss magnetic field was required to cut off the cylindrical magnetron diode with 500 volts on the anode, and 500 gauss moved the cutoff below 400 volts.

The theoretical cutoff voltages for 1000 and 500 gauss are 4800 and 1200 volts respectively. The presence of oscillations in the diode is strongly suspected but has not been directly observed as yet.

Under pulsed conditions the sole-anode drift space probe has been a definite aid in observing the output. There appears to be a high frequency oscillation on the output pulse. The oscillation is always damped to some degree, but the amount of this damping seems to be a function of conditions in the magnetron diode and the size of the gating pulse.

The larger the gating pulse the faster the damping. This might indicate that the large current is pulled out faster with the larger gate pulse, thus producing the desired effect. The pulse has been viewed on an oscilloscope with a frequency response to 30 mc (-3 db) and 41 mc (-6 db). The pulse applied is 100 microseconds long and the oscillation usually lasts half to three quarters of this length.

When viewed on a spectrum analyzer the only response above 10 mc is found at 120 mc. It has not yet been definitely established whether

or not this is the oscillation viewed on the oscilloscope or is a feed-through from the pulser. The 120 mc oscillation does not change with the magnetic field.

D.3 Conclusions. After experiencing many difficulties the hybrid crossed-field gun has been reassembled and some testing has been accomplished. The addition of coaxial probes has permitted a closer observation of the output pulse and the presence of high frequency oscillation suggests the possibility of a high leading edge current pulse in the output. The very low cutoff potential for the cylindrical magnetron section suggests the presence of strong oscillations but their presence has not yet been observed.

D.4 Program for the Next Period. Further study of the output pulse will be made to determine definitely whether or not there is a high current pulse on the leading edge. An effort will be made to obtain a nanosecond pulser for more direct observation of the pulse. The reason for the lack of detectable oscillation from the magnetron diode or why the cutoff voltage is so low will be determined.

E. Digital Computer Studies of Crossed-Field Guns (J. E. Boers)

E.1 Introduction. The digital computer program for the analysis of crossed-field electron guns has been further refined during the last period. The work on the program has been divided into two main divisions--first, to improve the accuracy of the representation of the gun, and second, to ease the handling of the input data to the program. The first will be referred to as "internal" and the second as "external" program modifications.

E.2 Computer Program Modifications.

a. Internal Computer Program Modifications. The CEMFEG-2 (for Crossed Electric and Magnetic Field Electron Gun) FORTRAN program has been modified so that nonuniform emission from the cathode is automatically taken into account. Since the current densities in the gun program are directly proportioned to the number of electron paths within a given distance, it was possible to simulate nonuniform emission from the cathode by starting more electrons in regions where the electric fields were higher. Previously these starting points were read in as external data, but now the program itself will determine both the number and location of the required trajectories.

Current densities along the cathode are computed by employing Child's law with the voltages being those of the first matrix point off the cathode, and the distances the length of one square of the matrix. The minimum of the current densities thus computed is then found and all the other values are then divided into it. This produces a normalized set of numbers which can be used to find the separation between trajectories, i.e., the maximum will be 1.0, which will be proportional to the separation between electrons at the point of lowest emission, and at all other points these numbers will be smaller.

Half the difference between the new and the previous current density is added to the previous one and is used for the new space-charge calculation. It was found that if the new current density was used directly the program would oscillate quite widely about the correct value. Whether or not half the difference is an optimum value has not been determined but the results obtained have been quite satisfactory.

Due to the added changes that now take place from one cycle to the next it is necessary to run the program a few additional cycles, or a total of 8 to 10 cycles before reasonable convergence is obtained. Cycle time varies from one to three minutes depending upon the stage of the calculations.

b. External Computer Program Changes. The number of data cards needed for the input to the program has been substantially reduced and some additional flexibility has been added.

The method of reading in the electrode voltages was modified so that it is no longer necessary to read in each point individually as before but only the end points of a given electrode and the value for that electrode. In addition, voltages can now be read in along the lower electrodes by the same method.

Also, since the trajectory starting points are now computed by the program itself, it is no longer necessary to read in these values reducing the amount of data still further.

Altogether the number of input data cards has been reduced from over 100 to less than 30 cards.

E.3 Computer Applications. The computer program was checked out on the modified Kino gun described in the previous report, but no significant changes in the results previously obtained have been found.

E.4 Conclusions. The crossed-field electron gun program (CEMFEG-2) has been improved in two ways. First, automatic calculation of nonuniform emission from the cathode has been made an integral part of the program. An additional benefit of this calculation has been the self-determination by the program of the current from the cathode. The handling of the input data has been improved, adding more flexibility, while at the same time reducing the total amount of information needed.

E.5 Program for the Next Period. Recent work with an axially symmetric digital program, where the cathode shape is generally more complex than in crossed-field guns, has shown that the accuracy of the electron trajectories is greatly improved by starting the electrons at the first matrix point off the cathode, i.e., most of the error in the trajectory seems to occur in the region just off the cathode where the field representation is poorest due to the finite size of the matrix and the exponential character of the voltage. The error in velocity at the exit plane of the axially symmetric gun was reduced from as high as 2.0 percent to less than 0.01 percent by starting the electrons with the proper velocity and direction at the first matrix point.

The possibility of improving the accuracy of the crossed-field program by this method should be investigated. The crossed-field case is slightly more complex due to the action of the magnetic field and some study of the region near the cathode may have to be made.

VI. GENERAL CONCLUSIONS (G. T. Konrad)

The topics of study discussed in this interim report represent the various phases of the research program. All of these investigations are directed toward extending the state of the art in microwave and quantum electronics. The major portion of the theoretical work has been devoted to low-noise phenomena and beam-plasma interactions. The experimental work has been in the general area of electromagnetic generation, particularly in the short wavelength regions. This includes several plasma devices, masers and a Cerenkov radiation device. In addition, crossed-field electron guns and high-thermal-conductivity dielectric materials have been studied from both experimental as well as theoretical points of view.

The results obtained in all the areas described have been quite encouraging. During the next period all this work will be continued along the lines outlined at the end of the individual sections.

DISTRIBUTION LIST

No. Copies	Agency
7	Aeronautical Systems Division, Attn: ASRNET-1, Wright-Patterson Air Force Base, Ohio
1	Air Force Cambridge Research Laboratories, Attn: Tube Group, L. G. Hanscom Field, Bedford, Massachusetts
1	Chief, Bureau of Ships, Code 691A4, Attn: Mr. H. J. Riegger, Department of the Navy, Washington 25, D. C.
1	Chief, Bureau of Ships, Attn: Mr. Charles Walker, Department of the Navy, Washington 25, D. C.
1	Commanding Officer, Diamond Ordnance Fuze Laboratories, Attn: Microwave Tube Branch, Washington 25, D. C.
1	Electronic Systems Division, Attn: ESRDE, Major J. W. Van Horn, L..G. Hanscom Field, Bedford, Massachusetts
1	Rome Air Development Center, Attn: RALTP, Mr. H. Chiosa, Griffiss Air Force Base, New York
1	Commanding Officer, USAERDL, Attn: Mr. Harold J. Hersh, SIGRA/SL-PRM, Ft. Monmouth, New Jersey
1	Commanding Officer, USAERDL, Attn: Mr. Irving Reingold, Microwave Tubes Branch, Ft. Monmouth, New Jersey
1	Commanding Officer, U. S. Naval Ordnance Laboratory, Attn: Miss Virginia L. Parker, Corona, California
30	ASTIA (TISIA), Arlington Hall Station, Arlington 12, Virginia
4	Advisory Group on Electron Devices, Attn: Mr. H. N. Serig, 346 Broadway, 8th Floor, New York 13, New York
1	Bendix Corporation, Systems Planning Division, Ann Arbor, Michigan, Attn: Technical Library
1	Mr. A. G. Peifer, Bendix Corporation, Research Laboratories, Northwestern Highway and 10-1/2 Mile Road, Detroit 35, Michigan
1	Bendix Corporation, Research Laboratories, Northwestern Highway and 10-1/2 Mile Road, Detroit 35, Michigan, Attn: Technical Library
1	California Institute of Technology, Department of Electrical Engineering, Pasadena, California, Attn: Professor Roy Gould

No. Copies	Agency
1	Cornell University, Department of Electrical Engineering, Ithaca, New York, Attn: Professor L. Eastman
1	Dr. Rajindar P. Wadhwa, Electron Tube Division, Litton Industries, 960 Industrial Way, San Carlos, California
1	General Electric Company, Electron Tube Division of Research Laboratory, Schenectady, New York, Attn: Dr. E. D. McArthur
1	General Electric Microwave Laboratory, 601 California Avenue, Palo Alto, California, Attn: Mr. S. Webber
1	Hughes Aircraft Company, Florence and Teals, Culver City, California, Attn: Mr. Nicholas E. Devereux, Technical Document Center
1	University of Illinois, Department of Electrical Engineering, Urbana, Illinois, Attn: Professor Paul D. Coleman
1	Litton Industries, 960 Industrial Way, San Carlos, California, Attn: Dr. Joseph Hull
1	Massachusetts Institute of Technology, Research Laboratory of Electronics, Cambridge 39, Massachusetts, Attn: Documents Library
1	Microwave Electronics Corporation, 4061 Transport Street, Palo Alto, California, Attn: Dr. S. F. Kaisel
1	Microwave Associates, Attn: Dr. P. Chorney, Burlington, Massachusetts
1	University of Minnesota, Department of Electrical Engineering, Minneapolis, Minnesota, Attn: Dr. W. G. Shepherd
1	Polytechnic Institute of Brooklyn, Documents Library, Brooklyn, New York
1	Raytheon Company, Spencer Laboratory, Burlington, Massachusetts, Attn: Mr. W. Teich
1	RCA Laboratories, Princeton, New Jersey, Attn: Library
1	Sperry Corporation, Electronic Tube Division, Gainesville, Florida, Attn: Library
1	Sperry Gyroscope Company, Great Neck, New York, Attn: Engineering Library
1	Stanford University, Microwave Laboratory, Stanford, California, Attn: Dr. M. Chodorow
1	Stanford University, Electronics Laboratories, Stanford, California, Attn: Dr. A. E. Siegman

No. Copies	Agency
1	Sylvania Microwave Tube Laboratory, 500 Evelyn Avenue, Mountain View, California, Attn: Dr. J. Needle
1	Sylvania Electric Products Inc., Applied Research Laboratory, 40 Sylvan Road, Waltham 54, Massachusetts, Attn: Mrs. Mary E. Bufka, Librarian
1	Varian Associates, 611 Hansen Way, Palo Alto, California, Attn: Technical Library
1	Watkins-Johnson Company, 3333 Hillview Avenue, Palo Alto, California, Attn: Dr. D. A. Watkins
1	Mr. Gerald Klein, Manager, Microwave Tubes Section, Applied Research Department, Westinghouse Electric Corporation, Box 746, Baltimore 3, Maryland
1	Westinghouse Electric Corporation, P. O. 284, Elmira, New York, Attn: Mr. Daniel Buck
1	The University of Michigan, Office of Research Administration, Mortimer E. Cooley Building, Ann Arbor, Michigan, Attn: Project Files
21	The University of Michigan, Electron Physics Laboratory, 3505 East Engineering Building, Ann Arbor, Michigan
1	Dr. Om P. Gandhi, Central Electronics Engineering Research Institute, Pilani, Rajasthan, India

AD _____

THE UNIVERSITY OF MICHIGAN, ELECTRON PHYSICS LABORATORY, ANN ARBOR, MICHIGAN. APPLIED RESEARCH IN MICROWAVE AND QUANTUM ELECTRONICS, by J. E. Rowe, et al. February, 1963, 150 pp. incl. illus. (Project No. 4156, Task No. 415605)

This report summarizes the work done to date on the general program of applied research in microwave and quantum electronics. All the investigations carried out are directed toward extending the state of the art in microwave and quantum electronics. The research is theoretical as well as experimental in nature.

The theoretical work is largely devoted to an investigation of low-noise phenomena and beam-plasma interactions. The experimental work is concerned with electromagnetic generation, particularly in the short wavelength regions. This includes several plasma devices, masers, and a Cherenkov radiation device. In addition crossed-field electron guns and high-thermal-conductivity dielectric materials for high-average-power microwave tubes are studied from a theoretical as well as experimental point of view.

UNCLASSIFIED

1. High-Thermal-Conductivity Materials
2. Low-Noise Investigations
3. Plasma and Quantum Electronics
4. Crossed-Field Electron Gun Studies

I. Rowe, J. E.
II. Detweiler, H. K.
III. Haddad, G. I.
IV. Noh, G.
V. Konrad, G. T.
VI. Lin, Y. C.
VII. Lomax, H. J.
VIII. Mansuri, H. A.
IX. Rowe, J. E.
X. Singh, A.
XI. Wen, C. P.
XII. Yeh, C.

UNCLASSIFIED

AD _____

THE UNIVERSITY OF MICHIGAN, ELECTRON PHYSICS LABORATORY, ANN ARBOR, MICHIGAN. APPLIED RESEARCH IN MICROWAVE AND QUANTUM ELECTRONICS, by J. E. Rowe, et al. February, 1963, 150 pp. incl. illus. (Project No. 4156, Task No. 415605)

This report summarizes the work done to date on the general program of applied research in microwave and quantum electronics. All the investigations carried out are directed toward extending the state of the art in microwave and quantum electronics. The research is theoretical as well as experimental in nature.

The theoretical work is largely devoted to an investigation of low-noise phenomena and beam-plasma interactions. The experimental work is concerned with electromagnetic generation, particularly in the short wavelength regions. This includes several plasma devices, masers, and a Cherenkov radiation device. In addition crossed-field electron guns and high-thermal-conductivity dielectric materials for high-average-power microwave tubes are studied from a theoretical as well as experimental point of view.

UNCLASSIFIED

1. High-Thermal-Conductivity Materials
2. Low-Noise Investigations
3. Plasma and Quantum Electronics
4. Crossed-Field Electron Gun Studies

I. Rowe, J. E.
II. Detweiler, H. K.
III. Haddad, G. I.
IV. Noh, G.
V. Konrad, G. T.
VI. Lin, Y. C.
VII. Lomax, H. J.
VIII. Mansuri, H. A.
IX. Rowe, J. E.
X. Singh, A.
XI. Wen, C. P.
XII. Yeh, C.

UNCLASSIFIED